A COMPARISON OF BIOCOLLOID AND COLLOID TRANSPORT IN SINGLE, SATURATED ROCK FRACTURES

A Comparison of Biocolloid and Colloid Transport in Single, Saturated Rock Fractures

By

JUNLEI QU, B.E.

A Thesis

Submitted to the School of Graduate Studies

In Partial Fulfillment of the Requirements

for the Degree

Master of Applied Science

McMaster University

MASTER OF APPLIED SCIENCE (2010) McMaster University
(Civil Engineering) Hamilton, Ontario

TITLE: A Comparison of Biocolloid and Colloid Transport in Single, Saturated Rock Fractures
AUTHOR: Junlei Qu, B.E. (Hohai University)
SUPERVISOR: Dr. Sarah E. Dickson
NUMBER OF PAGES: iv, 94

ABSTRACT

To obtain a better understanding of groundwater contamination, experiments of biocolloid and colloid transport in single, saturated fractures are conducted to have research in contaminants transport in fractured media. Hydraulic tests and solute tracer tests were conducted to characterize fractures. Due to the relatively large volume in the recirculation system, a back-calculation is employed in the analysis of tracer tests.

E. coli RS-2GFP tracer tests were conducted on three fractures at specific discharges of 0.1, 1 and 10 cm/min. With higher specific discharges, the percent recovery is higher in F2 and F3, as well as the colloid experiments, which is likely due to higher specific discharges providing biocolloids less opportunity to attach to the fracture walls. But this did not occur in F1, which is likely due to the smaller aperture size.

Comparing the synthetic replicas with real fractures in similar specific discharges, recovery of biocolloid was smaller than colloid. In colloid tracer tests, higher recovery appeared in the fractures with larger aperture field, but this is not clearly seen in biocolloid tracer tests. These indicate that the biological properties of bacteria, and the difference of fracture region and the tortuosity influence the transport.

ACKNOWLEDGEMENT

There are many people who have supported me during the program. I would first like to thank my supervisor, Dr. Sarah Dickson for her excellent guidance and supervision. Her enthusiasm and sound knowledge deeply influenced me, and brought me into the colorful science world. Her innovative ideas and endless support helped me go through every difficulty in the research.

I am grateful for the assistance of Anna Robertson and Peter Koudys. Their experienced technical skills and analytical work were greatly helpful to my research. The advice on the thesis from Anna provided me a clearer idea.

Many thanks to Sandrina for teaming up with me on this research. We spent countless days and nights together on the experiments and working on the data. It made the research more enjoyable and allowed the sharing of ideas. Thanks to Qinghuai for his previous research, share of achievements and helpful advice. Thanks to fellow graduate students for their friendship.

Thanks to my parents. It is their unreserved support and warmth travelled across the sea helped me go through the hard time, and encourage me to go on.

TABLE OF CONTENTS

LIST OF FIGURES

LIST OF TABLES

1 Introduction

Groundwater is the major source of drinking water for more than 25% of the population of the world (Clark and King, 2004) and constitutes more than half of the drinking water consumed by the United States and Europe. Use of this water by agriculture, industry, mining, and urbanization stresses the supply and diminishes its quality, which can cause disease and illness (Gleick, 2004). It is reported that almost half of all waterborne disease originates from groundwater contamination (Craun, 1984).

As a ubiquitous aquifer material, fractured rock is being investigated more and more frequently in the field of groundwater contamination. The fact that organic contaminants are reduced in fractures (Mclinn & Rehm, 1997) demonstrated the importance of fractures in the contamination of groundwater. Thus the role of fractures in groundwater dissolved contaminants has been thoroughly researched. Conversely, research in microbiological transport through fractures has generally been neglected. Since pathogenic protozoa, bacteria and viruses in groundwater can cause acute illness, pathogen contamination is a significant issue. Colloid sized (0.001 to 10 μm) pathogens (e.g., viruses, bacteria, protozoa) and toxic chemicals that adhere to similar sized mineral particles (e.g., clays and oxide precipitates) can be transported with groundwater (Saiers, 2006). Because the solutes' and colloids' transport behaviours (velocity, transport mechanisms, etc.) are different (Harvey et al, 1989), it is necessary to research colloid-sized tracers transport mechanisms.

From conservative tracer tests, it has been noted that flow rates, flow pathways (Hartmann, 2007), and the properties of subsurface media (Chen, 2007) may influence the recovery of tracers. From microorganism transport tests, it has been demonstrated that subsurface hydrogeology conditions (Lehman *et al.*, 2001), exterior conditions such as precipitation (Celico, 2004), and groundwater velocity (Mailloux, 2003) are all factors influencing colloid transport. Other experiments have demonstrated that the type and property of microorganisms are also factors (Pang and Simunek, 2006).

Typically, microorganisms can migrate long distances in both vertical and horizontal directions in the subsurface, which increases the potential for the contamination of groundwater, particularly if the microorganisms are able to survive for extended period. The travel distance of microorganisms depends on the type of media and groundwater flow rate (Abu-Ashour *et al.*, 1994). For example, in oil production, water injected into reservoirs to maintain pressure eventually reaches the production well. During this process, sulphate reducing bacteria travel to the substrate well along with the injection water (Beeder *et al.*, 1996). A bacterial indicator was used as a tracer demonstrating that microorganisms present in the injection water will eventually contaminate the well. Fractures in clay tills increase the bulk hydraulic conductivity of the clay, and hence increase the probability for contaminant migration. Fracture orientation, length, degree of interconnection, and aperture are also influential factors (Hinsby *et al.*, 1996).

Because of the natural configuration of fractures, various transport functions exist in biocolloid and colloid transport, including: attachment, detachment, dispersion, advection, straining, etc. It is important to determine whether, and how, biocolloids and colloids are retained in rock fractures during the transport process. Since most research on biocolloid and colloid transport in groundwater to date has focused on unconsolidated porous media, it is important to initiate research in rock fractures.

The objective of this work is to improve the understanding of biocolloid transport in fractured rocks, and to compare this with colloid transport. Specifically, this research was designed to determine the effects of flow rate and aperture field characteristics on colloid and biocolloid retention in fractured rock. This research employed lab-scale experiments in three natural fractures and three transparent fracture replicas. Two of these replicas are of real fractures employed in these experiments. Experiments were conducted under a range of specific discharges, and with both colloid and microbial tracers.

This thesis contains four additional chapters: Chapter 2 offers a general review of microbial transport in subsurface environments, Chapter 3 describes the experimental methods employed in this work, Chapter 4 presents the results and discussion, and Chapter 5 gives the conclusion reached from this work.

2. Literature Review

Microorganisms present in fractures have the ability to degrade many contaminants through biochemical reactions; this can be demonstrated through measuring the concentration of various contaminants at upstream and downstream locations. Microorganisms have different effects in groundwater, such as posing a potential hazard, or by attenuating chemical contaminants (Mclinn & Rehm, 1997). Microorganisms may move through the subsurface environment faster than conservative tracers, the properties of their communities influence the transport behaviour.

2.1 Biodegradation in Fractures

Chemical concentrations reveal the degree of degradation occurring in fractures. For example, the role of fractured dolomite in the degradation of petroleum contaminants was studied in a field experiment conducted by Mclinn and Rehm (1997). The carbon dioxide present in the pore gas increased, while the oxygen decreased, when an aerobically degrading petroleum was released nearby. In this process, the quantity of oxygen used depends on the specific organic chemical being consumed. Therefore, it is possible to analyze the state of degradation of the organic contaminant by monitoring the oxygen concentration. The investigators also found that the lowest concentration of oxygen corresponded to the highest gasoline concentration; demonstrating that the degradation of petroleum in this fracture is aerobic, with no other source of organic

carbon in the field. At the same time, the level of carbon dioxide, which is a by-product of aerobic degradation, was highest where the gasoline concentration was highest. Thus it can be concluded that the petroleum was removed by aerobic degradation from naturally conducted chemical reactions.

2.2 The Role of Microorganisms as Biobarriers in Fractures

2.2.1 Bioclogging

Numerous experiments have demonstrated that the clogging of pores in unconsolidated media and apertures in fractured media results in decreased values of hydraulic conductivity (K) (Ross *et al.*, 2002). For example, when injecting microorganisms into a core system model, K decreased significantly after a period of time (Shaw *et al.*, 1985). The biofilm presented the properties of continuously sorbing metals attaching bacteria, even under variable exterior environmental conditions, such as few nutrients or chemical injections (Cunningham *et al.*, 1997). In the experiment conducted by Cunningham *et al.* (1997) in synthetic glass parallel plate fractures, 140 hours after the injection of microorganisms, while continuously providing oxygen and nutrients, K decreased by two orders of magnitude in a sigmoid pattern. Such variation originated from the disturbance of biofilms at the inlet of the fractures, and can be observed from the pressure variation between the start and the end of the experiment, while the hydraulic aperture decreased sharply. The observed flow rate decreased significantly during the test under constant head conditions. An experiment conducted in porous media revealed a

similar phenomenon, including the magnitude and time required to decrease K (Vandevivere & Baveye, 1992). A similar experiment conducted by Vandevivere and Baveye (1992) revealed that the reduction of K in porous media was larger than that in fractures.

The degree of clogging in limestone fractures can be determined through monitoring the variation of hydraulic conductivity (K). Microorganisms that form biofilms are injected into fractures, forming biobarriers in fractured rocks (Ross *et al.*, 2001). These biobarriers are formed by extracellular polymeric substances (EPS) secreted by bacteria, and their ability to contain groundwater through acting as a barrier, or to treat contaminants through biodegradation are utilized to control contaminant transport in groundwater. The extent of bioclogging is influenced by the microorganisms present, and the chemical composition of both the rocks and the groundwater. Biofilm formation is different in fractured and porous media, since there is higher fluid shear stress in porous media (Ross *et al.*, 2001).

2.2.2 The Influence of Bioclogging

The influence of biobarriers can be analysed by comparing results prior to biostimulation and after. The injection of nutrients contained in groundwater and fractures will greatly affect the microorganisms' subsistence, and hence have an effect on biofilm structure, EPS composition, and bioclogging. Ross *et al.* (1998) designed experiments to analyse the microbes' growth after biostimulation in various physicochemical conditions,

and their ability to form biomass, EPS, and biofilm. The authors attributed the growth of microorganisms to the inorganic salt, amino acids, and divalent ions present in the nutrient injections; these constituents increased the interactions between the microbes and media surfaces.

Bioclogging also influences solute transport. Generally, transport in fractures is influenced by Taylorian dispersion and macrodispersion, due to different solute velocity and various fracture apertures (Hill & Sleep, 2002). However, after a biofilm formed, the apertures decrease, which results in an exponential increase in macrodispersion. This increase showed that bioclogging can have a significant influence on subsurface environments and contaminant transport (Hill & Sleep, 2002).

The influence of biofilms on groundwater flow were analysed in an experiment that consisted of a glass parallel plate fracture (Hill & Sleep, 2002). Microorganisms were inoculated with nutrients and oxygen supplied to the system, and biofilms were formed over a period of time. This revealed that flow channels and low permeability zones formed within the fracture. Both the hydraulic conductivity and the friction loss aperture were observed to decrease sharply, while the mass balance aperture did not change significantly, revealing that it was not greatly influenced in the effective porosity of the fracture.

In another experiment conducted by Hill & Sleep (2002), with the growth of a

microorganism cluster, a low permeability zone was formed in the centre of the fracture. This observation suggested that little horizontal mixing, transverse to the flow direction, occurred. In the experiment, the flow path was more tortuous than previous experiments in the same fracture due to the growth of the biofilms. In this case, the velocity profile was not parabolic, but varied across the width of the fracture with the flow channels and low permeability zones. Similar breakthrough curves from three different tracer experiments suggested that advection in low permeability zones was more important to solute transport, than mass transfer between the velocity channels (Hill & Sleep, 2002).

2.3. Microbial Transport through Soil and Fractures

2.3.1 *E. coli* Characteristics

E. coli is a gram-negative, facultatively anaerobic, rod-shaped bacteria in a range of 2.0–6.0 μm (Bergey *et al.*, 1984). *E. coli* has a negative surface charge and a relatively low die-off or inactivation rate coefficient. It can travel long distances in subsurface environment and thus be a useful indicator of contamination of groundwater (Foppen, 2006). The inactivation or die-off of *E. coli* is affected by multiple factors, such as the bacterial strain, temperature, predation, antagonism, light, soil type, pH, toxic substances, and dissolved oxygen. Generally, after *E. coli* groups are introduced into water environments, they gradually die off, accompanied by changes in their characteristics.

E. coli is the preferred indicator of fecal contaminants, due to its relatively simple, fast, and reliable detection properties. It is the only member of the thermotolerant coliform group found in feces of warm-blooded animals and the amount is far more than other thermotolerant coliforms in both human and animal excreta (Medema *et al.*, 2003).

Bacterial attachment behaviour is affected by cell surface charge, hydrophobicity, size, and the presence of particular bacterial structures such as flagella, fimbriae, and extracellular lipopolysaccharides (LPSs) (Gilbert *et al.*, 1991). *E. coli* is hydrophilic more than hydrophobic. As noted by Gilbert *et al.* (1991), for relatively hydrophilic organisms such as *E. coli*, the hydrophobicity did not dominate the adhesion process. Instead, the

primary controller of adhesion appeared to be the zeta potential. For example, cell surface charge is not measured directly, but can be determined via the electrophoretic mobility, which reflects the zeta potential (defined as the potential drop across the mobile part of the double layer that is responsible for electrokinetic phenomena (Stumm and Morgan, 1996).

However, zeta potential has two shortcomings in characterizing the interaction between *E. coli* and medium surfaces (DeKerchove and Elimelech, 2005). It typically applies to hard spherical particles, whereas biological cells are of soft ion-permeable layers consisting of charged and non-charged LPS structures around the cell. Zeta potential is a macroscopic scaled parameter that is not sensitive to small scaled variations in the cell surface. Therefore, the zeta potential value alone cannot reflect the distribution of charges, which might result in an erroneous understanding of interactions between *E. coli* and the medium surface.

2.3.2 Transport Mechanisms

Laboratory and field experiments have demonstrated that the transport velocity of microbes is greater than that of chemical tracers such as chloride and bromide (Harvey *et al.*, 1989). Experiments indicated that transport mechanisms may include physical, geochemical and biological processes. Physical processes include advection and hydrodynamic dispersion. Microorganisms transport by advection traveled with the bulk water flow. Hydrodynamic dispersion is the spreading of microorganisms from both microscopic and macroscopic effects, which can be measured by concentration and travel time. Molecular diffusion, mechanical mixing, and the mobility of the microbes themselves are also involved in dispersion (Yates and Yates, 1990). In turn, dispersion causes dilution and attenuation in the contaminant concentration. However, the effect of diffusion is considered negligible compared to mechanical mixing in bacterial transport, whereas it is still important for small-sized viruses. For mechanical mixing, there are mainly three processes: fluid velocity distribution in pore spaces, variations in pore velocities for different sizes and roughnesses, and convergence and divergence for pore channels, which all result in mixing.

Geochemical processes, including filtration, adsorption/desorption, and sedimentation, usually hinder microbe transport (McDowell-Boyer *et al.*, 1986). Filtration occurs when the particles are too large to penetrate soil, so they accumulate on the soil surface, further reducing soil permeability. Physico-chemical filtration occurs according to the ratio of particle to soil grain size. Most researchers believe that the effect of

filtration is negligible on virus movement, while its effect on bacteria is not clear yet (McDowell-Boyer *et al.*, 1986). Adsorption is the process of collecting particles on the interface in aqueous suspension, which plays an important role in removing microbes, and especially small viruses in soil (Gerba *et al.* 1975). The process of adsorption is reversible, though this is influenced by temperature, pH, ion concentration in the surrounding environment, configuration of soil, and type of microbes involved. Sedimentation is gravity's effect on particles deposition. This effect might be overestimated because the microorganisms are too small and neutrally buoyant to settle, so sedimentation only impacts large particles (>5μm), with efficiency being proportional to particle size.

Biological processes of growth and survival also affect transport mechanisms because they affect the microorganisms concentrations. Transport is also controlled by the intrinsic characteristics of microorganisms, such as type, size, and surface properties. In an experiment conducted by Gannon *et al.* (1991), researchers found that some cells were low in recovery because of strong attachment to soil. Bacteria motility also influences transport, for example, some microorganisms move towards nutrients, which brings about transport. Harvey (1989) indicated that transport speed due to chemotaxis can be faster than that due to Brownian motion.

Aside from above three processes, the transport of microorganisms through the vadose zone is influenced by infiltration rates, dispersive mixing, and the processes that affect microbial mobilization (Saiers, 2006). Torkzaban *et al.* (2006) focused on microbial

deposition and release from interfaces, and they found that the attachment to interfaces dominate the deposition of experimental bacteriophages (MS2 and ΦX174). Also, the sensitivity to pH showed that electrostatic interactions have a larger influence on attachment than hydrophobic interactions, and advection is an important contributor to microbial transport.

However, Bradford *et al.* (2006) showed that biocolloid transport is influenced by straining. They conducted pore-scale experiments and reflected *E. coli* was retained by straining, which occurred when colloids were trapped in small pore spaces. Experiments also demonstrated that straining is influenced by specific discharge and grain texture. Auset and Keller (2006) demonstrated that straining mainly caused colloid retention with rough surface media. Bradford *et al.* (2006) hypothesized that once biocolloids accumulated to sufficient sizes, shear forces disrupted them, and resulted in release and down-gradient transport.

Tufenkji (2006) found that bacterial deposition is controlled by a broad rate of distribution rather than by only one discrete rate. She hypothesized that those distributions are due to charge heterogeneity originating from various bacterial cell surface properties. Cortis *et al.* (2006) also demonstrated from the modeling and experimental data that physicochemical heterogeneity governs the microbial mobility.

2.3.3 Factors that Influence Microbial Transport

Many factors have been demonstrated to affect the survival and transport mechanisms of microorganisms in groundwater. They are mainly interactions between soil, water, microorganisms, and the surrounding environment. Factors affecting the survival may include the physiological state of the microorganism, the physical and chemical nature of the groundwater, atmospheric conditions, and biological interactions. Factors affecting the movement of microbes may include the physical characteristics of the soil, the soil environment, chemical factors, and microbial properties.

Celico (2004) conducted field (spring water monitoring) and laboratory (column tests with soil blocks) scale experiments to determine the distribution of precipitation versus time, and bacteria migration in soil breakthrough curves, and provided convincing evidence for controlling local groundwater contamination. In the field experiment, precipitation events were characterized by rainy intervals and provided breakthrough curves, while column tests simulated pulse infiltration, which caused breakthroughs characterized by different concentrations of bacteria. Celico found that pulse infiltration produced variation in quantities of microorganisms versus time, which brought about a discrete bacteria transport. This corresponds to the field-scale condition, in which rainy intervals acted as pulse infiltration, and the bacteria were then transported through the unsaturated zones intermittently. In the experiment, soil block heterogeneities did not influence the breakthrough, so the results obtained could be generally extended.

Lehman *et al.* (2001) conducted a series of experiments in both packed columns

and fractures to analyze the influence of different hydrogeologic conditions. In the packed columns, about 99% of the total biomass was attached to the medium, which was identical to the phenomenon found in field analysis of unconsolidated, sedimentary aquifers. It was observed by Lehman *et al.* (2001) that medium type could impact the categories and population of microorganisms attached, which influenced the transport. Differences in microorganism communities could be observed by the growth of aerobic heterotrophs from the groundwater but not from the substrate medium, and there were also differences in the carbon source usage patterns. In the hydrogeology scale, the numbers of aerobic heterotrophs and phenol oxidizers, which were used as comparable tracers in the experiment, were similar in the effluent, but the attached communities in fractures were larger than those in packed columns.

Experiments conducted by Mailloux (2003) showed that the velocity of bacteria and bromide plumes were correlated to the hydraulic conductivity of the medium. The plumes followed the higher permeability zone, but were not correlated with the hydraulic gradient. The bacterial breakthrough was found not to be related to the permeability of the layers. This proved that heterogeneity in both the vertical and horizontal directions impact the first moment of injected tracers as well as the direction of plume movement. The fastest arrival times (or lowest first moments) were observed in zones of higher hydraulic conductivity. A plume movement off the main flow pathway was also observed. This was not caused by gradient, but by heterogeneity. Direction was controlled by areas of high hydraulic conductivity. Even after traveling a small distance, there are large differences in

attachment in different grain-sized zones. Variations of sorbed profiles were also found in various grain-sized zones, which indicates that physical heterogeneity is an important factor influencing attachment.

The protist *Spumella guttula* was used as the tracer in transport experiments by Harvey (2002). Low-nutrient, porous media-grown *S. guttula* was compared to traditional high-nutrient broth-grown protists. About one-third of porous medium-grown protists were transported at least 2.8 m, compared with only 2% of the broth-grown ones. It was also found that a staining procedure resulted in much less attachment and more transport of *S. guttula* than a staining-and-fixation procedure. The experiments showed that attachment is not correlated to pH (over the pH range of 3 to 9), which is different from prey bacteria, revealing that there is a different attachment mechanism. The way that protists grew affected their transport behavior. Smaller (2 to 3 μm) porous medium-grown protists ones moved farther than larger (4 to 5μm) broth-grown ones, and the transport phenomena of the smaller ones were more similar to a conservative tracer (bromide) and microspheres of similar sizes than to the larger potists. For bacteria, cell size, motility, and hydrophobicity can be affected by nutrients prior to injection into the subsurface. For nanoflagellate transport, culturing methods and procedures affecting size, density, and surface characteristics are all important factors.

2.3.4 Microbial and Conservative Tracer Tests, and the Comparison

Experiments conducted by Smith *et al.* (1985) showed that microorganisms were found to move faster than conservative tracers, which the author attributed to the continuous macropore media. Many other experiments showed the same results, showing that microorganisms are carried by preferential flow through macropores, cracks, fractures, and channels formed by plant roots or animals, which brings about their fast movement.

In the lab scale experiments conducted by Zvikelsky and Weisbrod (2006), small sized colloids (0.02 μm latex microspheres) were most easily retained by the fracture cores. The maximum breakthrough concentration in colloids was larger than that of dissolved conservative tracers. The colloid breakthrough curves lacked tailing, suggesting smaller exchanges between fracture and matrix than that of solutes. They also pointed out that colloid size and the medium's properties (such as fracture aperture width and matrix permeability) would influence colloid transport.

Since contaminants can bind to colloids, colloids transport may worse contamination situations. Pang and Simunek (2006) conducted laboratory experiments of cadmium with bacteria transport in gravels, and found cadmium adsorption to the bacteria depended on type and mobilization of bacteria.

In the experiments conducted by McKay *et al.* (1993), the setup included source

tank located in the centre and two collector tanks with the intervals of 6.2 m and 4 m respectively. Phage concentration in the injection tank did not change significantly, which was consistent with phage survival experiments, while the concentration in the source tank declined greatly due to the microorganisms' inactivation and attachment to the medium. The phage in the nearer collector tank showed significant attenuation of the initial concentration, while the concentration is out of the detection limit in the tank that is 6.2 m away from the source. The great decrease in the nearer tank was believed to be due to phage attachment to the fractures surfaces and its limited diffusion into large pores.

In tracer experiments that study attachment, diffusion, and flow velocity (Hinsby *et al.*, 1996), colloid sized bacteriophage (PRD-1 with larger diameter and MS-2 with smaller diameter), carboxylated latex, and chloride were employed as tracers. The results showed rapid initial breakthrough in both experiments, indicating that flow rates in fractures with large apertures had similar velocities, which contributed to microorganism transport. The sharp curves showed that little dispersion existed in the transport processes. Concentration in steady state is much smaller than injection concentration, which is likely due to the filtration and electrostatic or hydrophobic attraction processes. This result is identical to observations in previous experiments. Since no additional fractures have an impact on discharge of the bacteriophage after reaching steady state, the time used to obtain steady state could indicate the range of groundwater velocity.

Bacteria and microsphere tracer experiments were conducted in a field-scale

fractured bedrock to investigate colloid behaviour in transport; most of the colloids presented different breakthrough curves (Becker *et al.*, 2003). The results indicate that minor differences in the physical properties of bacteria may cause major differences in transport. It was found that bacteria and microspheres both had poor recoveries, indicating that they were heavily removed in the system (Becker *et al.*, 2003). Coccus (ML3) bacteria arrived slightly earlier than deuterated water, which means that there was enhanced transport compared to the solute tracer, which may be attributable to hydrodynamic chromatography and hydrodynamic dispersion. Gram-positive rod bacteria (ML1) appeared to be more retained than nonmotile Gram-negative rod bacteria (ML2m), so Gram staining could be an indicator for interactions between bacteria and fracture surface under certain conditions (Becker *et al.*, 2003). Gram positive cocci were observed to transport farther than Gram positive rod bacteria, which indicated that spheroid shapes may reduce attachment. The reason may be that rod shapes have a greater cell surface area available for contact to medium surface compared to spheric ones of the same length. Additionally, rod-shaped bacteria may overcome electrostatic repulsion better between approaching particles and medium surface. However, cell shape would not influence the straining of bacteria if the aperture size was larger than 5 μm. In addition, it is uncertain that cell shape would have a significant impact, since it is impossible to separate cell shape from cell size, and typically cell size is more important. When the cell size is the only variable, smaller particles are recovered more efficiently. No identical breakthrough curves can be found, and microspheres appeared very different from bacteria. Larger bacteria motility seemed to delay transport, and motile bacteria experienced more

diffusion than nonmotile ones in the same sizes and shapes. In theory, colloids with high diffusion rates may be highly removed when other factors are equal. In addition, motile strains are more likely to travel to stagnant water, at which point the transport is delayed or ceased. Stagnant water typically occurs adjacent to mobile water in fractures, with diffusion between mobile and immobile water, resulting in delay in particle transport.

Generally, solute tracer transport in a fractured fine porous medium would be retarded by diffusion into the porous matrix (McKay *et al.*, 1993). However, since the flow velocity is difficult to measure, the degree of retardation is difficult to determine. In contrast, colloid particles do not retard significantly due to their larger size, which prevents them from diffusing into the porous matrix. As a result, colloid transport velocity can be measured as the lower limit of flow velocity. Phage size is small relative to the hydraulically determined equivalent fracture aperture, so the concentration during transport may vary significantly and it may reach velocities similar to that of the flow in the fracture. Different properties of microorganisms also cause differences in behaviour during transport, and hydrophobic phage is harder to adsorb, while hydrophilic phage sorbs more easily, and is therefore more retarded in groundwater environments.

3 Materials and Methods

Experiments to investigate biocolloid and colloid transport through fractures were designed. The goal of these experiments was to measure the biocolloid concentration differences between the upstream and downstream ends of the fracture, in order to evaluate the role of fractures in retaining colloids and biocolloids. Three fractures were employed in these laboratory-scale experiments. Hydraulic and solute tracer tests were conducted to characterize the aperture fields, in order to evaluate the effect of aperture field variability on the retention of biocolloids.

3.1 Fractures Setup

The fractures employed in these experiments were those collected, prepared, and employed by Zheng (2008), Sekerak (2004), and Dickson (2001). Two granite rock samples, from the Zheng (2008) and Sekerak (2004) experiments, were removed from an outcrop beside Highway 118, just west of Carnarvon, Ontario. A dolomitic limestone fracture, prepared by Dickson (2001), was collected from an outcrop located in Kingston, Ontario. These outcrops were chosen due to the presence of prominent stylolites and bedding planes, which provided convenient planes of weakness for inducing fractures in the lab. The rocks were cut into cube shapes and the surfaces were ground smooth. Shallow saw cuts were made along the length of the sample, perpendicular to the plane of weakness, to stabilize metal triangular bars along the plane of weakness. Carbon fiber

reinforced polymer (CFRP) (Fyfe Company: Tyfo SCH-35) was applied to the surface of each sample to reinforce it in all planes, except that of the weakness. The triangular bars transferred the load, applied by a uniaxial compression machine, directly on to the plane of weakness. Metal banding was wrapped perpendicular to the plane of weakness, prior to the applied loads, to ensure that the sample remained intact upon fracturing. This methodology is similar to the natural formation of fractures by compression or stress relief. Further details regarding the collection and preparation of those fractures are available in Dickson (2001).

Figure 3-1 shows a schematic fracture prepared for the experiments. Figure 3-2 and 3-3 show schematic and photographic representations of the experimental apparatus respectively. The longitudinal sides of the samples were then sealed as no-flow boundaries using silicone (GE Silicone Window and Door), and 1 cm thick plexiglass caps were employed to create flow cells on both the upstream and downstream ends of the fracture.

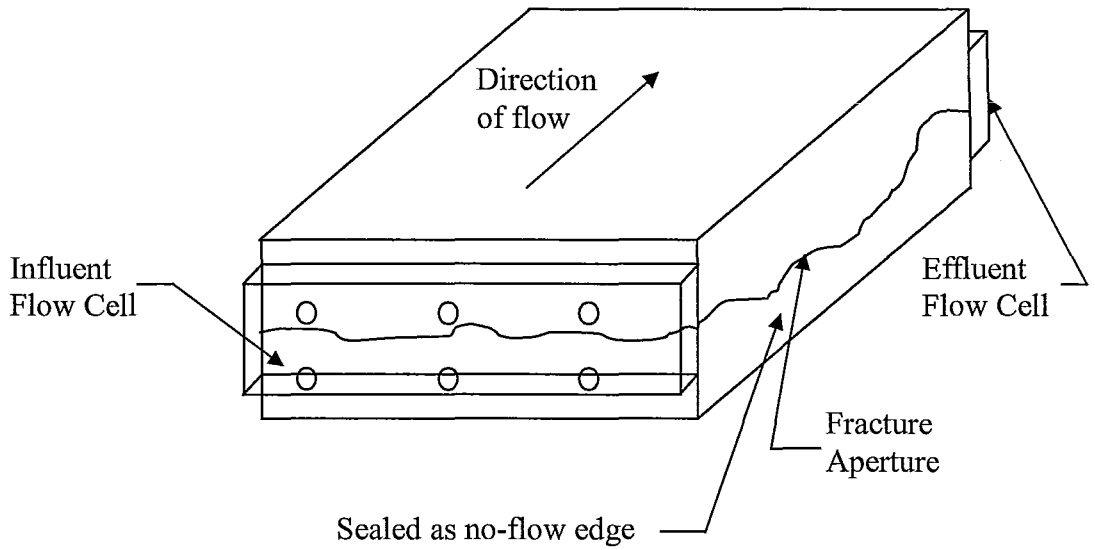

Figure 3-1. Schematic diagram of a fracture prepared for experimentation.

Six 5-mm holes were drilled on each flow cell. The upper center hole on the upstream flow cell was equipped with a Swagelock fitting through which the influent water was pumped. An upper hole on the downstream flow cell was equipped with a Swagelock fitting through which the effluent could exit. A recirculation system was set up on each flow cell by threading Teflon tubing (Tygon clear R3603) through two holes, located diagonally across each flow cell (Figure 3-2). The Teflon tubing was perforated every 2 mm along its length. A glass vial (Chromatographic Specialties Inc. C223710C) was fitted with spigots, hole caps and teflon-backed septa (Chromatographic Specialties Inc. C242C), and connected to either end of the Teflon tubing using pump tubing (MasterFlex 06404-14) to form a closed loop. These vials were employed as sampling

and injection ports. A pump (MasterFlex L/S 7523-70) was located on the pump tubing, which served to recirculate the entire volume of the flow cells, sampling/injection vial, and recirculation tubing. The remaining holes in the flow cell were sealed with Swagelock fittings and tubing (Nalgene 380 PVC), and sealed with clamps. Prior to running any experiments, trial experiments were conducted to ensure the system was leak-free.

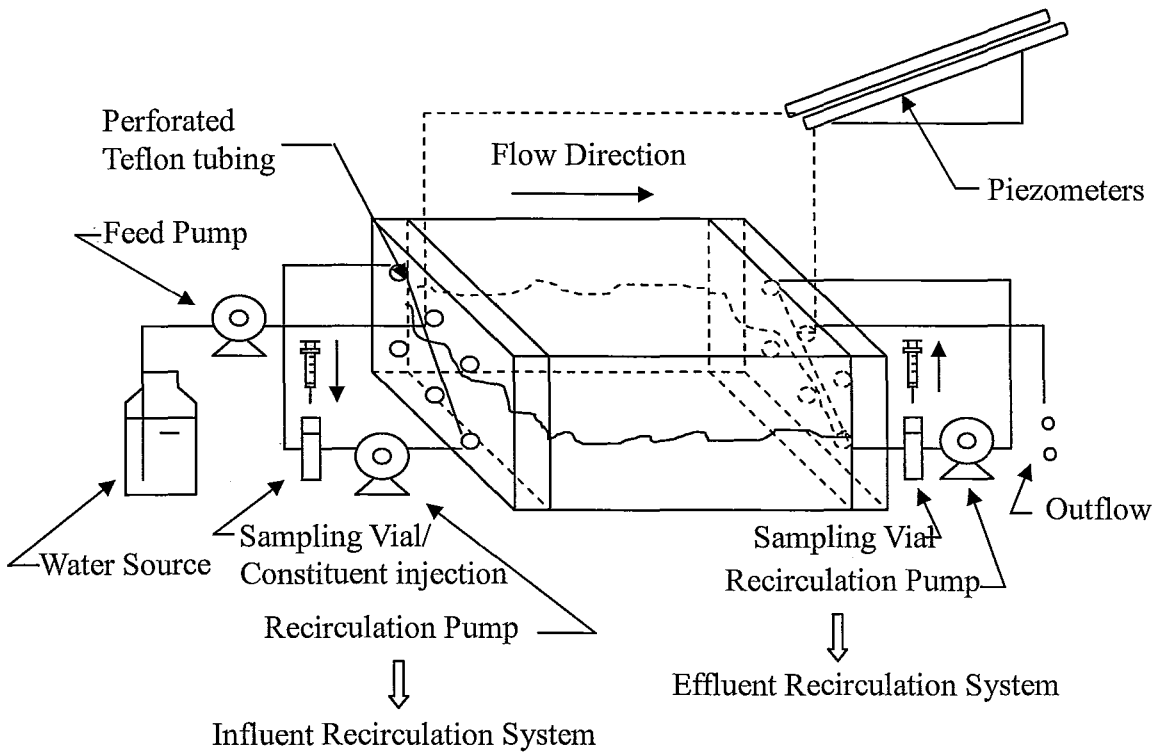

Figure 3-2. Schematic diagram of the experimental apparatus.

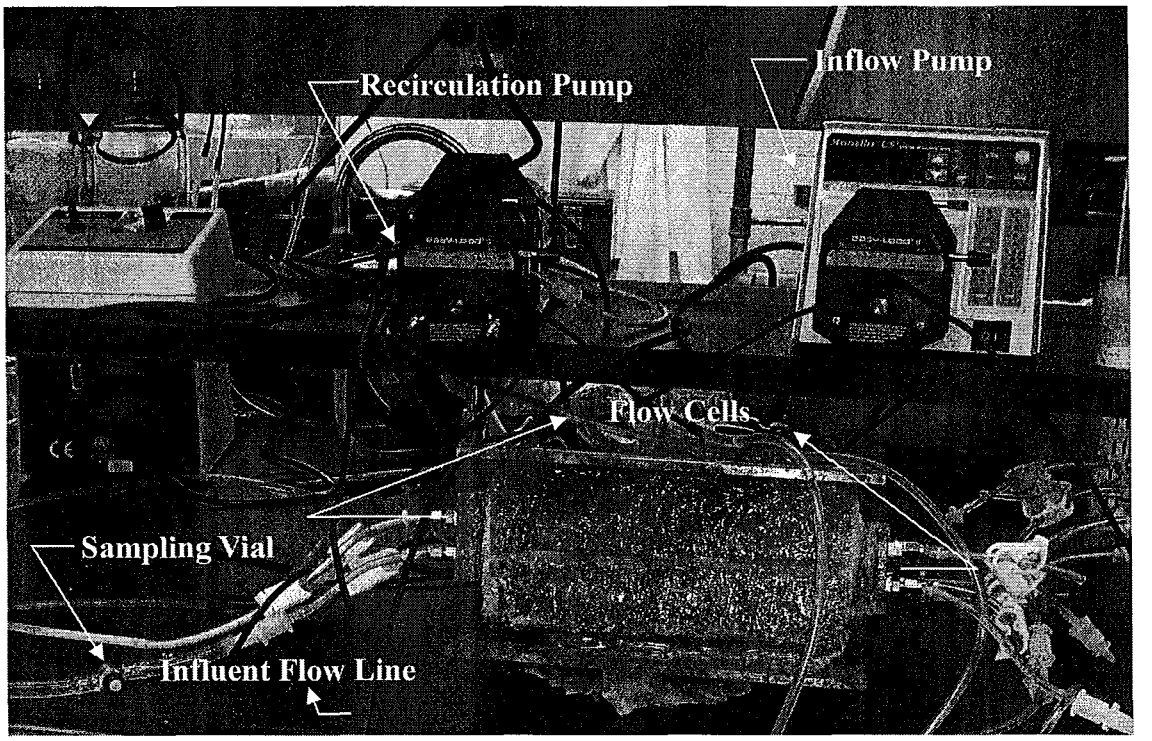

Figure 3-3. Photograph of the experimental apparatus.

Fracture Plane Saturation

The water employed in all of these experiments was specially prepared as follows. Milli-Q water was adjusted to a pH of approximately 8 to prevent carbonate compounds in the rock from dissolving into the water passing through the fracture. The water was also degassed by bubbling helium through it. This prevented the possibility of any gas coming out of solution, due to temperature changes in the lab, within the fracture plane, as the goal of these experiments is to investigate colloid and biocolloid transport in fully saturated environments. Prior to pumping, carbon dioxide was run through each fracture for approximately 10 minutes. Carbon dioxide is much more soluble in water than air is, and therefore this step ensured that no gas pockets were remained in the fracture upon

saturation. The buffered, deionized, degassed water (DDW) was then pumped through the fracture overnight (about 16-18 hours) prior to conducting any hydraulic or tracer experiments.

3.2 Hydraulic Tests

Hydraulic tests were conducted, under a range of flow rates, to determine the equivalent hydraulic aperture. Buffered DDW was pumped through the water-saturated fracture under a constant flow rate. Both the flow rate and head loss were measured for each hydraulic test. The flow rate was determined by measuring the volume of water exiting the fracture over a specified time interval. An inclined piezometer was employed to measure the head loss between upstream and downstream flow cells (i.e., across the fracture plane). Two parallel inclined glass tubes, with a 1 cm diameter and approximately 50 cm in length, were set on a stand at angles of approximately 17, 35, and 17 degrees for F1, F2, and F3 respectively (Figure 3-2). One glass tube was connected to the upstream flow cell with flexible tubing, and the other was connected to the downstream flow cell in the same manner. Hydraulic tests were conducted only after the piezometer readings became steady at the specified flow rate. The difference between the water surface elevations in the upstream and downstream piezometers was measured using a ruler with 1 mm graduations. The length and angles of the inclined tubes were measured to calculate the hydraulic head loss using trigonometry. Hydraulic tests were conducted on each fracture under a number of different flow rates (0.06-0.1 mL/s), and the measuring of each flow rate was repeated three times to ensure repeatability.

3.3 Solute Tracer Tests

Solute tracer tests were conducted to measure the equivalent mass balance and frictional loss apertures. Bromide, in the form of sodium bromide, was selected as the tracer for these experiments, due to its conservative properties and the fact that it is easy to quantify.

Prior to conducting any solute tracer tests, the fracture was saturated according to the method described in Section 3.1. Dye tests were also conducted prior to the solute tracer tests to determine the mixing time required in the upstream flow cell. The feed pump was turned off, leaving only the recirculation pump running, and 0.3 mL of dye (Acid Red 052, Spectra Colors Corp.) was injected into the sampling vial located in the upstream recirculation system. The time required for the entire volume of the upstream flow cell to reach a uniform color was recorded. These dye tests were conducted on the influent recirculation systems of all three fractures.

Buffered DDW was pumped through the saturated fractures overnight before the solute tracer tests were conducted. 0.3 mL of 10 g/L NaBr was injected into the upstream recirculation sampling vial, and the recirculation pump was run with the feed pump off for the time required to fully mix the influent flow cell and recirculation system. The feed pump was then turned on, pumping buffered DDW through the fracture.

Background water samples were taken prior to the start of these experiments to

quantify any residual bromide remaining in the fracture from previous solute tracer experiments. Samples were withdrawn from the downstream sampling vial at strategic time intervals throughout each experiment (i.e. dense sampling in the beginning of the experiment to capture the peak, and more sparse sampling over time to capture the tail). Sampling was ceased once the bromide concentration fell below the method detection limit (MDL) of the HPLC. At each sampling event, approximately 2 mL of sample was withdrawn from the downstream sampling vial with a disposable plastic syringe (BD, 309585), and injected into an HPLC analysis vial (Chromatographic Specialties Inc. C223700C). Since the upstream and downstream recirculation pumps were running throughout each test, the bromide concentration in the sampling vial was representative of the flow cell and recirculation system together.

Each Tracer test was conducted several times at the same flow rate to ensure that the whole breakthrough curve was captured, and that the experiment was repeatable. Mass balance calculations were conducted on the mass of bromide injected for quality assurance purposes.

3.4 *E. coli* RS-2GFP Tracer Tests

The Environmental Systems laboratory is a level 1 biohazard lab, and therefore pathogens are not permissible. *Escherichia coli* RS-2GFP was selected as a suitable biocolloid surrogate for *E. coli* O157: H7. It is a non-toxic, non-pathogenic and non-hazardous bacterial strain previously employed in experiments conducted by Saini *et al.* (2001, 2003). It is resistant to the antibiotics kanamycin and rifampicin. This strain is a derivant of RS-1; the green fluorescent protein (*gfp*) expressed gene enables the bacteria to express green fluorescent protein, and the protein excitation is optimal under ultraviolet light (365 nm) or at 488 nm; emission optimum is 510 nm and hence the green fluorescence. The *E. coli* RS-2GFP was obtained from the Emelko Laboratory in the Department of Civil Engineering at the University of Waterloo. The Waterloo culture originated from Dr. Larry Halverson from the Department of Agriculture and Biosystems Engineering at Iowa State University, Ames, IA, USA.

Prior to commencing the *E. coli* RS-2GFP tracer tests, the fracture plane was saturated according to the method described in Section 3.5.2. One percent phosphate buffered saline (PBS) solution was then run through the fractures overnight to remove any residual constituents from previous experiments. In order to establish the appropriate *E. coli* RS-2GFP concentration in the influent flow cell, the feed pump was stopped, and 3 mL of approximately 10E08 CFU/mL *E. coli* RS-2GFP suspension was injected into the upstream sampling vial. The recirculation pump was turned on for the requisite amount of time, established by the dye tests, required to fully mix the influent flow cell. At this time,

the feed pump was turned on marking the beginning of the experiment (t=0). A background sample was drawn from the downstream sampling vial at t=0.

Samples were drawn from the downstream sampling vial using a 3 mL syringe (BD, 309585), and diluted in a series of test tubes with 1% PBS for subsequent analysis according to the method described in Section 3.5.2. Samples were collected frequently at the beginning each experiment to ensure that the peak concentration was captured, and less and less frequently as the experiment progressed and the *E. coli* RS-2GFP concentration began to tail. Sampling was ceased when the *E. coli* RS-2GFP was predicted to be below the detectable limit based on the solute tracer tests. Each *E. coli* RS-2GFP experiment was repeated under the same conditions at least three times to ensure repeatability.

3.5 Analytical Techniques

3.5.1 Equipment List

HPLC

High-performance liquid chromatography (HPLC) (Varian ProStar 330) was used to quantify the bromide in the samples from the solute tracer tests. The equipment contained an auto sampler (Varian, 410), a solvent delivery module (Varian, 230), and a conductivity detector (Dionex, CD25). A guard column (Dionex AG12A) and a 4 x 200 mm column (Dionex, AS12A) with an anion suppressor (Dionex, AMMSIII 4mm) were employed.

Autoclave

The autoclave was Hirayama Hiclave HV-50. It was employed at 121 °C for 20 min; the total sterilization process was approximately 2 hours long.

Spectrophotometer

A spectrophotometer (Beckman Coulter DU 530) was employed to test the optical density of the *E. coli* RS-2GFP culture. The blank and bacterial suspensions were prepared in the same medium, and analyzed at 520 nm.

Centrifuge

The centrifuge (Beckman Coulter Allegra 25R) was set at 8500 rpm, resulting in a

force of 5000 g, and run for 10 minutes to centrifugate the *E. coli* RS-2GFP culture.

Incubator

The incubator (VWR 1575R) temperature was set to 37 °C, and a rotational speed of 180 RPM to grow the *E. coli* RS-2GFP culture.

Counters

A colony counter (Stuart SC6) was employed to count *E. coli* RS-2GFP colonies precisely.

3.5.2 Reagent List

PBS Stock Solution

A 10% PBS solution was employed to serially dilute effluent *E. coli* RS-2GFP samples in a series of test tubes and to saturate the experimental fracture planes prior to the *E. coli* RS-2GFP tracer experiments. The recipe for the PBS solution is as follows:

- Sodium Chloride (NaCl), 80.0 g
- Potassium Chloride (KCl), 2.0 g
- Sodium Phosphate (Na_2HPO_4), 14.4 g
- Potassium Dihydrogen Phosphate (KH_2PO_4), 2.4 g
- Milli-Q water, 1L

The pH of this solution was adjusted to 7.4 using NaOH. The PBS solution was prepared and stored in plastic bottles. Dilutions were prepared as required.

Antibiotics

The antibiotics were prepared as follows:

- Kanamycin: 1 g of kanamycim was added to 100 mL of DDW, filter sterilized through a 0.22 μm filter, and dispensed into 5 mL bottles. It was stored at -80 °C.

- Rifampicin: 0.1 g of Rifampicin was added to 100 mL of methanol, and stored in an amber bottle, at 4 °C.

Broth

The broth was prepared in an Erlenmeyer flask using the following recipe:

- HiVeg Hydrolysate (HIMEDIA RM030v-500G), 10 g

- Yeast Extract (Bacto BD 212750), 5 g

- Sodium Chloride (NaCl), 10 g

- Milli-Q water, 1L

After autoclaving and cooling, 10 mL of each Kanamycin and Rifampicin were added to 1 L of broth.

Luria-Bertani (LB) Agar

Luria-Bertani agar was prepared using the following recipe:

- HiVeg Lysate, 10 g

- Yeast Extract, 5 g

- Sodium Chloride (NaCl), 10 g

- Agar (Bioshop AGR003.500), 15 g

- Milli-Q water, 1L

These ingredients for the LB agar were combined and slowly warmed on a stirred hotplate, until entirely dissolved. Once the agar had been autoclaved and cooled to approximately 65 °C, the two antibiotics were added as 10 mL each into per 1 L broth and mixed until uniform. Approximately 10 mL of agar was poured into pre-sterilized disposable plastic petri-dishes (FisherBrand P-D), distributed evenly across the dish surface, and allowed to cool. The plates were stored in a plastic sleeve, sealed with tape, dated, and placed in the refrigerator at 4 °C. Prior to use, the plates were dried by bringing them to room temperature.

Eluent

The eluent solution for the HPLC was comprised of 0.3 mM $NaHCO_3$ and 2.7mM Na_2CO_3; the two components' stocks were prepared as follows:

$NaHCO_3$ stock:

- Sodium Biocarbonate ($NaHCO_3$), 10.5g

- Milli-Q water, 250 mL

Na_2CO_3 stock:

- Sodium Carbonate (Na_2CO_3), 26.5g

- Milli-Q water, 250 mL

The eluent recipe was then prepared by adding 0.6 mL of the $NaHCO_3$ stock and 2.7 mL of the Na_2CO_3 stock to 1 L of Milli-Q water.

Regenerant

The regenerant for the chemical suppressor was a 12.5 mM H_2SO_4 solution; the recipe is as follows:

- Sulfuric Acid (H_2SO_4), 2.8 mL
- Milli-Q water, 4 L

3.5.3 Bromide Quantification

The HPLC was employed for Br^- quantification, according to Method 300.1 (Hautman *et al*, 1997). The electrical conductivity was set at approximately 14-20 μs, the regenerant was set at 2 mL/min, which originated from setting the gas pressure at 5 psi, and the eluent flow rate was 1 cm/min. A 10 g/L NaBr solution was diluted with Milli-Q water to prepare the standards according to the technique described by Standard Method 1020B (APHA *et al.* 2006). The standard concentrations prepared were 50 mg/L, 20 mg/L, 10 mg/L, 5 mg/L, and 1 mg/L. The standards were analyzed and a standard curve was prepared prior to the analysis of the samples. If the coefficient of determination (R^2) for the standard curve was larger than 0.995, the standard curve was deemed acceptable, and the samples were analyzed. Figure 3-4 a), b) and c) contain the bromide standard curves from three fractures. The MDL was calculated to be 0.13 mg/L according to Standard Method 1030C (APHA *et al.* 2006). The sample concentrations were then calculated by converting the area under the bromide breakthrough curve on the chromatogram, which was calculated automatically by the HPLC system control software (Varian Star Chromatography Workstation Version 6.20), to a concentration using the standard curve.

A sample chromatagram is included in Appendix A.

a) F1

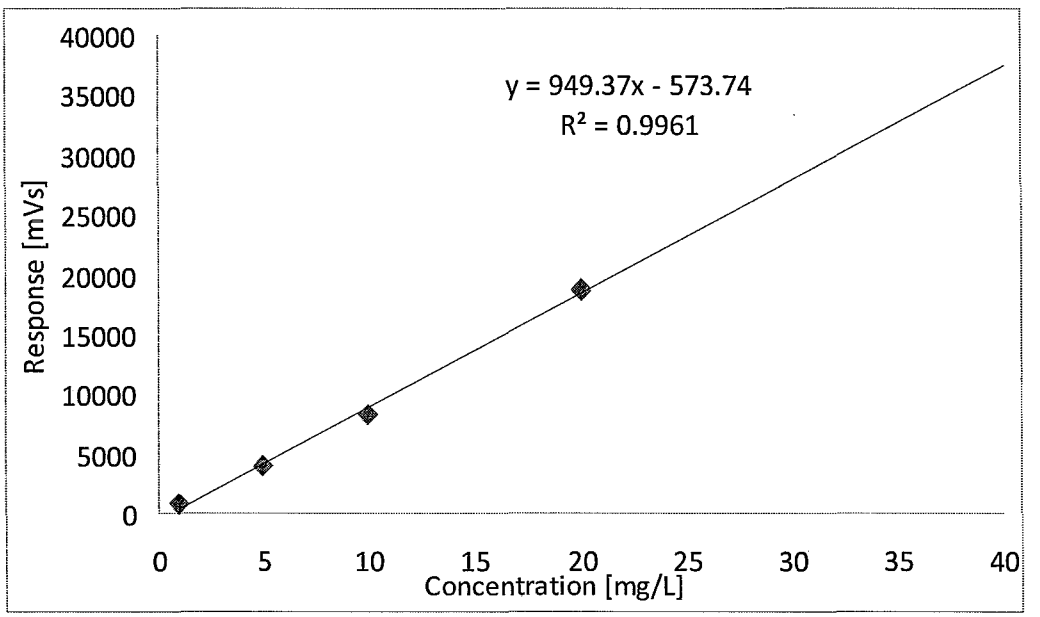

b) F2

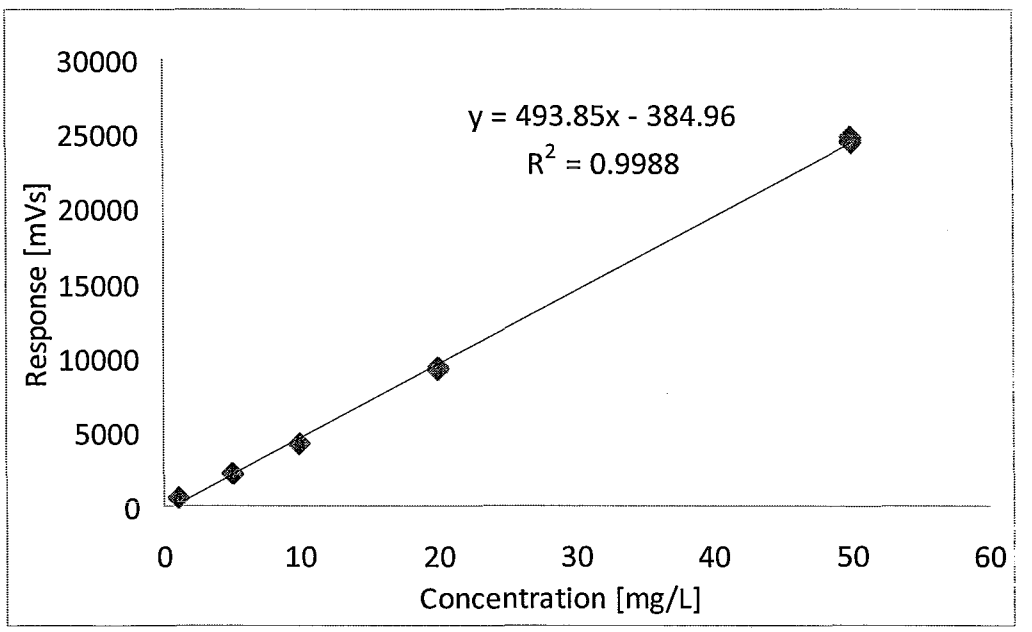

c) F3

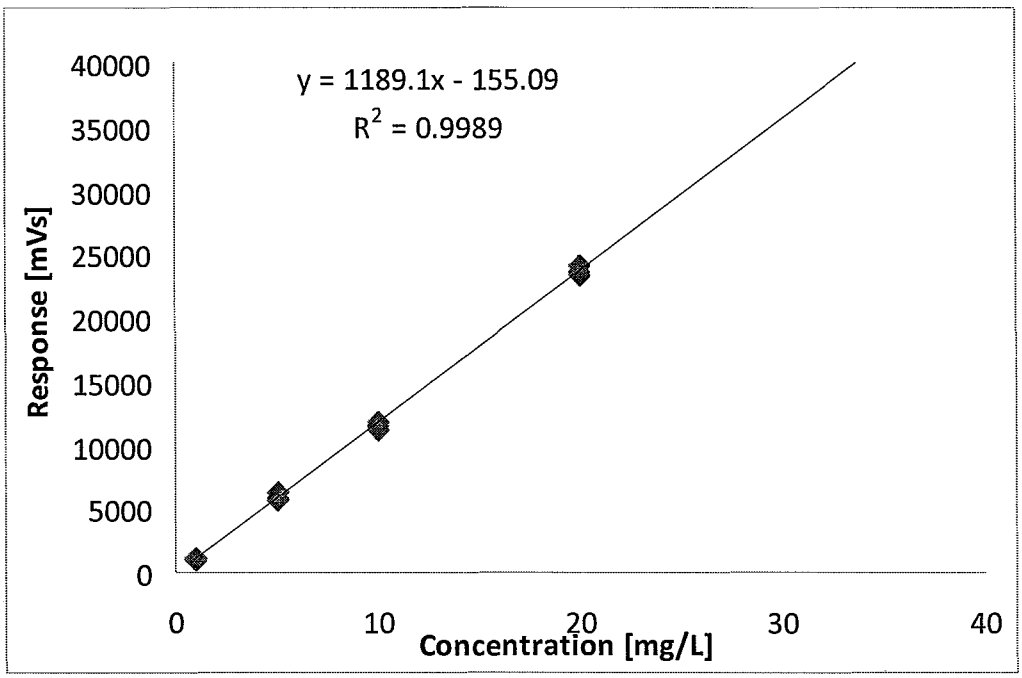

Figure 3-4. Solute tracer tests HPLC standards response curves on a) F1, b) F2 and c) F3.

3.5.4 *E. coli* RS-2GFP Enumeration

Inoculation Preparation

1 mL of the source *E. coli* RS-2GFP culture was combind with 100 mL of prepared broth in a 250 mL Erlenmeyer flask. The flask was incubated at 37 °C, and agitated at 180 rpm for 3 hours. The optical density was measured hourly in the spectrophotometer at a wavelength of 520 nm. Uninoculated broth was employed as the blank, and prepared in the same manner. The culture is approximately 10E8 cfu/mL in the log growth stage corresponding to an absorbency of 0.5 units. At this point, the culture was cooled, and 10% (v/v) sterilized glycerol was added. This solution was mixed well,

and dispensed into 2 mL cryogenic vials, and stored at -80 °C.

To prepare the *E. coli* RS-2GFP for an experiment, one 2 mL bottle of frozen inoculum was thawed at room temperature, and added to 125 mL of broth in a 250 mL Erlenmeyer flask. The flask was incubated at 37 °C, and agitated at 180 RPM overnight (15-18 hours). The optical density was measured using the spectrophotometer to ensure that it was between 0.5 and 1.8 units.

The inoculum was then centrifuged at 5000 g, the broth was decanted, and the *E. coli* RS-2GFP was resuspended in a sterilized 1% PBS solution. The cells were washed twice by centrifuging to separate, and re-suspended in a clean 1% PBS solution. After the final washing, the cells were suspended in 18 mL of PBS. The solution was stored at 4 °C until needed, for a maximum of 72 hours.

Enumeration

Serial dilutions tubes were prepared with 1% PBS solution. Four tubes per sample were prepared, and samples were diluted to a concentration in the range of 10^{-2}–10^{-6}. The tubes with PBS solution were autoclaved and cooled to room temperature before use.

During a sampling event, 0.1 mL of sample was withdrawn from the downstream sampling vial with a sterile syringe, and diluted in the serial dilution tubes. 0.1 mL of solution from each serial dilution tube was dispensed onto the prepared petri dishes, starting with the highest dilution to prevent any contamination. All dilutions were

prepared in triplicate. The samples were spread on the surface of the plates, left to dry, and then incubated for 24 hours at 37 °C.

After 24 hours, the colonies were counted and recorded, and the concentration was calculated. The general range for countable numbers of colonies on a plate is 30-300 (Standard Method 9215A, APHA *et al.* 2006), however, Emelko *et al.* (2008) investigated the organism counts from 1 to 1000, and demonstrated that counts as low as approximately 10 do not increase the uncertainty, and therefore a range of 8-300 was employed (i.e. the plates with colonies between 8 and 300 were reserved for analysis).

4 Results and Discussion

This chapter presents and discusses the results from the hydraulic, solute tracer, and *E. coli* RS-2GFP tracer tests conducted on each of the three fractures. Additionally, the results of the microsphere transport experiments conducted in synthetic fractures by Zheng (2008) are compared to these results.

4.1 Aperture Field Characterization

The goal of the hydraulic and solute tracer tests was to determine the fracture aperture field characteristics, including the equivalent cubic law (μ_c), mass balance (μ_m), and frictional loss (μ_l) apertures. Hydraulic tests also reflect the flow regime in the fracture, and therefore the validity of the cubic law. Three different fractures were employed in these experiments. The fracture dimensions are included in Table 4-2.

Hydraulic Tests

Hydraulic tests were conducted at three different flow rates, with each flow rate repeated to ensure consistency. The flow rates employed were selected to bound the range of specific discharges employed in the *E. coli* RS-2GFP tracer tests, and are listed in Table 4-2.

The equivalent hydraulic aperture was calculated using the cubic law,

$$\mu_c = \left(\frac{12\eta QL}{\gamma W|\Delta H|}\right)^{1/3} \qquad (4\text{-}1)$$

where Q ($L^3 \cdot T^{-1}$) is the volumetric flow rate, L (L) is the length of the fracture in the direction of flow, W (L) is the width of the fracture perpendicular to the direction of flow, ΔH (L) is the head loss across the fracture plane, η($M \bullet L^{-1} \bullet T^{-1}$) is the dynamic viscosity of the fluid, and γ($M \bullet L^{-2} \bullet T^{-2}$) is the specific weight of the fluid. The equivalent hydraulic apertures calculated for fractures F1, F2, and F3 respectively are reported in Table 4-2.

Figure 4-1 shows the specific discharge, based on the equivalent hydraulic aperture, versus head loss for F1, F2 and F3. The relationship is linear in all three cases, indicating that the flow regime is laminar, and the cubic law provides a reasonable estimate of the equivalent hydraulic aperture (Brush and Thomson, 2003). The Reynold's number calculated for each flow rate, presented in Table 4-2, is less than 1 in all cases. This also indicates that the flow regime is laminar. The specific discharge based on the equivalent hydraulic aperture, q_c, was calculated as follows:

$$q_c = \frac{Q}{\mu_c \cdot W} \qquad (4\text{-}2)$$

where μ_c (L) is the equivalent hydraulic aperture, and W (L) is the width of the fracture (perpendicular to the direction of flow). Q versus q was then plotted for each fracture to expedite the determination of the flow rate required for a specified specific discharge.

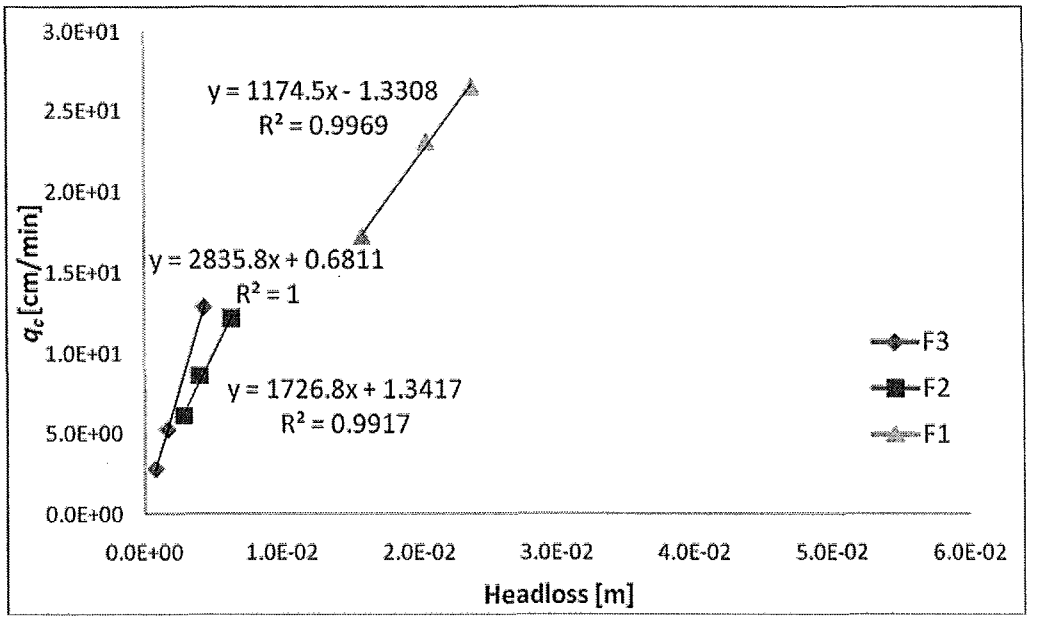

Figure 4-1. Specific discharge versus head loss for F1, F2, and F3.

Solute Tracer Tests

Solute tracer tests were conducted on each fracture to measure the mass balance and frictional loss apertures as follows (Tsang, 1992):

$$\mu_{\mathrm{m}} = \frac{Qt_m}{LW} \tag{4-3}$$

$$\mu_{\mathrm{l}} = L\left(\frac{12\eta}{\gamma|\Delta H|t_{\mathrm{m}}}\right)^{1/2} \tag{4-4}$$

where t_m (T) is the mean residence time of the tracer. The mean residence time is defined as (Fahim and Wakao, 1982):

$$t_m = \frac{\int_0^t C(t)_{\mathrm{out}} \cdot t\,dt}{\int_0^t C(t)_{out}\,dt} - \frac{\int_0^t C(t)_{in} \cdot t\,dt}{\int_0^t C(t)_{in}\,dt}. \tag{4-5}$$

and was approximated as:

$$t_m = \sum t \cdot E(t) \cdot \Delta t, \qquad (4\text{-}6a)$$

$$E(t) = \frac{C_{out}(t)}{\sum C_{out}(t) \cdot \Delta t} - \frac{C_{in}(t)}{\sum C_{in}(t) \cdot \Delta t}, \qquad (4\text{-}6b)$$

where $C_{out}(t)$ is the tracer concentration exiting the fracture at time t, $C_{in}(t)$ is the concentration entering the fracture at time t, and Δt is the time interval between sampling events. The equivalent mass balance and frictional loss apertures are tabulated in Table 4-2 together with the specific discharges at which the experiments were conducted. The bromide concentration in the upstream recirculation system decreased exponentially, and was modeled as follows (Zheng, 2008):

$$C_{in}(t) = \frac{M_{br}}{V_{recir}} * EXP(\frac{-Q \cdot t}{V_{recir}}) \qquad (4\text{-}7)$$

in which M_{br} is the total mass of bromide initially injected into the upstream flow cell, and V_{recir} is the volume of the upstream flow cell and recirculation system (Table 4-2).

It is important to note that the solute exiting the fracture plane is diluted upon entering the effluent flow cell. Therefore, the samples collected from the downstream sampling vial were not representative of the actual bromide concentration exiting the fracture. Thus, the measured sample concentrations were adjusted to determine the actual bromide concentration exiting the fracture. This was accomplished by conducting a mass balance on a continuous flow mixed reactor (CFMR) as follows:

$$C_{eff\text{-}frac}(t) = \frac{V_{recir}}{Q} * \frac{dC_{meas}(t)}{dt} + C_{meas}(t) \qquad (4\text{-}8a)$$

$$\approx C_{eff\text{-}frac}(t) = \frac{V_{recir}}{Q} * \frac{C^{t}_{meas} - C^{t-\Delta t}_{meas}}{\Delta t} + C^{t}_{meas} \qquad (4\text{-}8b)$$

where $C_{eff\text{-}frac}(t)$ represents the bromide concentration exiting the fracture, C_{meas} (t) represent the measured bromide concentration in the effluent flow cell, V_{recir} represents the volume of the downstream recirculation system and flow cell (Table 4-2), and Q represents the hydraulic flow rate.

The two curves shown on Figure 4-2 represent the measured and back-calculated (using equation 4-8b) bromide breakthrough curves from solute tracer experiments conducted in F1, F2, and F3. The peak concentration of back-calculated curves appeared sooner and higher than measured ones, demonstrating that the concentration of bromide has been diluted in the downstream recirculation system.

An examination of Table 4-2 reveals the following relationship amongst the cubic law (μ_c), mass balance (μ_m), and frictional loss (μ_l) aperture for all three fractures:

$$\mu_l < \mu_c < \mu_m \qquad (4\text{-}9)$$

This relationship is the same as that observed by others (e.g., Zheng *et al.*, 2008; Dickson and Thomson, 2003) and predicted by Tsang (1992). The fact that mass balance aperture is the equivalent aperture most closely related to the arithmetic mean aperture, and therefore most appropriate for describing solute transport in single fractures, was

demonstrated by Zheng *et al.* (2008).

a)

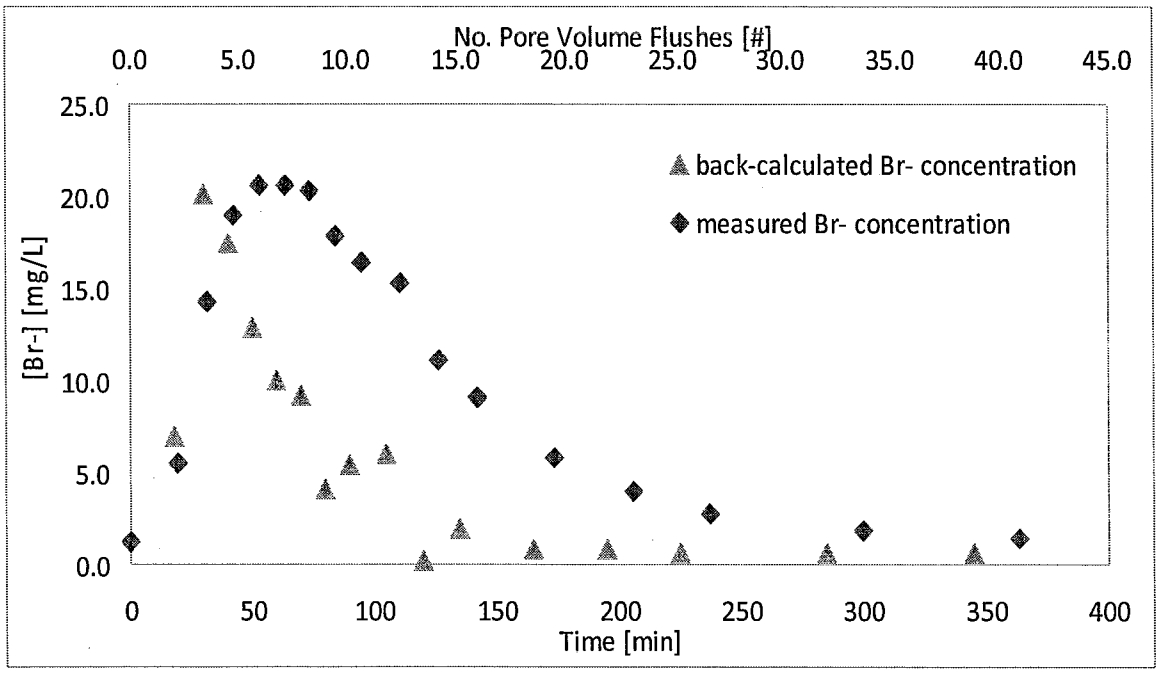

b)

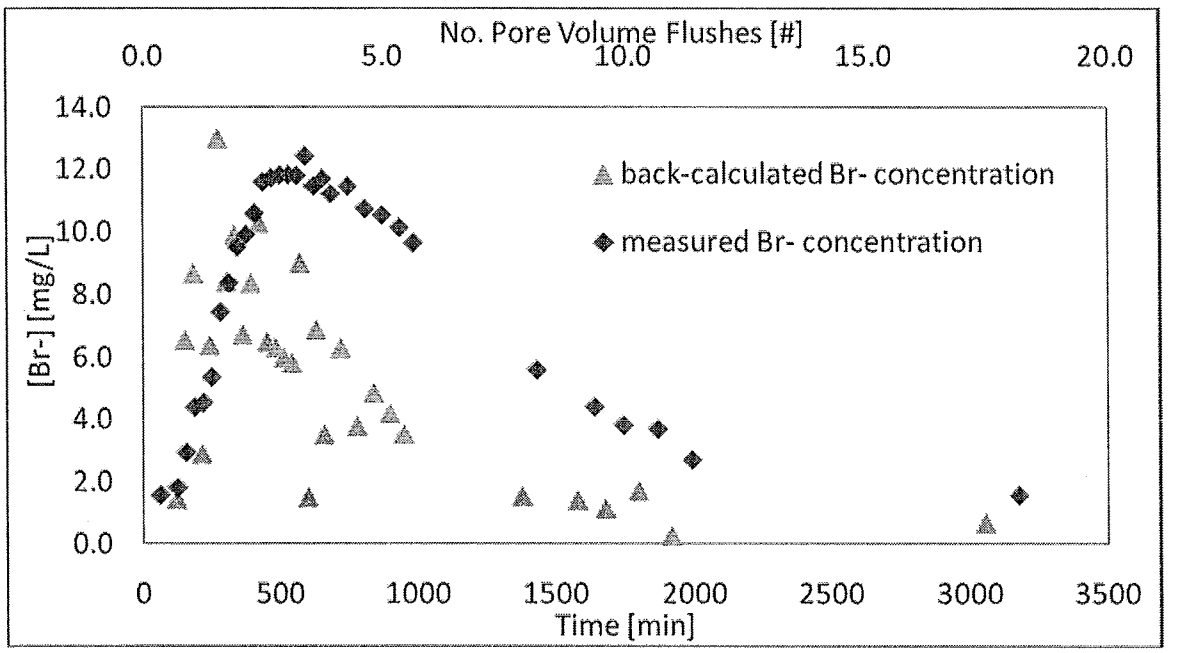

c)

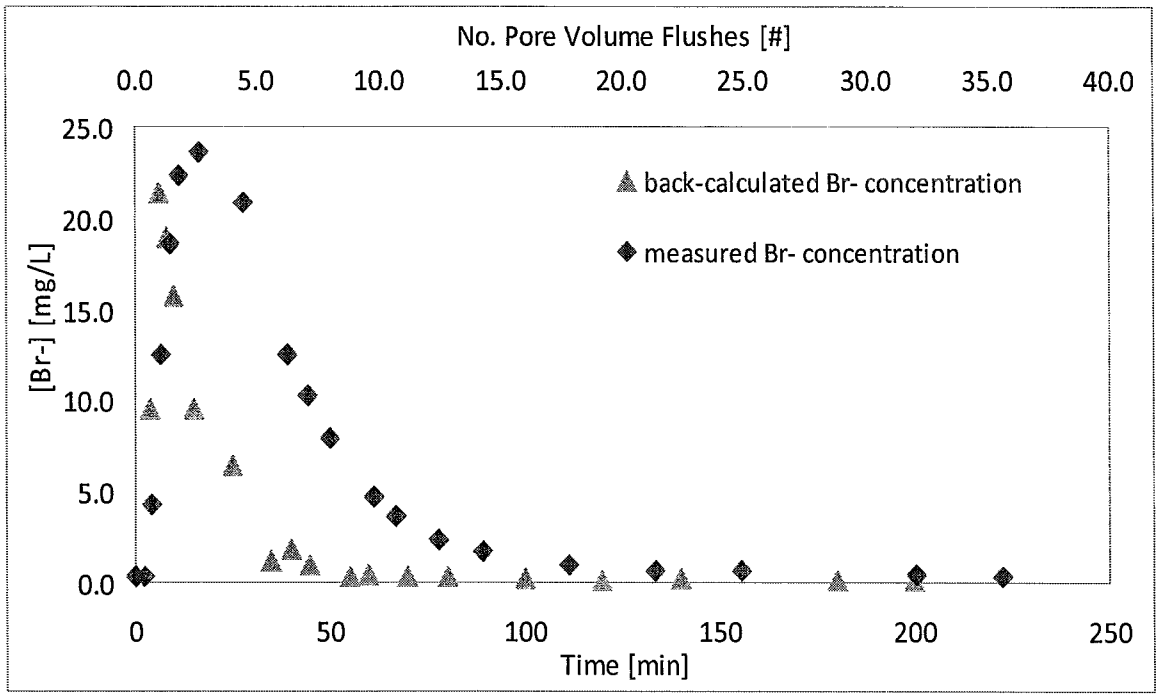

Figure 4-2. Measured and back-calculated bromide breakthrough curves for the solute tracer test conducted on a) F1 at 2.12 mL/min, b) F2 at 0.1 mL/min, and c) F3 at 10.3 mL/min.

A mass balance was conducted on the bromide for each tracer test to ensure that all measurements and calculations were conducted properly. Table 4-1 shows the percentage of bromide mass recovered from each solute tracer test. The recoveries range from 73% to 105%. The percentage recovery for F3 at the specific discharge of 10 cm/min was 105%. The fact that this is more than 100% is likely due to the summation effect of several sources of error, including the method employed for summing the area under the breakthrough curve, existing background concentrations of bromide from previous experiments, quantification error, and unsteady flow rates. As a result, it appears that more mass came out of the fracture than was injected, which is not actually the case.

Table 4-1 Bromide recovery from solute tracer tests.

Fracture ID	Percentage of recovery	q_c
F1	74%	3.2 cm/min
F2	75%	0.01 cm/min
F3	105%	10 cm/min

Conversely, the percentage recoveries for F1 and F2 are approximately 75%, which deviate from 100% further than is desirable. It is suspected that in the fractures with lower recoveries, some bromide became trapped in stagnant areas of the aperture field, which left more time for diffusion into the matrix. It is postulated that F3 doesn't have any extremely large aperture regions, where bromide would become stagnant, thus the recovery in F3 is relatively larger than the other two fractures. This demonstrates that the fracture characteristics have a great influence on solute transport.

Table 4-2[a] Fracture Field Characterization Data.

Fracture ID	Length [m]	Width [m]	Recirculation System Volume[b] [m^3]		Q (Hydraulic Tests) [mL/min]	μ_m [mm]	q_m[d] [mm/s]	μ_c [mm]	q_c [mm/s]	μ_l [mm]	q_l [mm/s]	Estimated fracture aperture volume[c] [mL]			Reynolds Number[e]
			Upstream	Downstream								Based on μ_m	Based on μ_c	Based on μ_l	
F1	0.16	0.24	1.06E-04	7.98E-05	9.45 8.29 6.06	1.06	0.50	0.22± 0.002	4.42 3.85 2.87	0.10	5.30	40.6	8.26	3.72	0.62-0.98
F2	0.22	0.295	1.27E-04	1.07E-04	9.61 6.43 4.53	2.99	0.03	0.33± 0.01	0.20 0.14 0.10	0.02	4.07	193.9	6.88	1.29	0.03-0.07
F3	0.23	0.37	1.19E-04	1.17E-04	13.33 5.70 3.29	1.32	1.27	0.50± 0.09	2.15 0.88 0.48	0.27	6.19	112.2	38.6	22.6	0.26-0.96

a. All experiments were conducted at 25±2 °C, and the value of the parameters used in these calculations corresponds those at 25°C (i.e., ρ=997 kg/m^3, η=0.00089 N·s/m^2).

b. Recirculation volume includes the volume of the flow cell, sampling vial and tubings.

c. Estimated fracture aperture volume = $L*W*\mu$, where μ represents μ_m, μ_c, or μ_l.

d. q is the corresponding specific discharge, $v=Q/W/\mu$, where μ represents μ_m, μ_c, or μ_l.

e. Reynolds Number = $\rho*q*\mu_c/\eta$.

4.2 *E. coli* RS-2GFP Tracer Tests

E. coli RS-2GFP tracer tests were conducted at three different specific discharges, q_c, which were selected to represent a range of typical groundwater flow rates in fractured environments: 10, 1, and 0.1 cm/min. Each tracer test was conducted a minimum of three times at each flow rate to ensure repeatability. Similar to the solute breakthrough curves, the measured *E. coli* RS-2GFP concentrations from the effluent sampling port were diluted in the downstream flow cell and recirculation system. Therefore, the measured *E. coli* RS-2GFP concentrations were back calculated using equation 4-8b.

E. coli RS-2GFP breakthrough curves containing both measured and back-calculated data for all fractures in triplicate experiments are plotted on Figure 4-3 a)-aa). The data presented in the measured curve on Figure 4-3 represents the log median *E. coli* RS-2GFP concentration enumerated from each sample. The error bars represent the range between the maximum or 1.5(Q3-Q1)+Q3, and the minimum or Q1-1.5(Q3-Q1), where Q1 and Q3 represent the first and third quartiles respectively. A sample calculation for the error bars is included in Appendix B. The data presented and analysed in the remainder of this chapter represent the back-calculated *E. coli* RS-2GFP concentrations exiting the fracture, unless otherwise stated.

The breakthrough curve trend shown in Figure 4-3 is typical of all the flow rates in all of the fractures. The effluent concentration soared quickly and remained steady through a relatively long-lasting peak, followed by a gradually decreasing tail. The

cumulative number of *E. coli* RS-2GFP exiting fracture was calculated for each experiment by estimating the area under the breakthrough curve. The percentage of *E. coli* RS-2GFP removal (i.e., the recovery), was then calculated for each *E. coli* RS-2GFP experiment. These data are reported in Table 4-3.

Figures 4-4 a), b), and c) show the log-normalized median effluent *E. coli* RS-2GFP concentrations from all three experiments conducted at q=10 cm/min in F1, F2 and F3 respectively. Similar figures for the experiments conducted at q=1 cm/min and q=0.1 cm/min are included in Appendix C. This figure demonstrates that the experimental results are repeatable, and therefore the data are considered reliable.

a) F1 0.1 cm/min #1

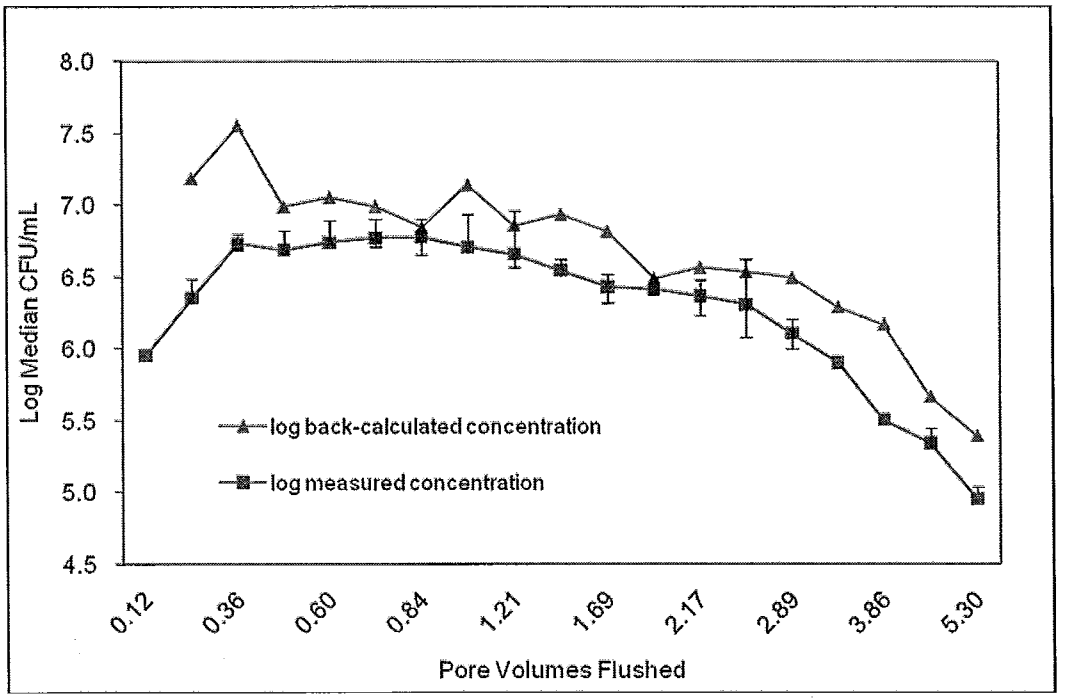

b) F1 0.1 cm/min #2

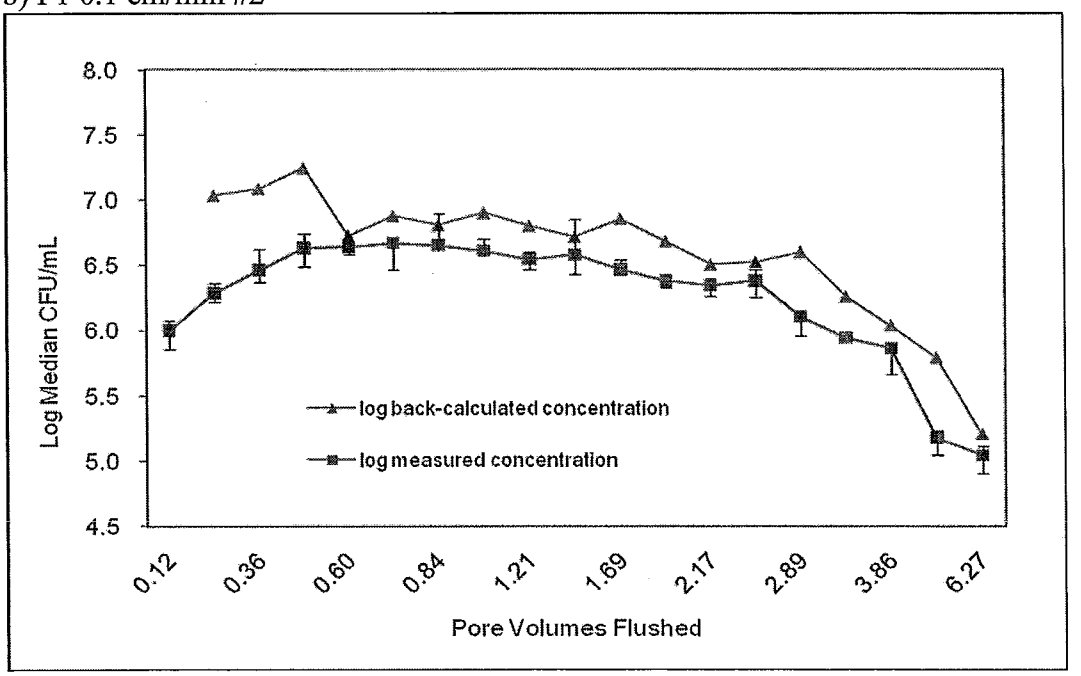

c) F1 0.1 cm/min #3

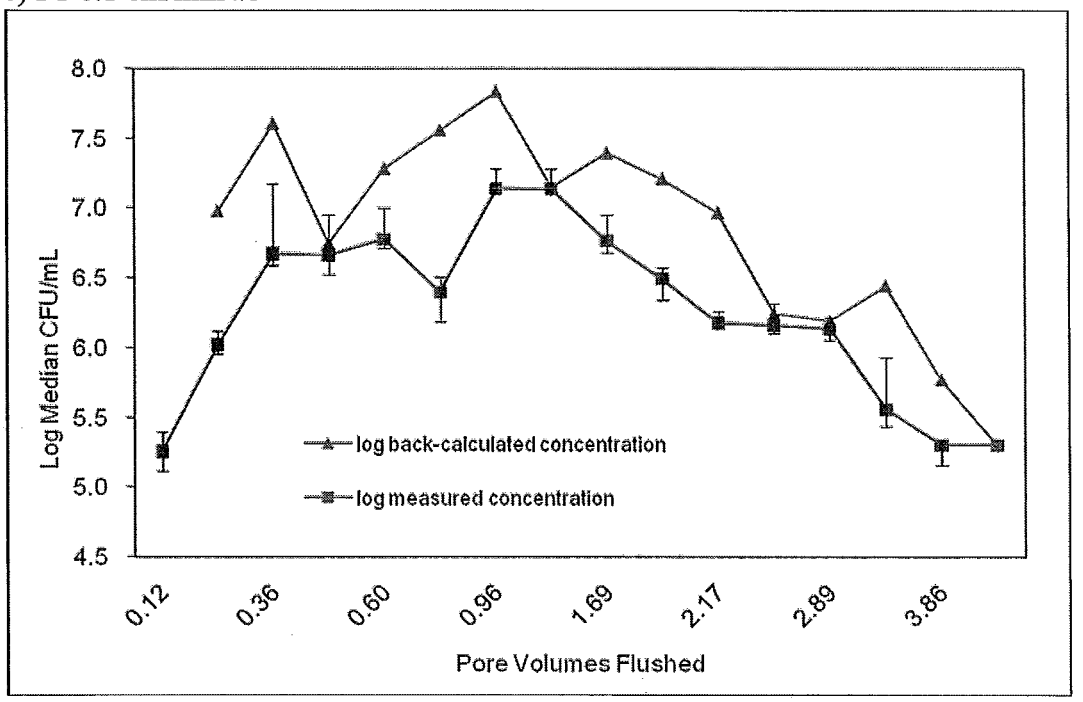

d) F1 1 cm/min #1

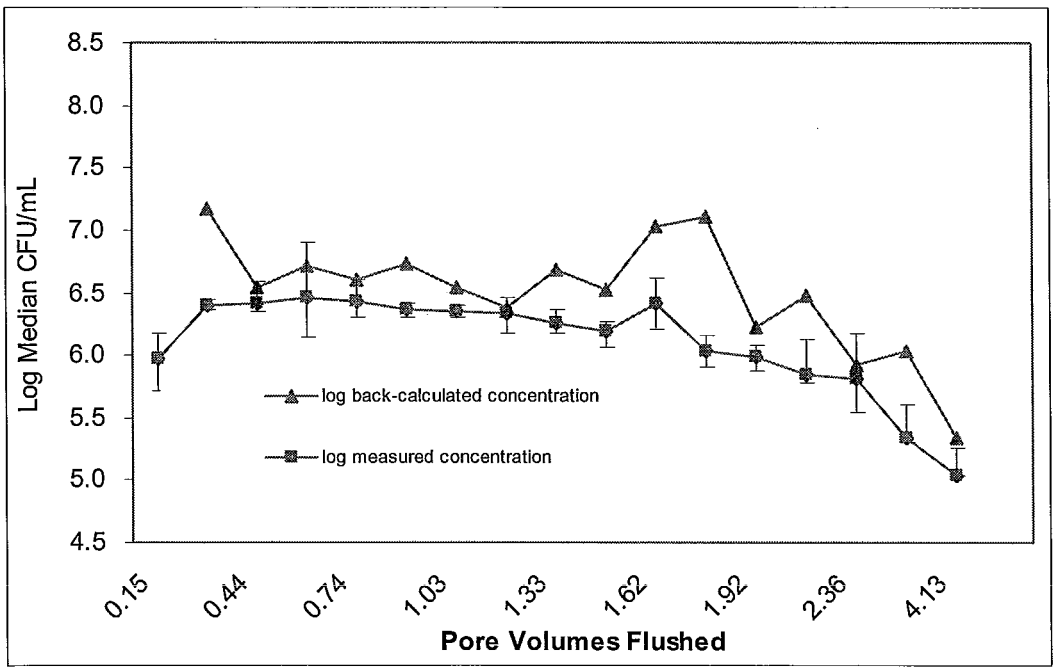

e) F1 1 cm/min #2

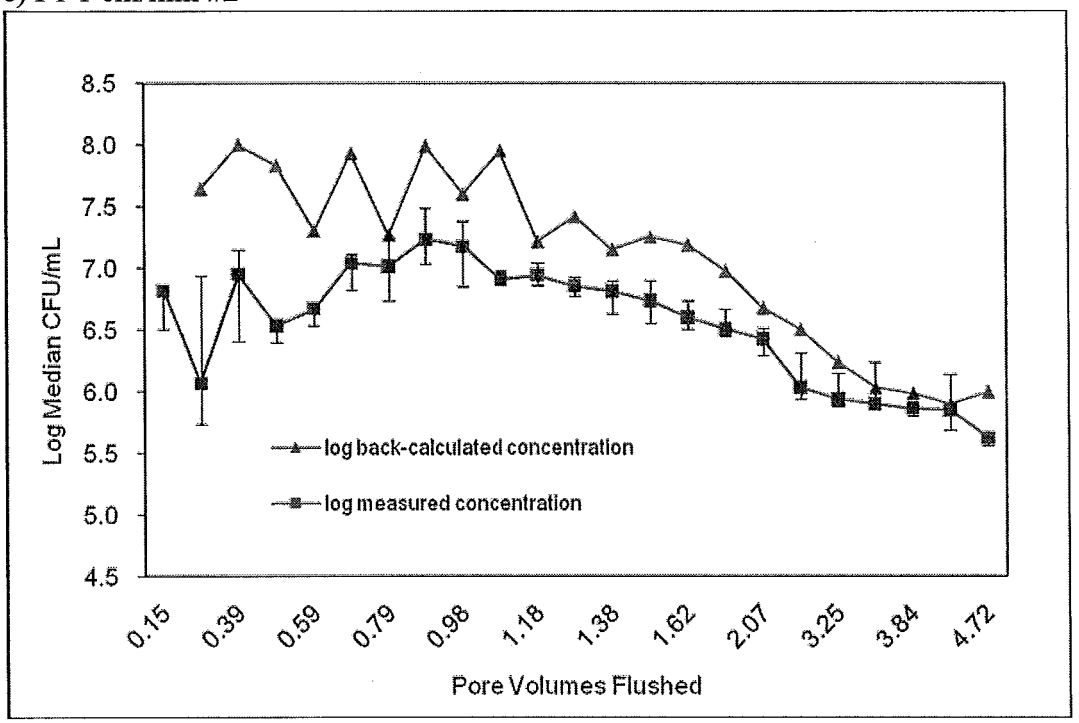

f) F1 1 cm/min #3

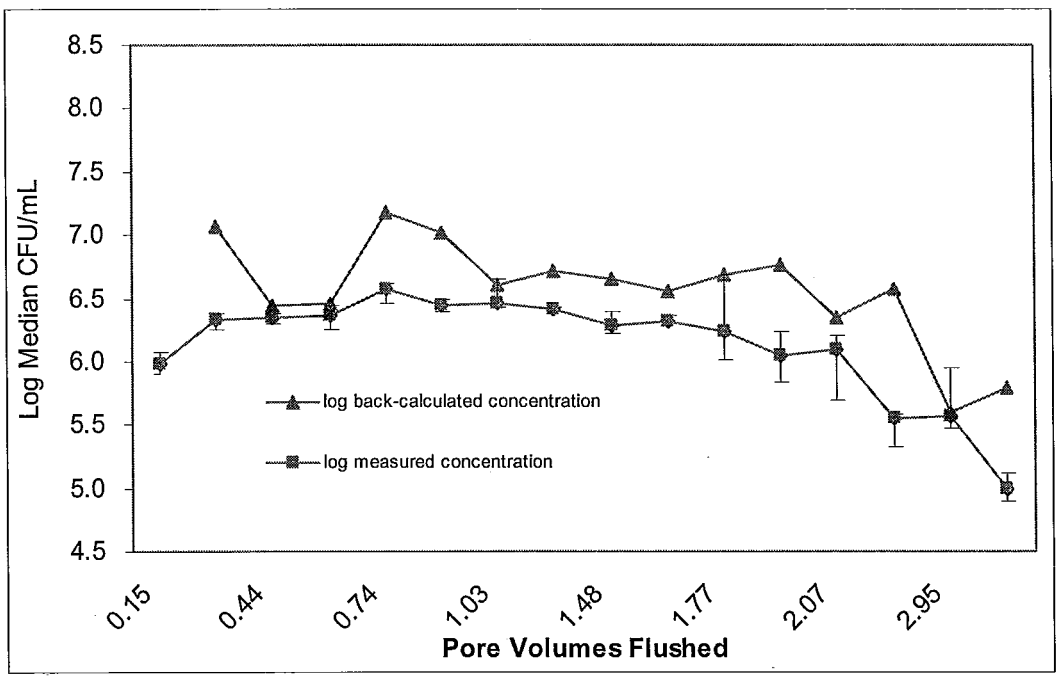

g) F1 10 cm/min #1

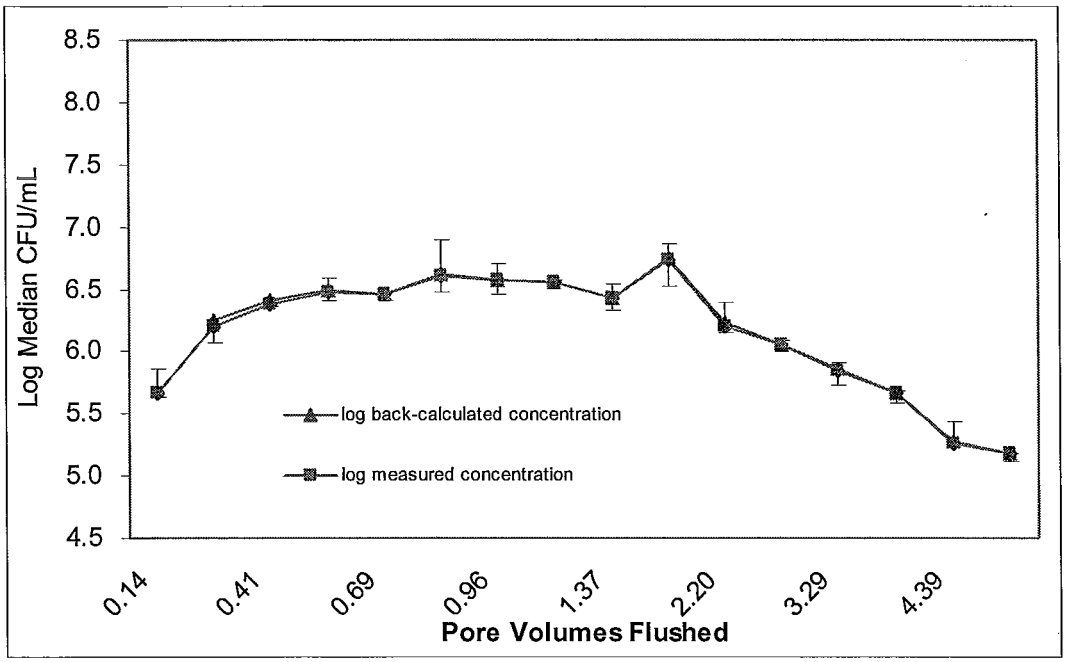

h) F1 10 cm/min #2

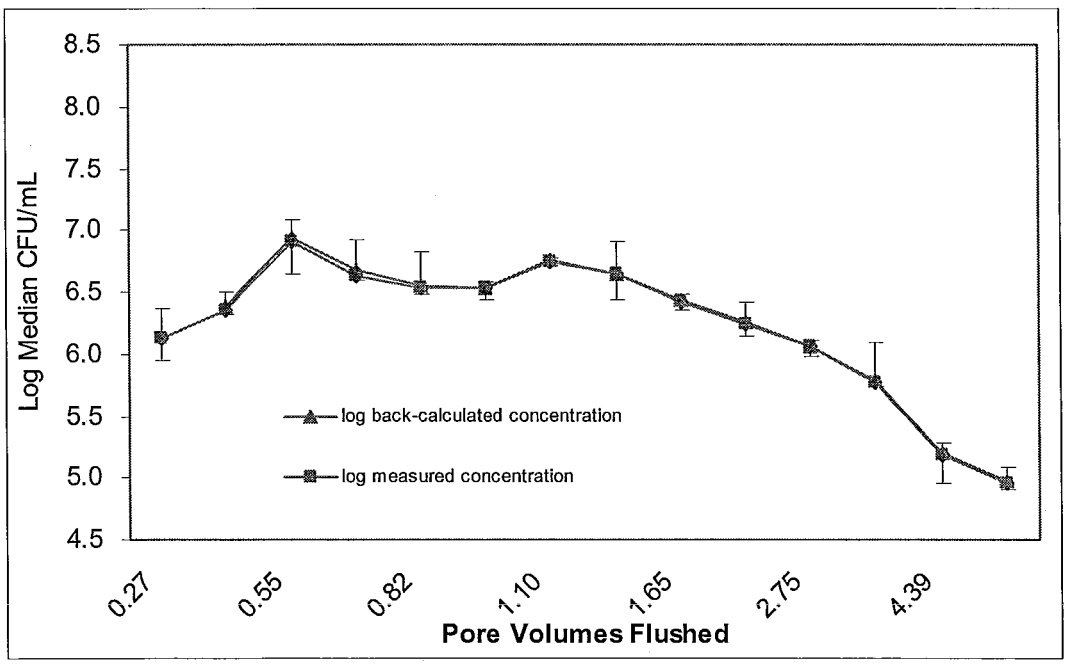

i) F1 10 cm/min #3

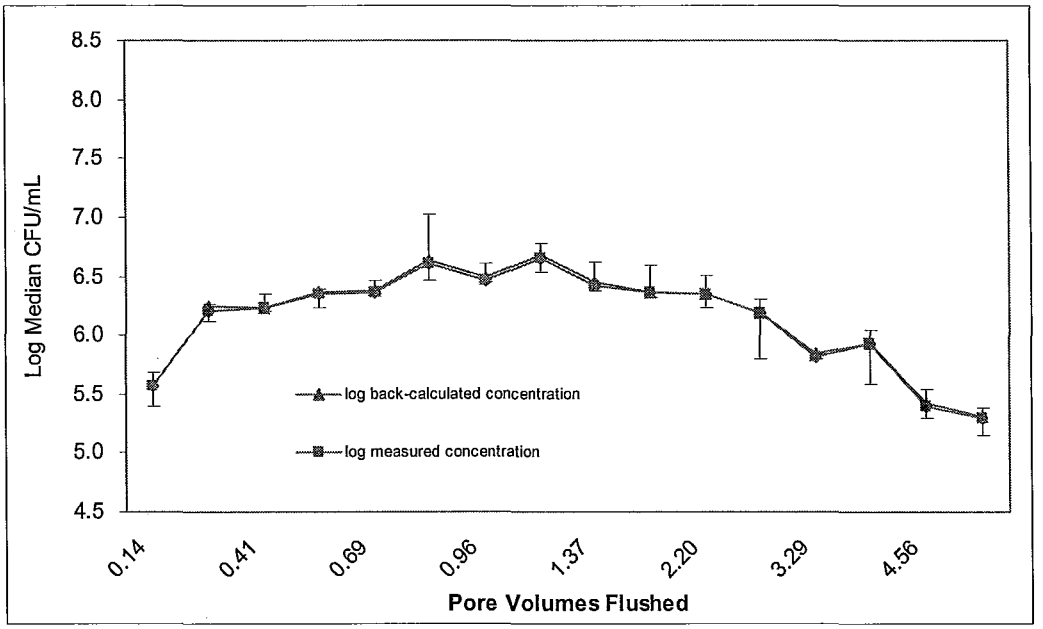

j) F2 0.1 cm/min #1

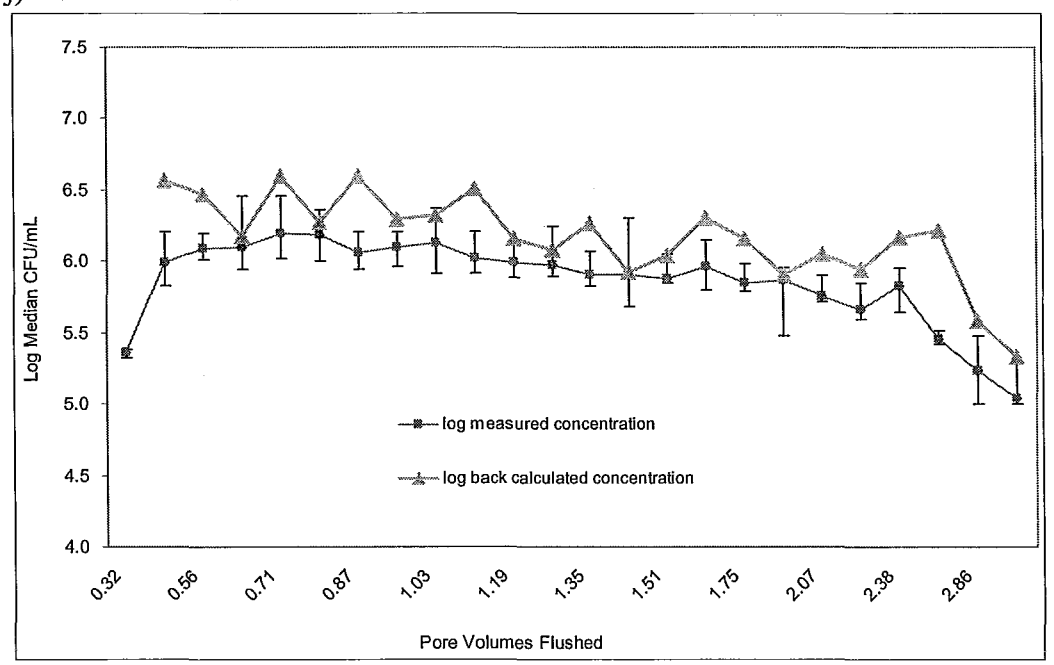

k) F2 0.1 cm/min #2

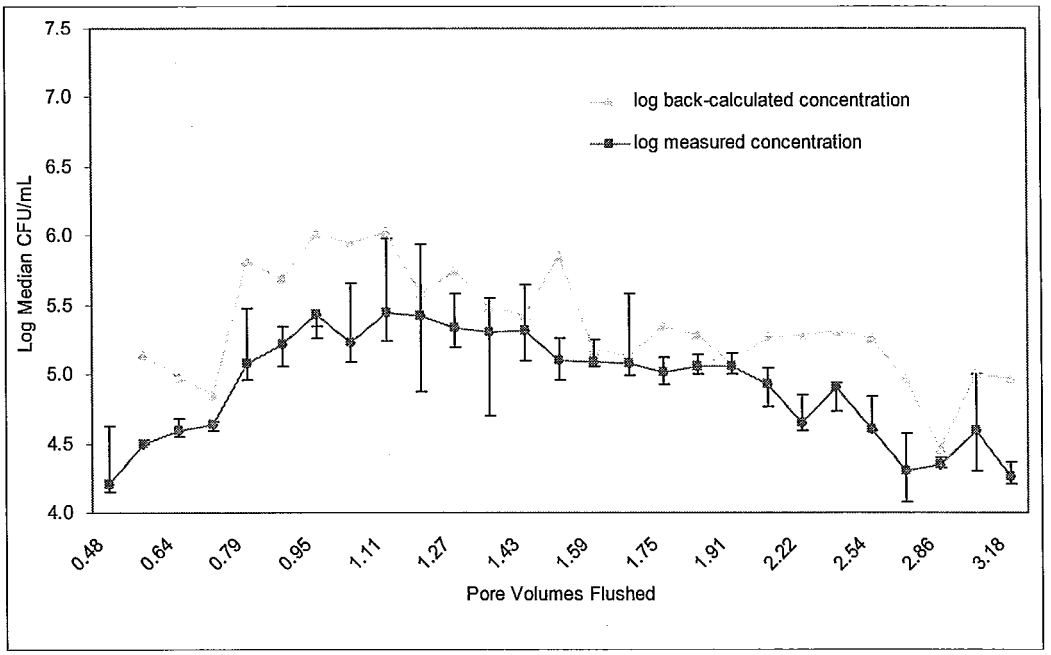

l) F2 0.1 cm/min #3

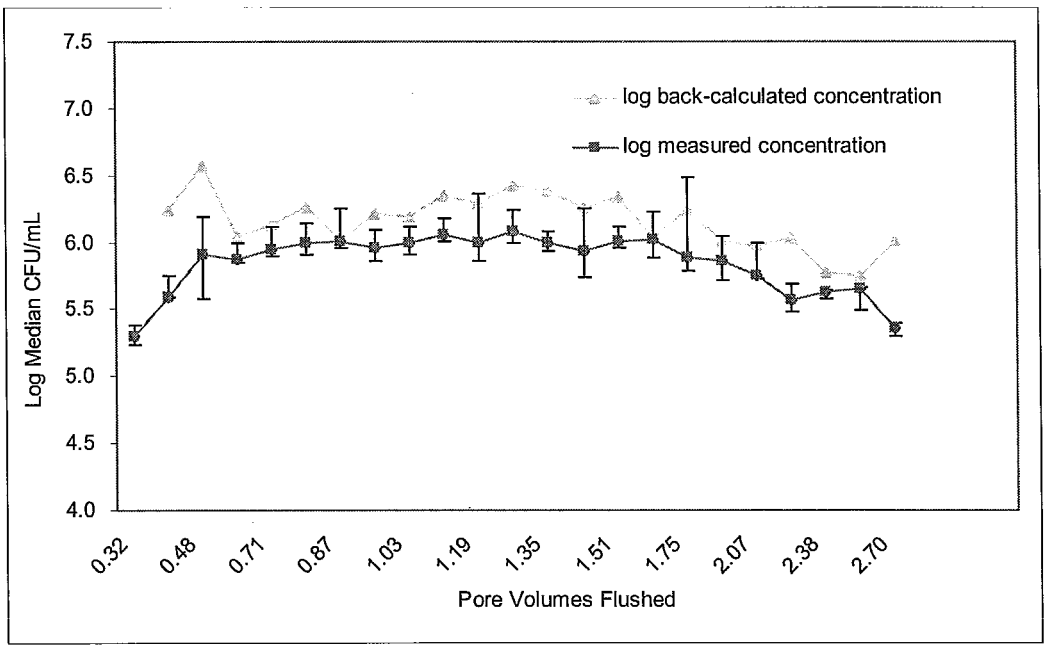

m) F2 1 cm/min #1

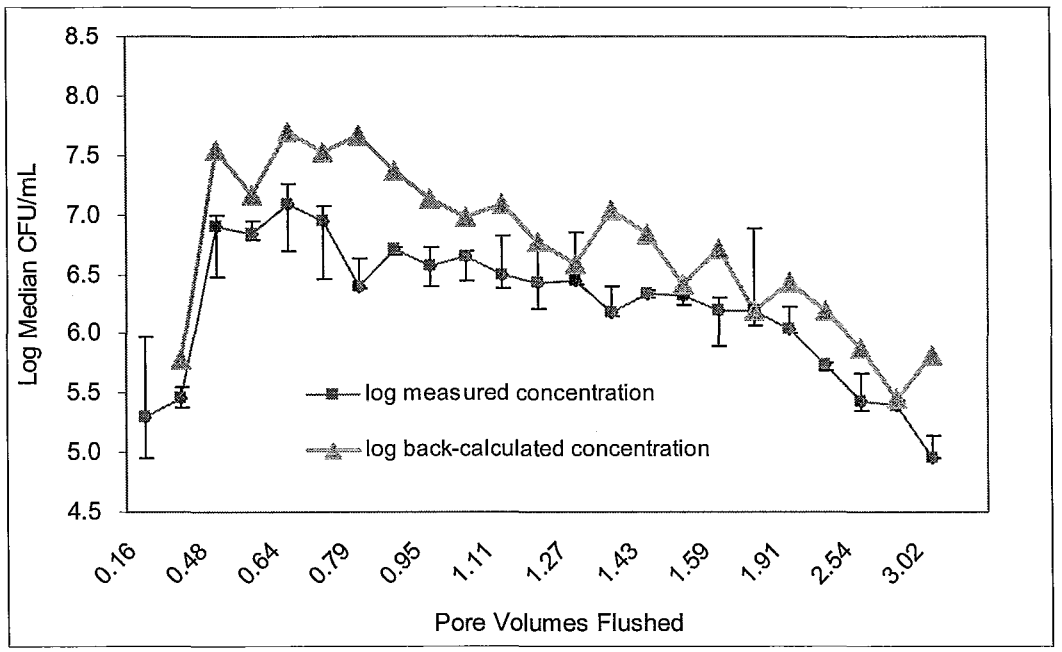

n) F2 1 cm/min #2

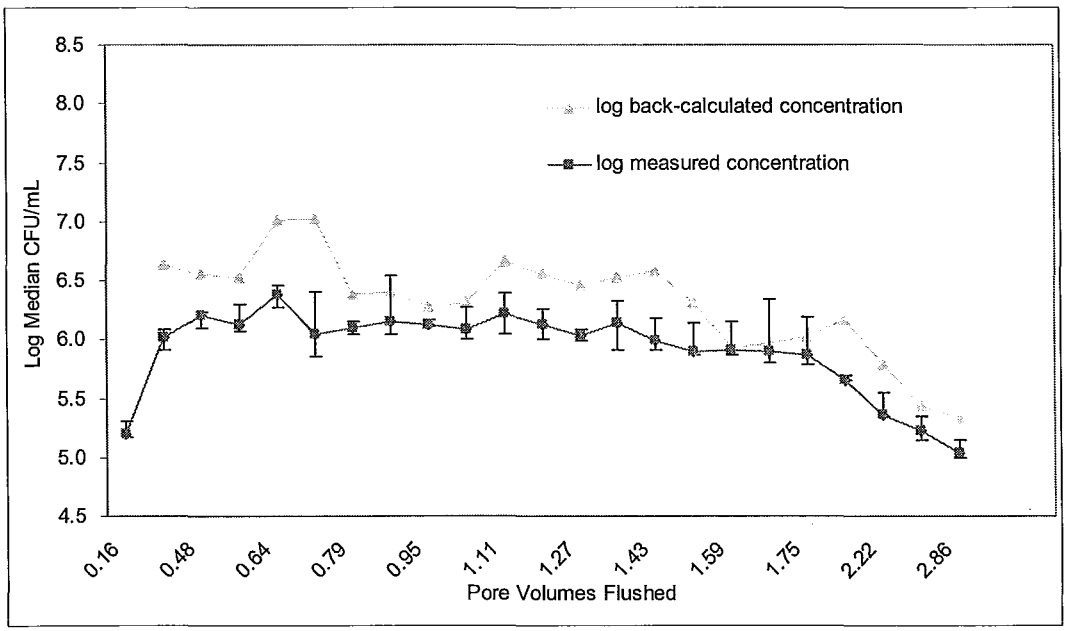

o) F2 1 cm/min #3

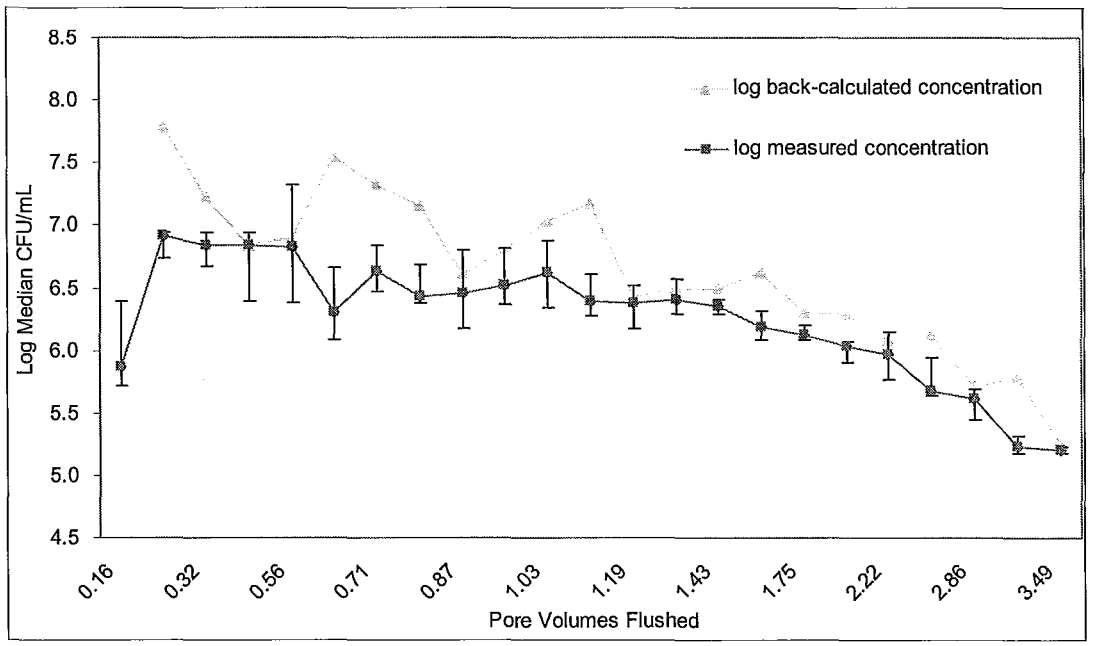

p) F2 10 cm/min #1

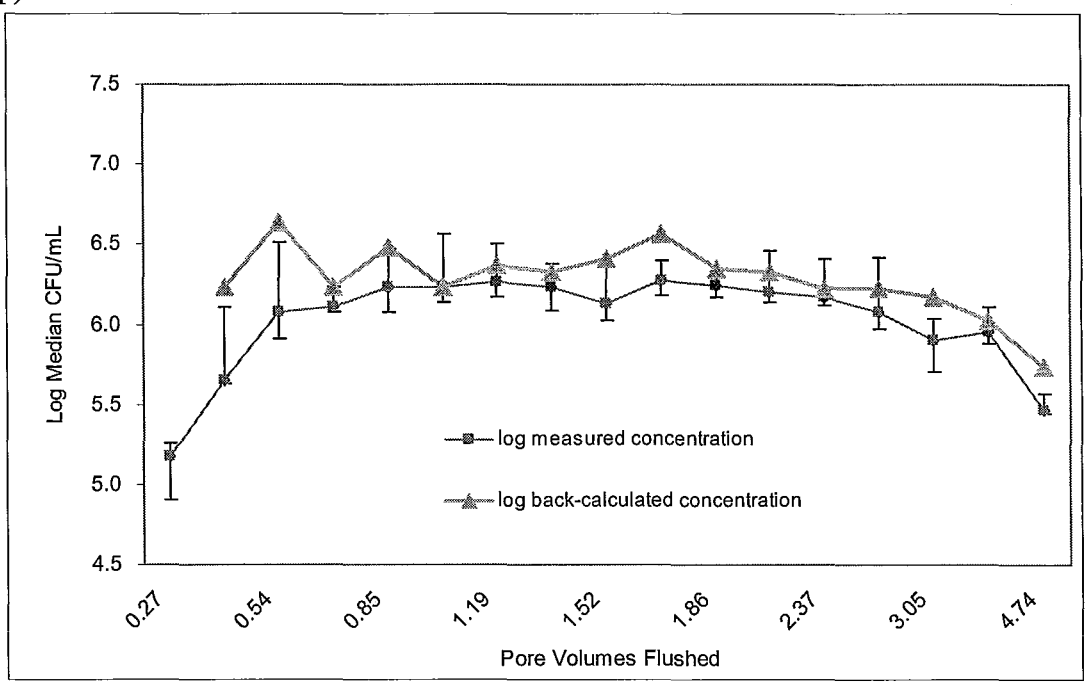

q) F2 10 cm/min #2

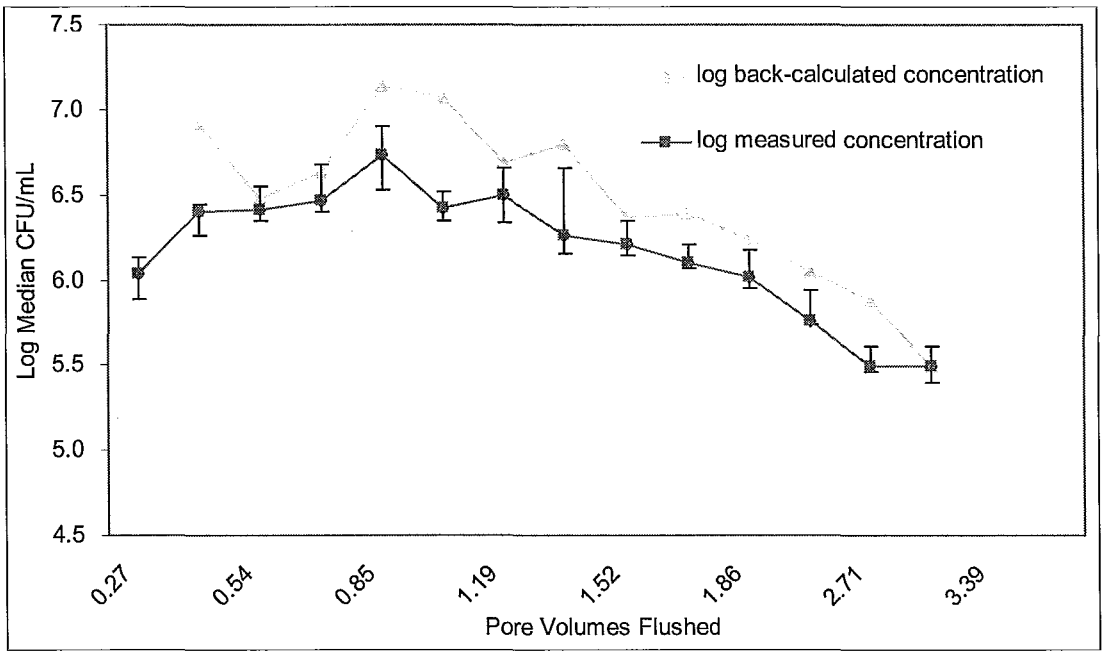

r) F2 10 cm/min #3

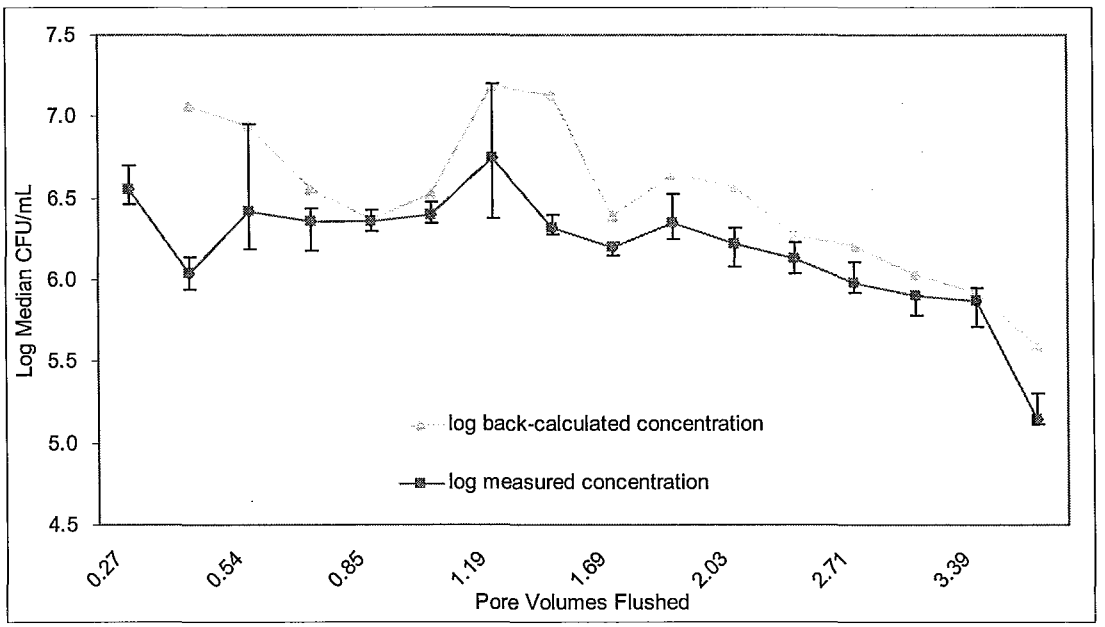

s) F3 0.1 cm/min #1

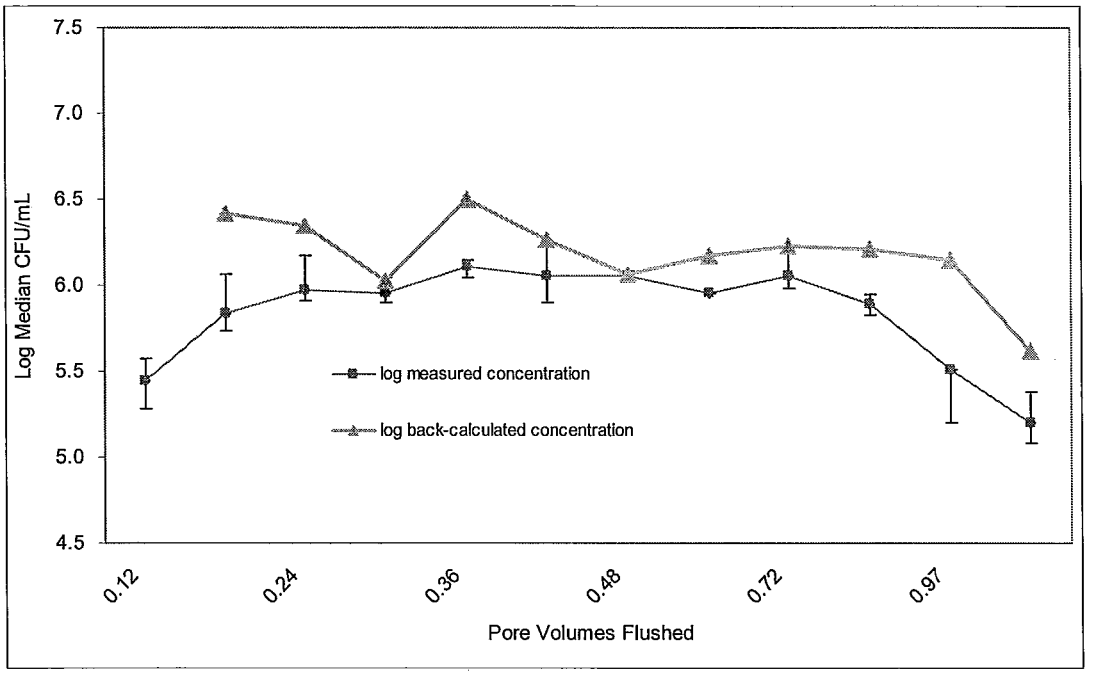

t) F3 0.1 cm/min #2

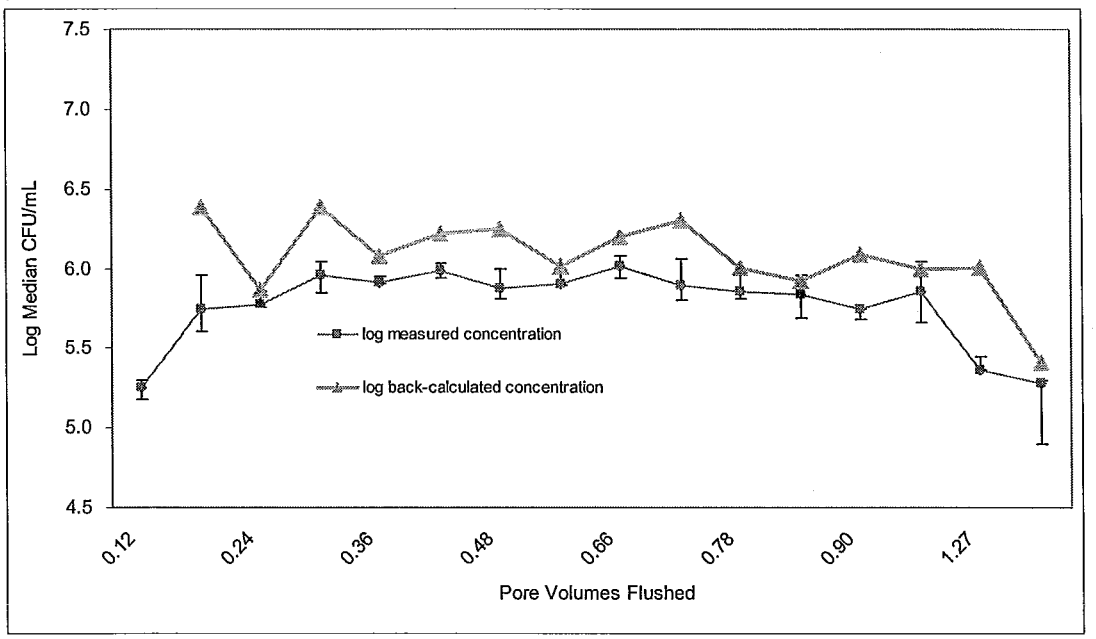

u) F3 0.1 cm/min #3

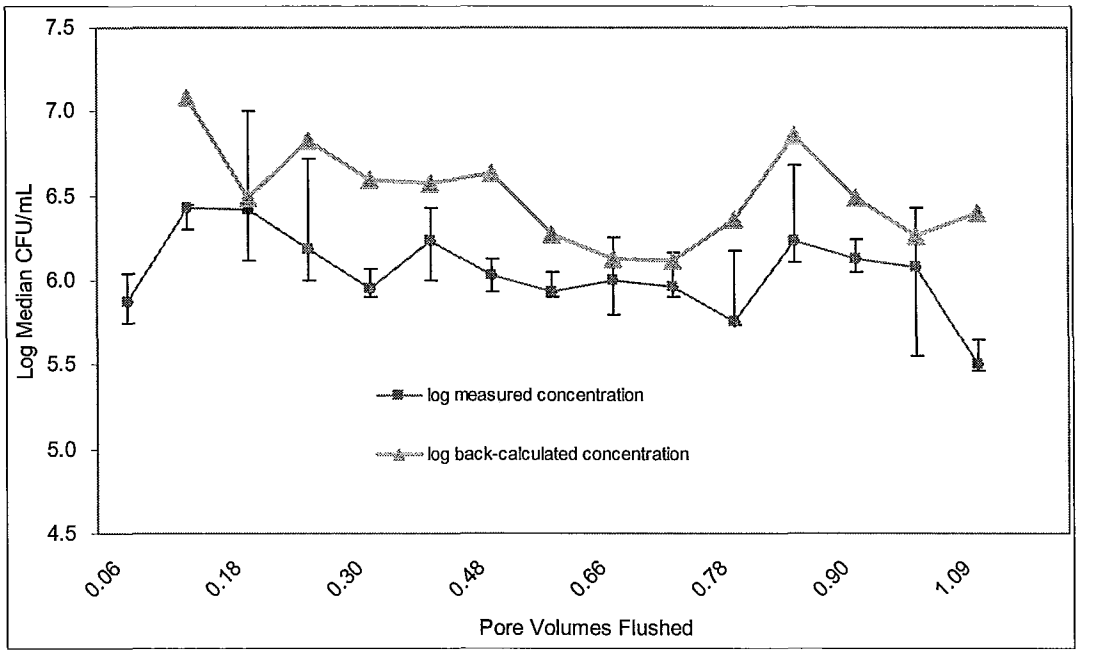

v) F3 1 cm/min #1

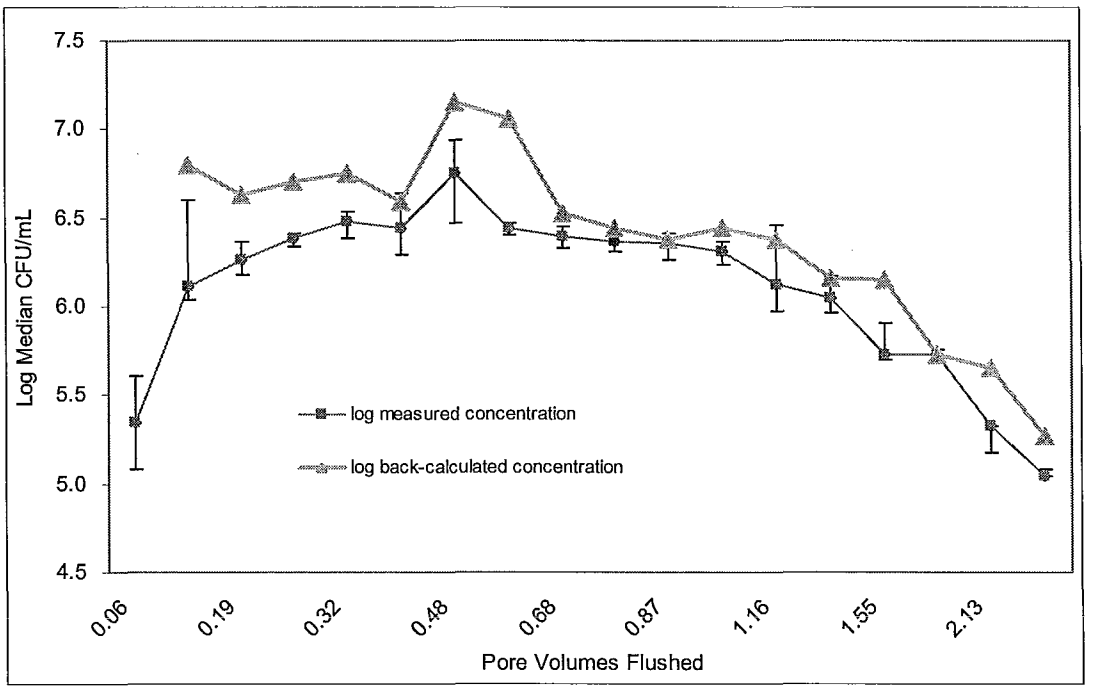

w) F3 1 cm/min #2

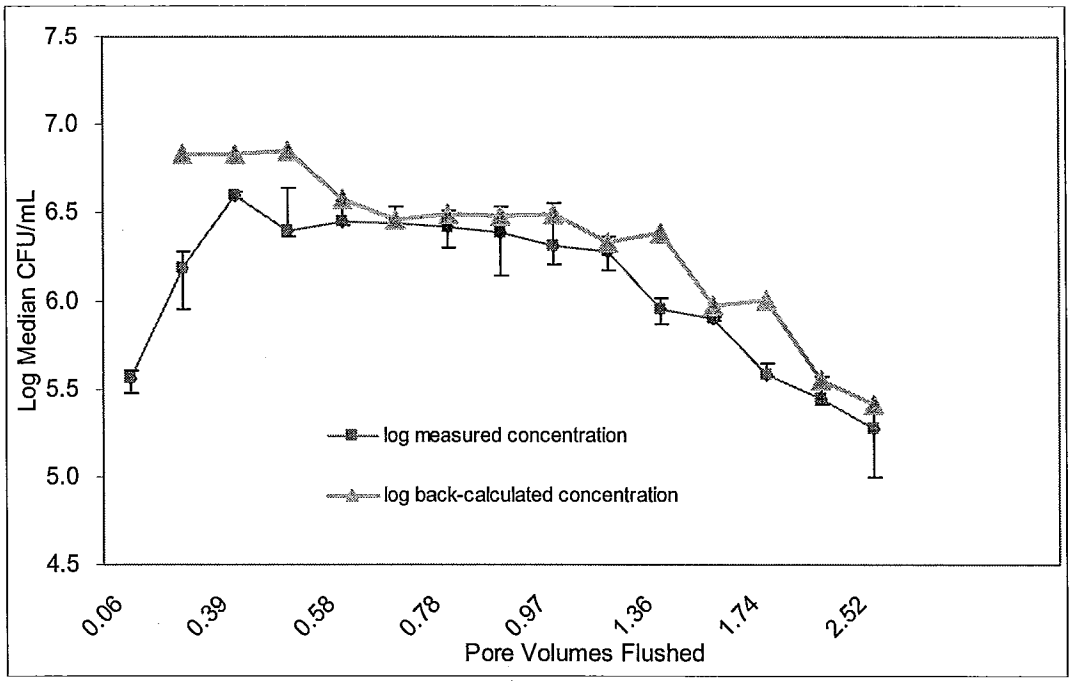

x) F3 1 cm/min #3

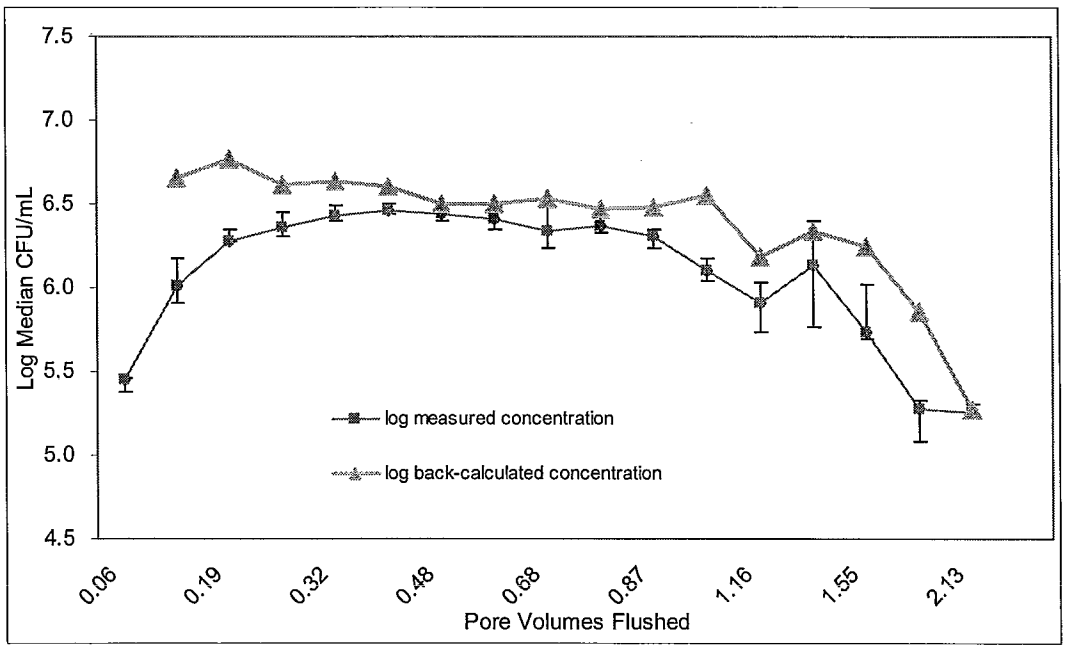

y) F3 10 cm/min #1

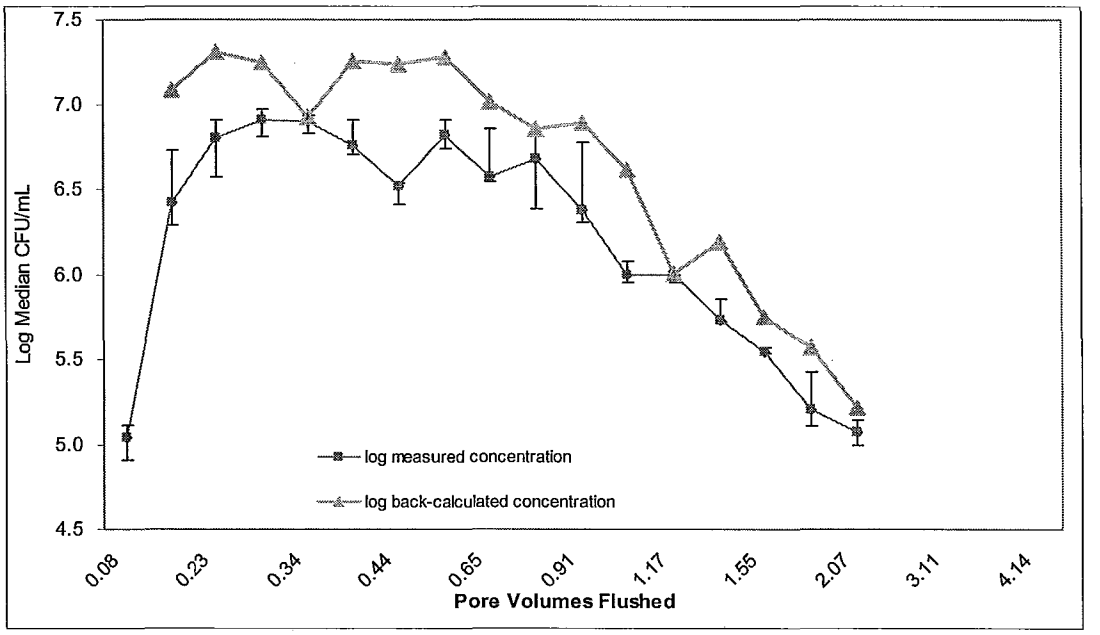

z) F3 10 cm/min #2

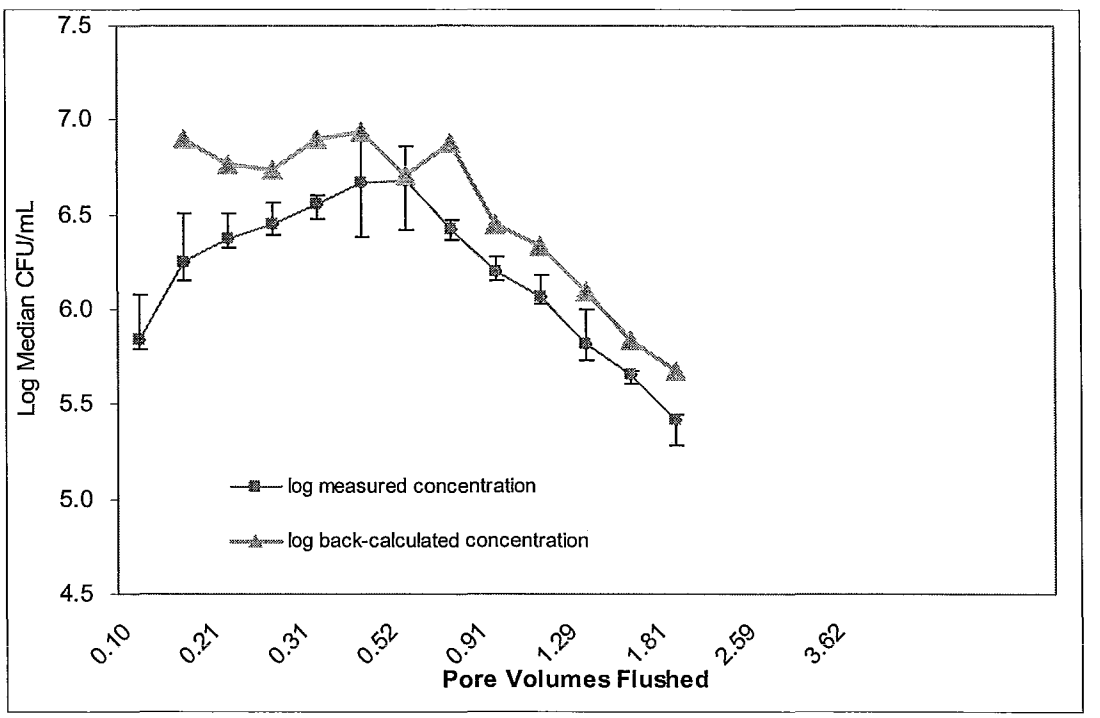

aa) F3 10 cm/min #3

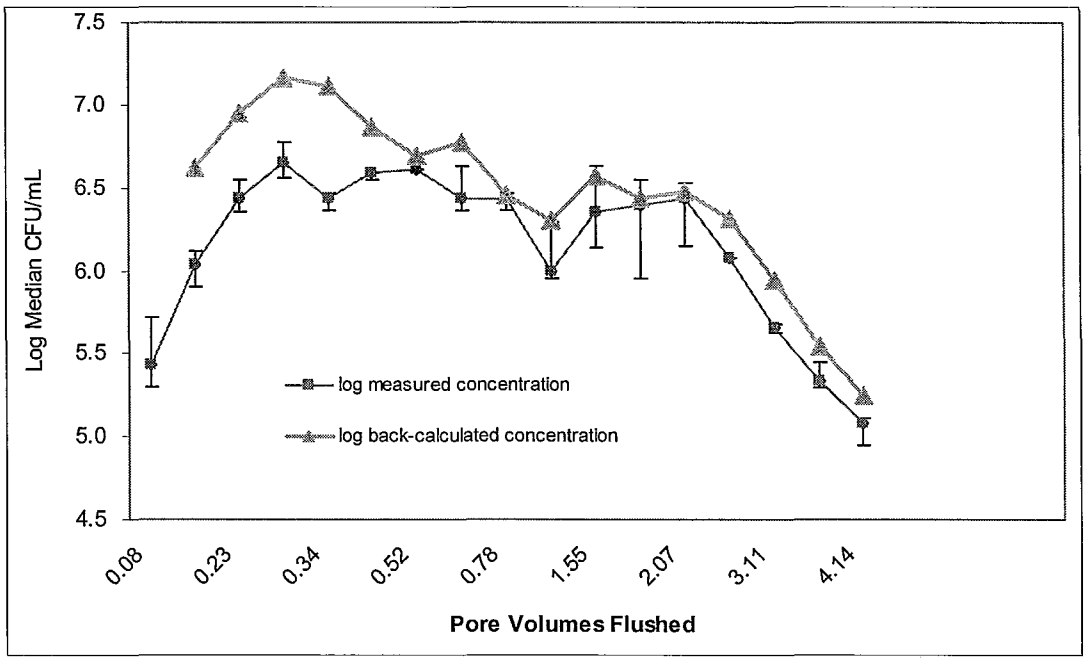

Figure 4-3. Log-back-calculated and log-measured *E. coli* RS-2GFP concentration breakthrough curves in F1, F2, and F3 at a specific discharge of 0.1, 1, and 10 cm/min, and in triplicate times (a~aa). Error bars represent the range between the maximum or 1.5(Q3-Q1)+Q3, and the minimum or Q1-1.5(Q3-Q1), where Q1 and Q3 represent the first and third quartiles respectively.

Table 4-3 *E. coli* RS-2GFP recovery for all three fractures at each specific discharge.

Fracture	Specific Discharge (cm/min)	Number of *E. coli* experiments conducted	Average *E. coli* recovery (%)	σ (%)
F1	0.1	3	66.8	12.7
	1	3	43.2	22.4
	10	3	42.8	9.2
F2	0.1	3	11.8	10.3
	1	3	43.7	14.9
	10	3	45.3	15.1
F3	0.1	3	24.8	21.6
	1	3	64.1	13.6
	10	3	56.9	9.6

a) F1

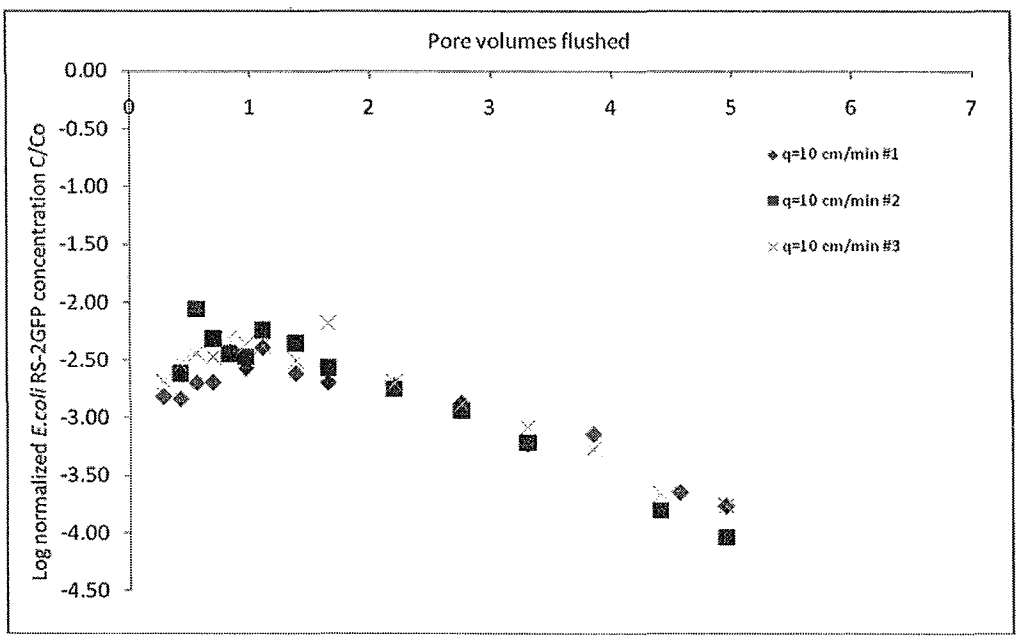

b) F2

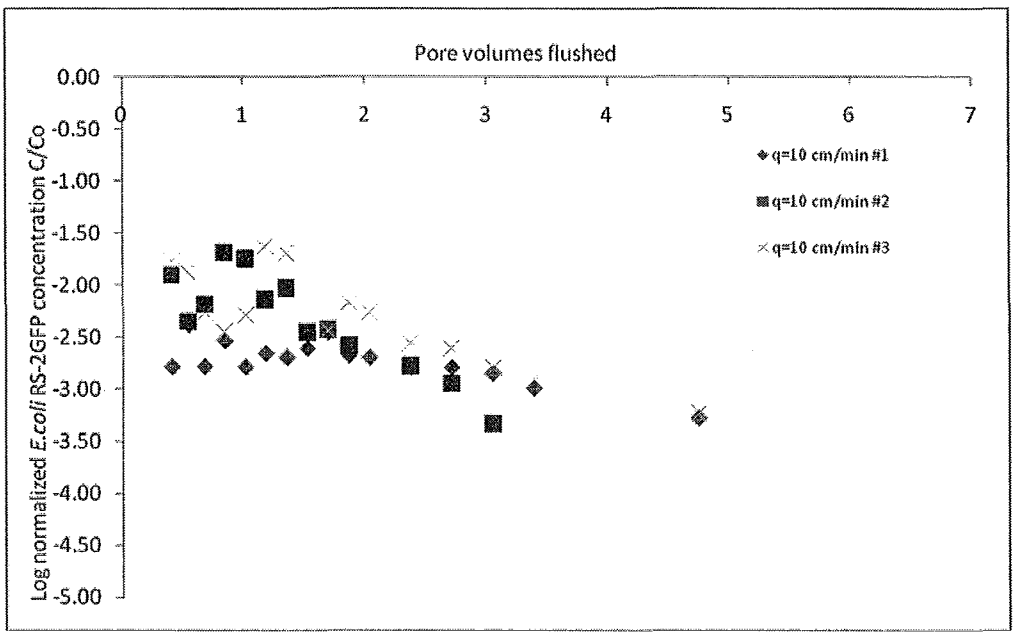

c) F3

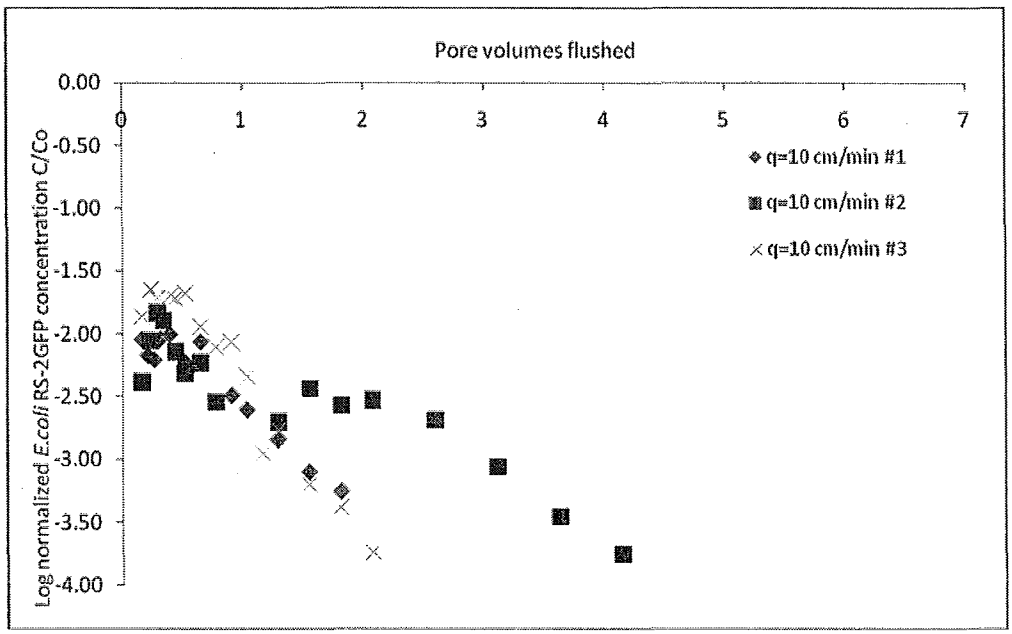

Figure 4-4 Log normalized breakthrough *E. coli* RS-2GFP curves for all repeat experiments conducted at 10 cm/min in a) F1, b) F2 and c) F3.

a) F1

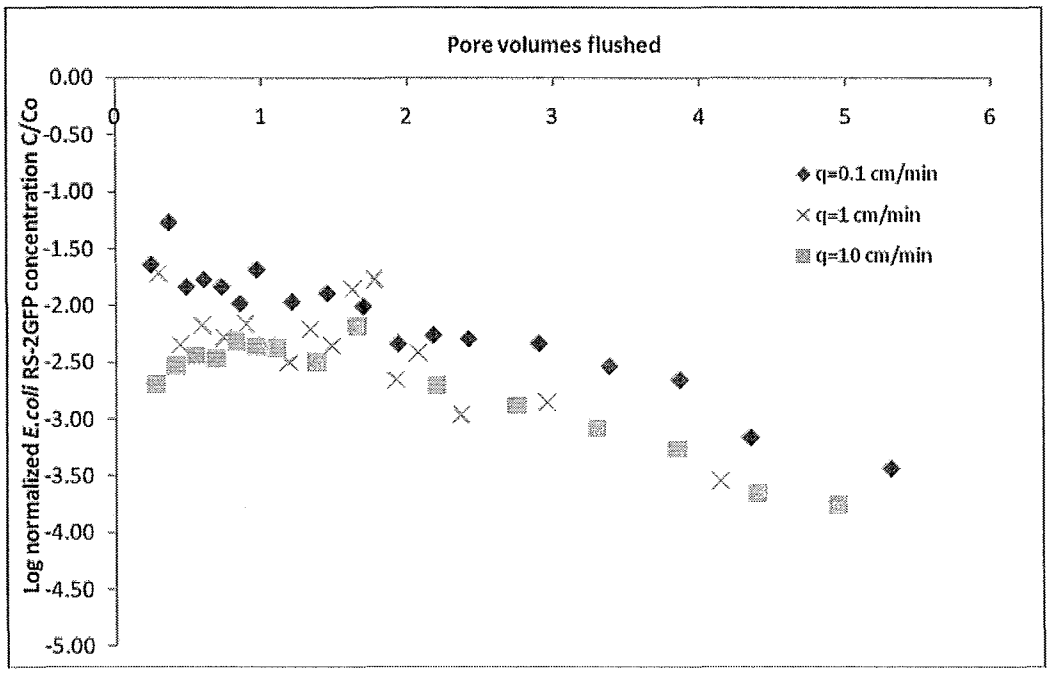
Pore volumes flushed
Log normalized E.coli RS-2GFP concentration C/Co
0.00
-0.50
-1.00
-1.50
-2.00
-2.50
-3.00
-3.50
-4.00
-4.50
-5.00
0
1
2
3
4
5
6
q=0.1 cm/min
q=1 cm/min
q=10 cm/min

b) F2

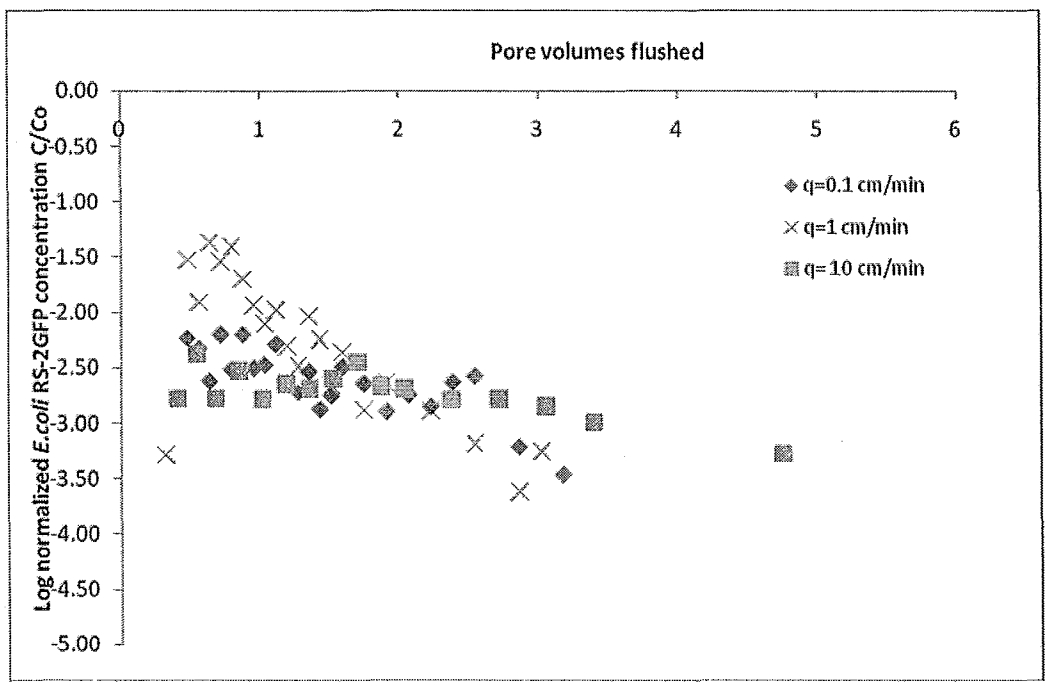
Pore volumes flushed
Log normalized E.coli RS-2GFP concentration C/Co
0.00
-0.50
-1.00
-1.50
-2.00
-2.50
-3.00
-3.50
-4.00
-4.50
-5.00
0
1
2
3
4
5
6
q=0.1 cm/min
q=1 cm/min
q=10 cm/min

c) F3

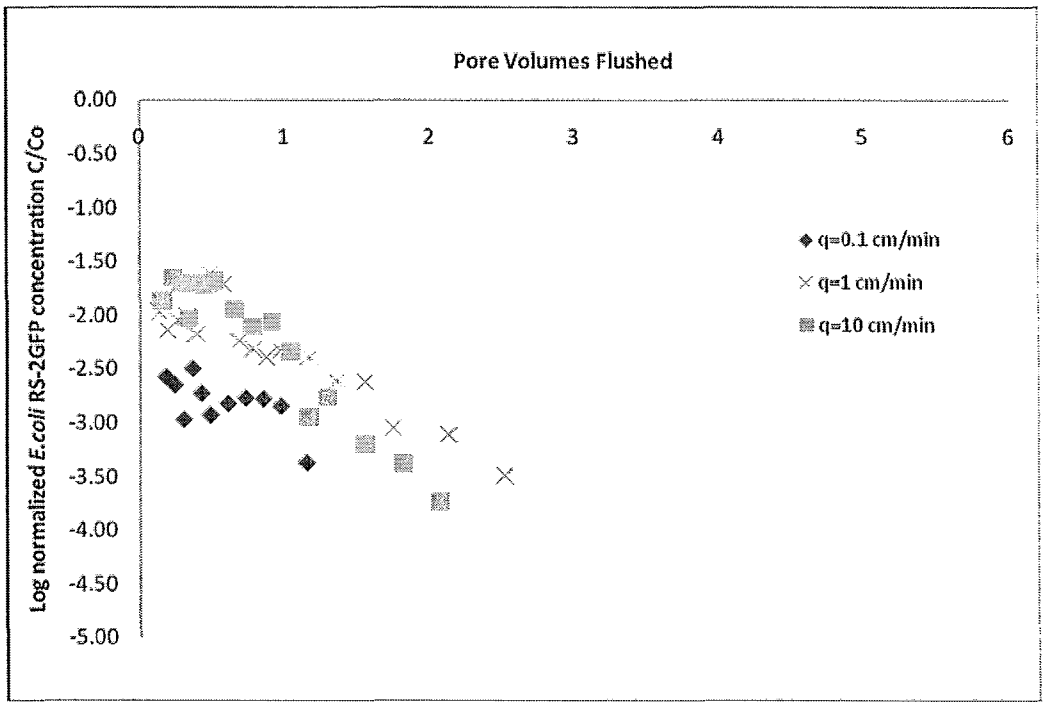

Figure 4-5. Log normalized median *E. coli* RS-2GFP breakthrough curves for 0.1, 1, and 10 cm/min, in a) F1, b) F2, and c) F3.

Figures 4-5 a), b), and c) show the log normalized median *E. coli* RS-2GFP breakthrough curves at all three specific discharges for F1, F2 and F3 respectively. The fact that recovery is largest at the highest specific discharges in F2 and F3, but smallest at the highest specific discharge in F1, suggests that different transport mechanisms are dominant in the different fractures. It is hypothesized that larger flow rates: 1) provide biocolloids with less opportunity to attach to the fracture wall, and 2) result in larger shear forces causing detachment. Therefore, larger flow rates should result in larger recoveries. Table 4-3, however, indicates that this postulation is only followed in F2 and F3. In F1, however, the opposite trend is observed. F1 does have a relatively small

aperture field compared to F2 and F3, and therefore it is possible that the resulting velocities in F1 did not provide ample time for any attachment to occur, and therefore other transport mechanisms were more dominant than attachment, such as straining and dispersion. This demonstrated that the specific discharges influence the transport, i.e., with higher specific discharge, there is higher recovery, but meanwhile the fracture characterization also plays a role on transport.

Figure 4-5 shows that tailing persisted the longest in F1, and the breakthrough peaks were earliest in F3. Comparing the transport time with the peak concentrations, a general trend can be identified in which longer transport times are associated with lower peak concentrations. This trend is consistent with the results found by McKay *et al.* (1999). This trend might relate to the variability between fracture apertures, in which the tortuosities of the flow pathways vary significantly. More straining occurs in small fracture apertures, which may result in more opportunity for the processes of attachment and detachment to occur, resulting in lower peak concentrations and slower transport.

A comparison of breakthrough curves at the same flow rate in different fractures may be instructive in determining the effects of aperture field characteristics on *E. coli* RS-2GFP retention in fractures. Plots of log normalized median *E. coli* RS-2GFP concentration versus time in all three fractures at each flow rate are given in Figure 4-6.

a). 0.1 cm/min.

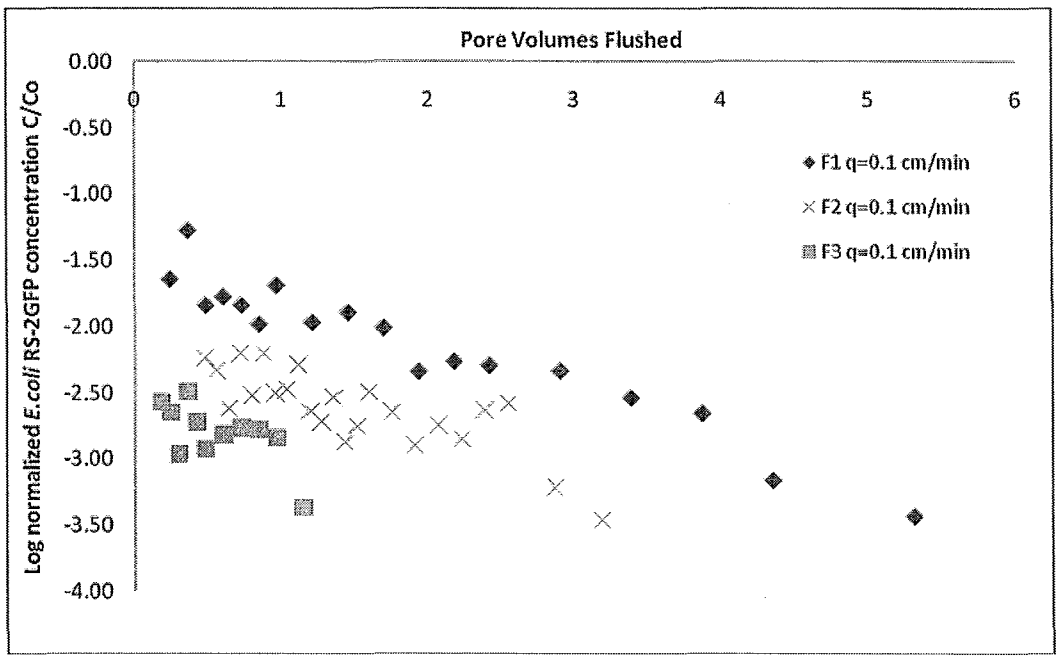

b). 1 cm/min.

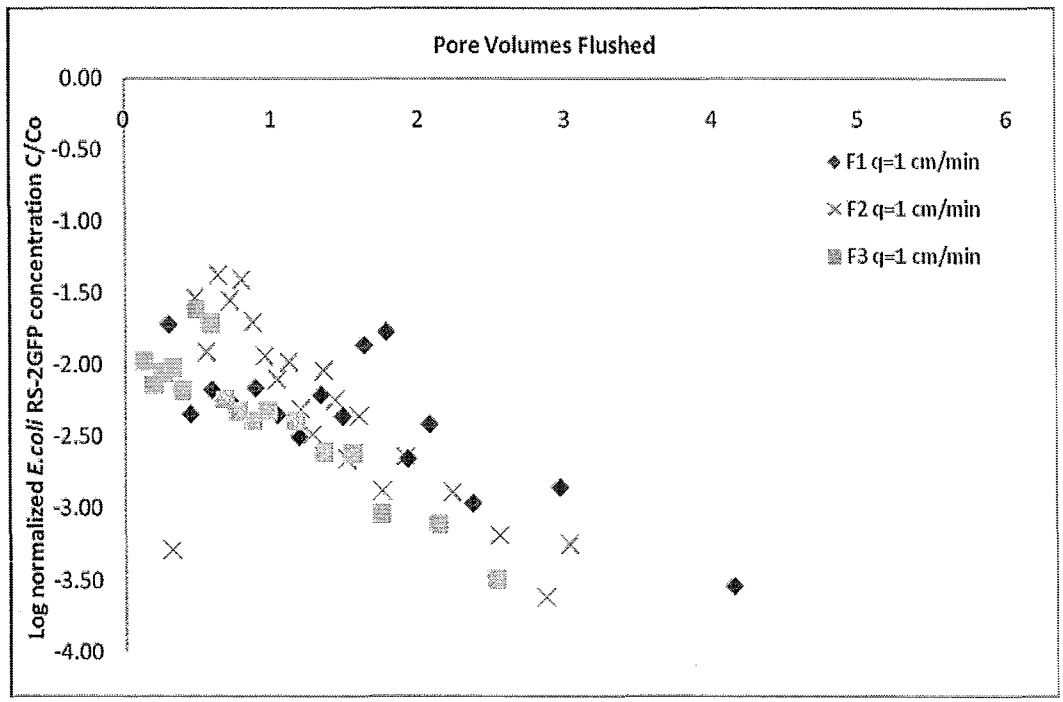

c). 10 cm/min

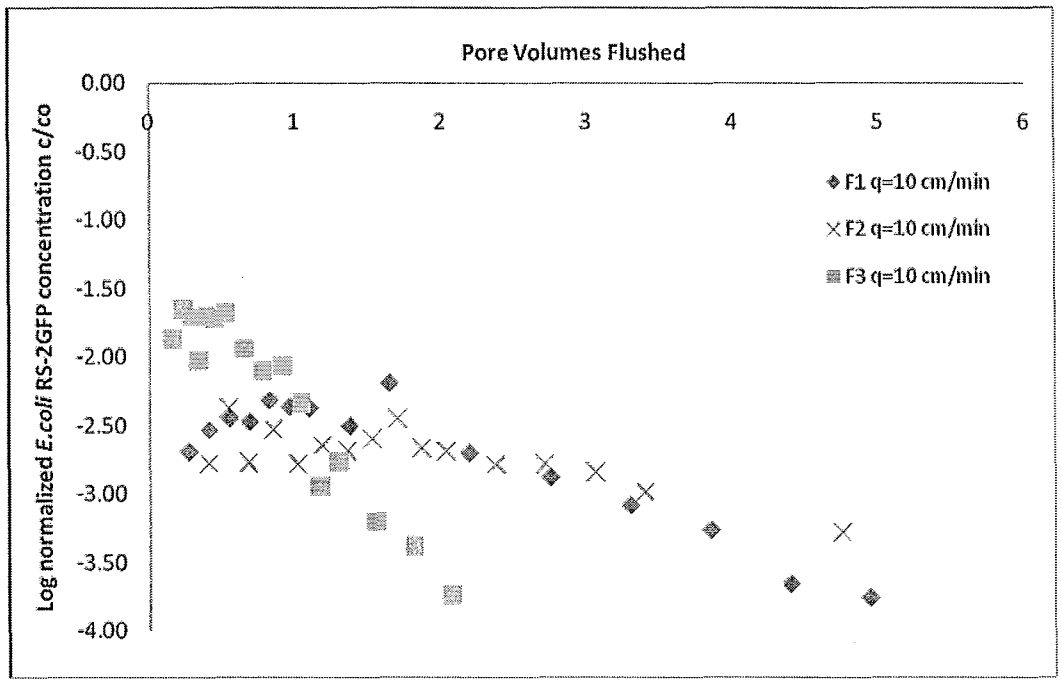

Figure 4-6. Log normalized median breakthrough curves in all three fractures at specific discharges of a) 0.1, b) 1, and c) 10 cm/min.

The relationship between the mass balance apertures, and therefore the arithmetic mean aperture, is F1<F3<F2. Figure 4-7 shows the percent recovery versus specific discharge for all experiments conducted in each fracture. It can be seen from this figure that at the lower specific discharge (0.1cm/min), the range of percent recovery is relatively large. At this low specific discharge, F1 has the largest mean recovery (66.8%), while the recoveries in F2 and F3 are relatively low (11.8 and 24.8% respectively). At the highest specific discharge (10 cm/min), the range of recoveries is much narrower, and F2 and F3 have higher mean recoveries (45.3 and 56.9% respectively), while F1 has a lower mean recovery (42.8%). This is likely due to the fact that higher specific discharges

enable the biocolloids to distribute uniformly across the flow profile, providing the biocolloids with less opportunity to transport towards the vicinity of the fracture wall. This has two effects: 1) Without access to the fracture wall there is less opportunity for attachment; and, 2) the velocity profile is such that the largest velocities occur in the centre of the fracture, resulting in the fastest transport.

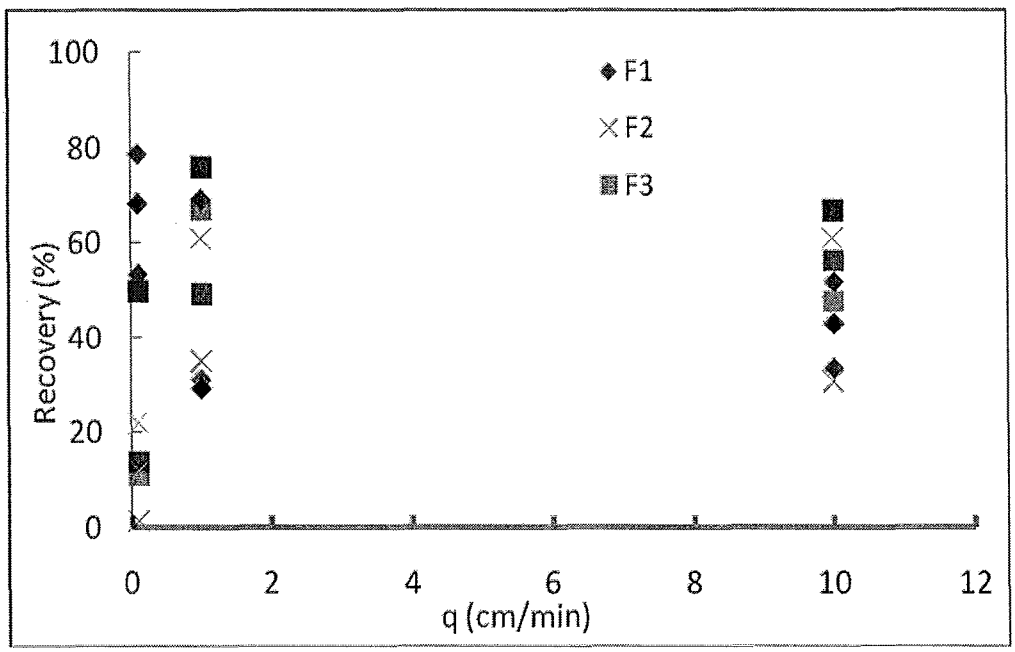

Figure 4-7 Recovery vs. specific discharges for all the repeated experiments on three fractures.

Since the *E. coli* RS-2GFP experiments are susceptible to variation in bacterial survival, inoculum preparation and enumeration, the experiments must be repeatable to be convincing. However, Figure 4-4 and Figure C included in Appendix C demonstrate that the result of triplicate experiments match each other quite well in terms of duration,

magnitude and shapes, demonstrating that the experiments are scientifically reliable. Therefore, it is concluded that different removal mechanisms are responsible for the seemingly conflicting results obtained from the different fractures, and not experimental error. It is postulated that both the flow rate and aperture field characteristics influence the removal mechanisms.

4.3 Colloid Tracer Tests

Polystyrene microspheres were used as colloid tracers in synthetic fractures in the physical experiments conducted by Zheng (2008). The purpose of Zheng's (2008) experiments was to investigate the effects of specific discharge, ionic strength and aperture field charateristics on colloid transport in saturated rock fractures. The microspheres employed by Zheng (2008) were monodisperse with a 1 μm diameter, a specific density of 1.05, and they fluoresced when excited under UV light of 535 nm (Zheng, 2008). The fracture casts employed by Zheng were of a similar scale to those employed in these experiments, and therefore it may be appropriate to compare the results of the colloid experiments in fracture casts to the *E. coli* RS-2GFP experiments conducted in natural rock fractures here to investigate the differences between biocolloid and colloid transport in rock fractures. Table 4-4 lists the characteristics of the fractures employed by Zheng (2008), hereafter refered to R1, R3 and R4. Further details regarding the fabrication of the fracture casts employed in the experiments themselves are available in Zheng (2008).

Figure 4-8 presents the percent of colloid recovery versus specific discharge for R1, R3 and R4, and Figure 4-9 shows a typical normalized breakthrough curve for R1 at a specific discharge of 10 cm/min. Results of colloid recovery at three specific discharges are tabulated in Table 4-5. Figure 4-8 demonstrates that as the specific discharge increases, the percent recovery also increases, which is not entirely consistent with the results of biocolloid experiments discussed in Section 4.2.

Table 4-4 Synthetic replicas field characterization.

Fracture ID	Length [cm]	Width [cm]	μ_m [mm]	μ_c [mm]	μ_l [mm]
R1	24.1	14.9	0.933	0.400	0.267
R3	34.9	23.0	1.653	0.533	0.380
R4	35.0	21.4	1.607	0.540	0.327

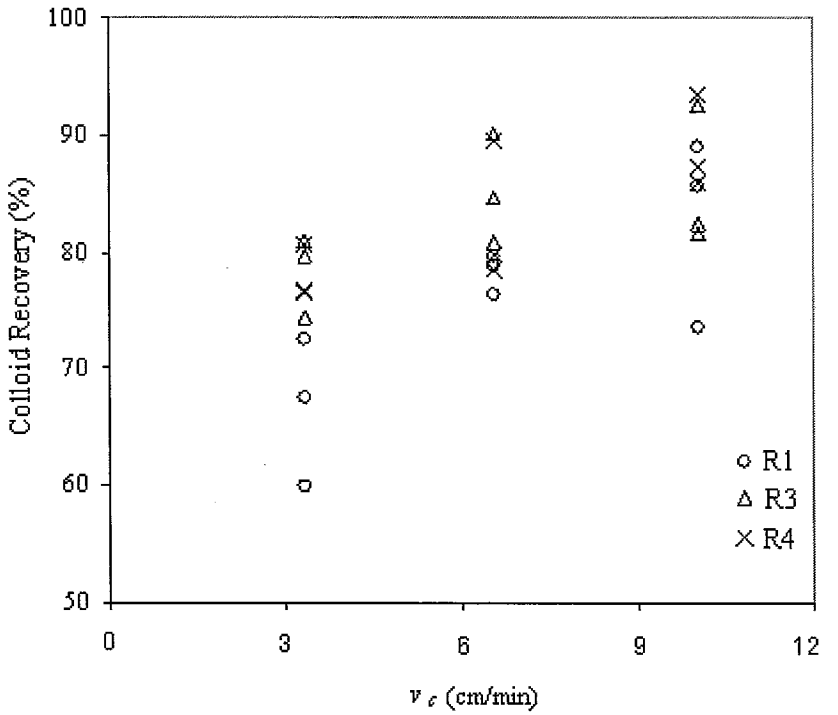

Figure 4-8. The effect of specific discharge (v_c), ionic strength (I_c) and aperture field variability on colloid recovery in R1, R3, and R4 (Zheng, 2008).

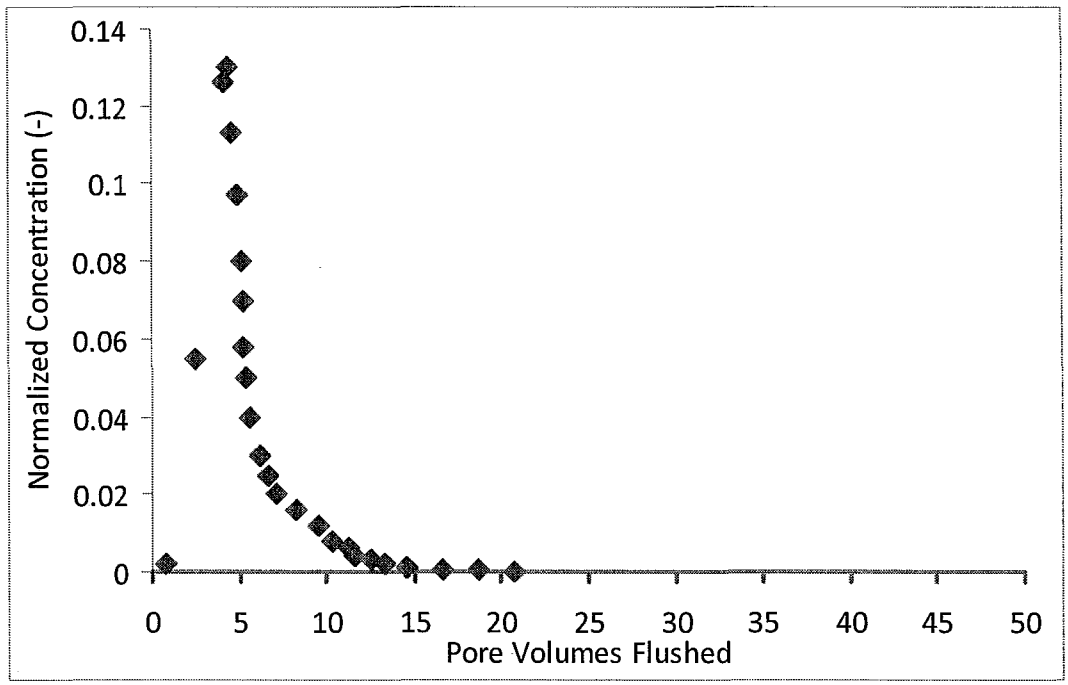

Figure 4-9. The typical normalized breakthrough curves for R1 (q=10.0 cm/min, I_c=0.01) (Zheng, 2008).

Table 4-5 Colloid recovery for all three synthetic fractures at each specific discharge.

Fracture	Specific Discharge (cm/min)	Number of colloid experiments conducted	Average *E. coli* recovery (%)	σ (%)
R1	3.3	3	66.7	6.4
	6.5	3	78.3	1.7
	10.0	3	81.5	10.2
R3	3.3	3	74.4	3.8
	6.5	3	80.6	3.0
	10.0	3	82.8	3.9
R4	3.3	3	77.9	2.4
	6.5	3	82.6	6.1
	10.0	3	88.9	4.0

This is likely due to the fact that under the higer flow rates, colloids have less opportunity to contact the wall of the fractures, and therefore less opportunity for the attachment processes to occur. The size of the mass balance apertures amongst the fracture replicas are ordered as follows: R1<R4<R3. Zheng (2008) hypothesized that in fractures with smaller apertures, colloids will have more collisions with the fracture walls, thereby providing more opportunity for attachment. Figure 4-8 clearly corroborates this hypothesis at all three specific discharges, with the percentage recovery ordered as follows R1<R4<R3; however, R3 and R4 have similar recoveries, which is coincident with their similar aperture sizes.

4.4 Comparison of *E. coli* RS-2GFP and colloids tracer tests results

Figure 4-10 clearly demonstrates that the colloid recovery increased with increasing flow rate, and that there is less of a spread in the recovery data, due to flow rates, in the larger fracture apertures. Figure 4-11 does not demonstrate these same trends for the biocolloid data. For biocolloids, the average recovery seems to decrease with aperture size at lower specific discharges. No clear relationship between aperture size and specific discharge, for biocolloid removal, is visible in Figure 4-11, indicating that perhaps dominant removal mechanisms are not consistent between fractures at a given specific discharge. It is likely that shear forces (i.e. detachment) are more important in smaller apertures at higher specific discharges, also there are less attachment due to little opportunities to contact the fracture wall.

To compare the biocolloid and colloid results, the recoveries from F1, F3 and their replicas R1 and R3, are tabulated in Table 4-6 and graphed versus specific discharge in Figure 4-12. Two similar specific discharges were compared. Biocolloid at 1 cm/min with colloid at 3.3 cm/min, and both biocolloid and colloid at 10 cm/min.

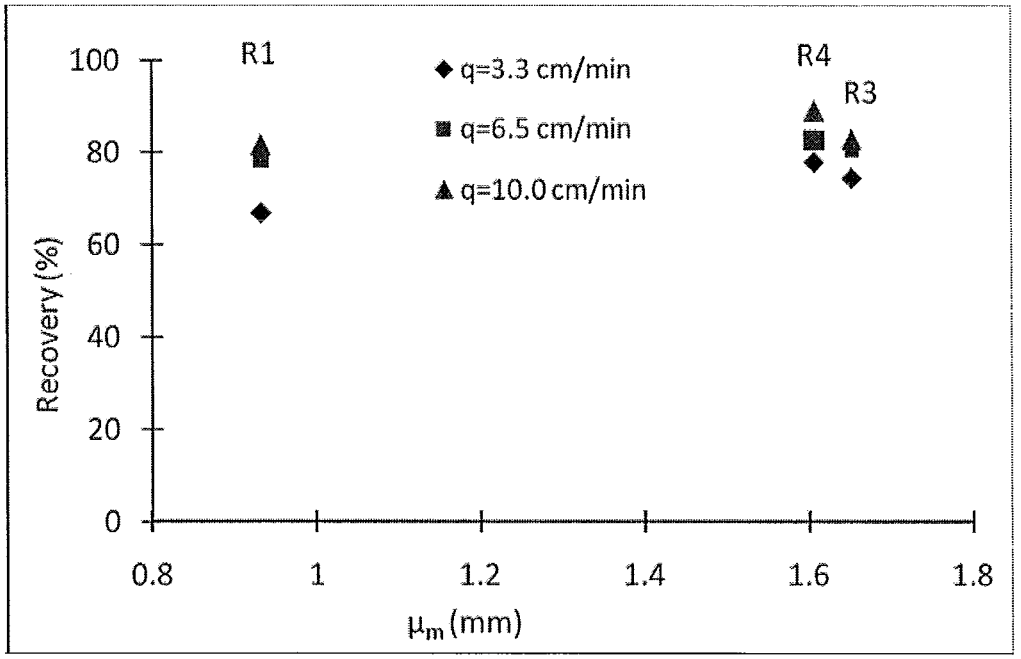

Figure 4-10. Colloid recovery (%) in three different fractures at specific discharges.

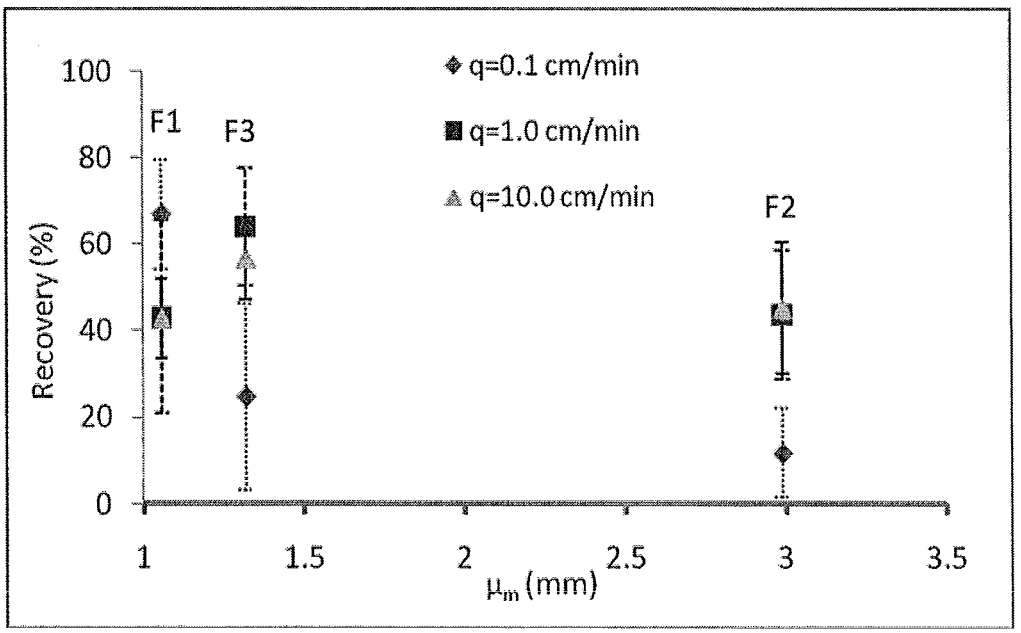

Figure 4-11. *E. coli* RS-2GFP recovery (%) in three different fractures at three specific discharges, the error bars shows the standard deviation from triplicate experiments (0.1 cm/min: ". .", 1.0 cm/min: "- -", 10 cm/min: "--").

Table 4-6 Biocolloid and colloid recovery for each fracture at each specific discharge

Fracture ID	Recovery (%)			μ_m (mm)
	q=1 (cm/min) q=3.3 (cm/min)		q=10 (cm/min)	
F1	43.2		42.8	1.056
R1		66.7	81.5	0.933
F3	64.1		56.9	1.319
R3		74.4	82.8	1.653

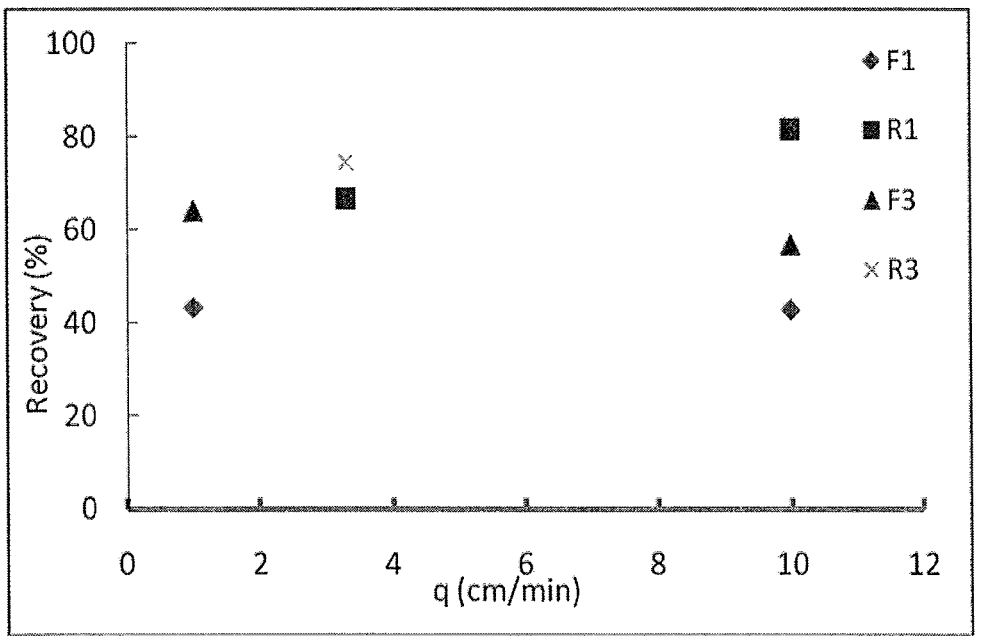

Figure 4-12. A comparison of biocolloid and colloid recovery in similar specific discharges.

Figure 4-12 shows that the percentage of recovery in the real fractures are smaller than those of the synthetic ones; however, the mass balance aperture sizes of real fractures are slightly larger than synthetic ones. This is not absolutely coincident with the hypothesis that smaller apertures will retain more colloids. This is likely due to the differences in surface properties between the real and synthetic fractures and the biocolloids and colloids. *E. coli* RS-2GFP has biological properties, e.g., they can grow and die off in the fractures, and it is possible for them to accumulate in fracture walls and cracks, or agglomeration. Polystyrene microspheres, on the other hand, have fewer biological effects and are dominated by physical processes, which demonstrates that the properties of microorganisms themselves can significantly influence the behavior of transport. The fracture material will also affect transport. While epoxy can replicate the details of the fracture wall, real fractures will have surfaces with more variability in aperture field, which provides more space and opportunities for straining and attachment.

5. Conclusions

The research involves experiments on different fracture fields and specific discharges. A comparison was conducted between biocolloid transport in rock fractures and colloid transport in synthetic fractures. The results reveal some of the factors influencing transport, thus furthering our understanding of fractured aquifer vulnerability to pathogen contamination.

- A linear relationship was found between flow rate and head loss over the range of flows employed in all three fractures, demonstrating that the flow in the fracture systems was laminar, and therefore the cubic law is valid. The aperture fields follow the trend: the mass balance aperture is larger than the cubic law aperture, which is larger than the friction law aperture. This is consistent with previous research.

- The percent recovery increased with specific discharge in F2 and F3, but not in F1. The fact that F1 has the smallest aperture likely contributes to this fact, as the resulting velocities in F1 may not provide ample time for the process of attachment to occur, and therefore other transport mechanisms may be more dominant than attachment in F1. Further, the larger velocities in F1 resulting in larger shear forces, and therefore detachment.

- Under the same specific discharge, it was found that smaller aperture fields produced lower and later peak particulate concentrations, resulting in a longer time required to

transport the particulates injected through the system. This indicates that the fracture aperture field has a large influence on preferential pathways and attachment mechanisms.

- Higher specific discharge result in a much smaller range of recoveries in the three fractures than lower specific discharges. This may be due to the fact that higher specific discharges enable biocolloids to distribute uniformly across the velocity profile, providing less opportunity to contact the fracture wall and attach.

- In the microspheres tracer tests, larger specific discharges resulted in higher colloid recovery in all cases, which is consistent with the results found in biocolloid experiments conducted on F2 and F3.

- Higher colloid recovery was observed with increasing aperture in the microsphere experiments, this was not clearly seen in the biocolloid experiments.

- In general, the recovery of *E. coli* RS-2GFP in real fractures was smaller than the recovery of microspheres in the fracture replicas. This indicates that the surface properties of the tracers, thus the properties of the biocolloids and fractures employed in this research, have a very large influence on biocolloid transport.

Recommendations

In addition to analysing colloid recovery in fractures, it is necessary to determine the specific mechanisms of removal in order to provide appropriate suggestions for preventing contamination of fractured aquifers in the future. It is important to conduct experiments in transparent replicas, to visualise the transport process. To pursue further knowledge of pathogen contamination, research is required investigating different types of microorganisms, since the biological property of microorganisms is a dominant factor influencing transport behaviour.

References

Abu-Ashour Jamal *et al.*, Transport of microorganisms through soil, Water, *Air and Soil Pollution, 75,* 141-158, 1994.

APHA, AWWA, WEF, *"Standard Methods for the Examination of Water and Wastewater"*, Standard Methods Online, 2006, [Online], Available: http://standardmethods.org/Store/index.cfm [Accessed: Jan. 21, 2010].

Auset, M., and A. A. Keller, Pore-scale visualization of colloid straining and filtration in saturated porous media using micromodels, *Water Resour. Res., 42*, W12S02, doi:10.1029/2005WR004639, 2006.

Becker Matthew W. *et al.*, Bacterial transport experiments in fractured crystalline bedrock, *Ground Water, Vol. 41, No. 5*, 682-689, 2003.

Beeder Janiche *et al.*, Penetration of sulphate reducers through a porous north sea oil reservoir, *Applied and Environmental Microbiology,* Sept, 3551-3553, 1996.

Bergey, D.H., Holt, J.G., Krieg, N.R., *Bergey's Manual of Systematic Bacteriology.* Williams & Wilkins, Baltimore, USA. ISBN 0-683-04108-8, 1984.

Bradford, S. A., J. Simunek, and S. L. Walker, Transport and straining of E. coli O157:H7 in saturated porous media, *Water Resour. Res., 42, W12S12,* doi:10.1029/2005WR004805, 2006.

Brush, D. J., and Thomson, N. R., Fluid flow in synthetic rough-walled fractures: Navier-Stokes, Stokes, and local cubic law simulations, *Water Resour. Res., Vol 39, No. 4*, 1085, 2003.

Celico Fulvio *et al.*, Influence of precipitation and soil on transport of fecal enterococci in fractured limestone aquifers, *Appl. Environ. Microbial., Vol. 70,* No. 5, 2843-2847, 2004.

Chen Jui-Sheng, Chen Chia-Shyun, and Chen Chih Yu, Analysis of solute transport in a divergent flow tracer test with scale-dependent dispersion, *Hydrological Processes, 21*, 2526-2536, 2007.

Clark, R., and J. King, *The Water Atlas*, New Press, New York, 127 pp., 2004.

Cortis, A., T. Harter, L. Hou, E. R. Atwill, A. I. Packman, and P. G. Green, Transport of Cryptosporidium parvum in porous media: Longterm elution experiments and continuous

time random walk filtration modeling, *Water Resour. Res., 42*, W12S13, doi:10.1029/2006WR004897, 2006.

Craun, G. F., *Health aspects of groundwater pollution, Groundwater Pollution Microbiology*, John Wiley & Sons, Inc., New York, 1984.

Cunningham, A., Warwood, B., Sturman, P., Horrigan, K., James, G., Costerton, J.W., & Hiebert, R., Biofilm processes in porous media-practical applications. In P.S. Amy & D.L. Haldeman (Ed.), *The microbiology of the deep subsurface*, 325-344, 1997.

DeKerchove, A.J., Elimelech, M.. Relevance of electrokinetic theory for 'soft' particles to bacterial cells: implications for bacterial adhesion. *Langmuir 21*, 6462–6472, 2005.

Dickson, S.E., Dissolution of entrapped DVAPLS in variable aperture fractures, Ph.D. thesis, University of Waterloo, Waterloo, Ontario, Canada, 2001.

Emelko *et al.*, Quantification of unvertainty in microbial data – reporting and regulatory implications, *Journal AWWA 100:3*, March 2008.

Fahim M. A., and Wakao N., Parameter estimation from tracer response measurements, *The chemincal Engineering Journal, Volume 25, Issue 1,* Page 1-8, 1982.

Foppen J.W.A., Schijven J.F., Evaluation of data from the literature on the transport and survival of Escherichia coli and thermotolerant coliforms in aquifers under saturated conditions, *Water Research Vol. 40,* 401-426, 2006.

Ganon, J. T., Manilal, V. B., and Alexander, M., *Appl. Environ. Microbiol, 57,* 190, 1991.

Gerba, C. P., Wallis, C., and Melnich, J. L., J. Irrig. *Drain. Div. 101,* 157, 1975.

Gilbert, P., Evans, D.J., Evans, E., Duguid, I.G., Brown, M.R.W., Surface characteristics and adhesion of Escherichia coli and Staphylococcus epidermis. *J. Appl. Bacteriol. 71,* 72–77, 1991.

Gleick, P. H., *The World's Water,* Island Press, Washington, D. C, 362 pp., 2004.

Hartmann S, Odling N.E., and West L.J., A multi-directional tracer test in the fractured Chalk aquifer of E. Yorkshire, UK, *Journal of Contaminant Hydrology, 94,* 315-331, 2007.

Harvey Ronald W., George Leah H., Smith Richard L, and LeBlanc Denis R., Transport of microspheres and indigenous bacteria through a sandy aquifer: results of natural- and forced-gradient tracer experiments, *Environ. Sci. Technol. 23,* 51-56, 1989.

Harvey Ronald W., Mayberry Naleen, Kinner Nancy E., Metge David W., and Novarino Franco, *Applied and Environmental Microbiology*, Apr. 2002, 1872-1881, 2002.

Hautman, D. P., Munch D. J., and Pfaff J. D, Method 300.1, Determination of inorganic anions in drinking water by ion chromatography, revision 1.0, National Exposure Research Laboratory Office of Research and Development, U.S. Environmental Protection Agency, Cincinnati, Ohio 45268, 1997.

Hill David D. and Sleep Brent E., Effects of biofilm growth on flow and transport through a glass parallel plate fracture, *Journal of Contaminant Hydrology, 56,* 227-246, 2002.

Hinsby K. et al, Fractures aperture measurements and migration of solutes, viruses, and immiscible creosote in a column of clay-rich till, *Ground Water, Vol. 34, No.6,* 1065-1075., 1996.

Lehman Michael R. *et al.*, Attached and unattached microbial communities in a simulated basalt aquifer under fracture- and porous-flow conditions, *Appl. Environ. Microbial., Vol. 67, No. 6,* 2799-2809, 2001.

Mailloux Brian J., Fuller Mark E., Onstott Tullis C., Hall James, Dong Hailiang, DeFlaun Mary F., Streger Sheryl H., Rothmel Randi K., Green Maria, Swift Donald J.P., and Radke Jon, *Water Resources Research, Vol. 39, No. 6,* 1142, doi:10.1029/2002WR001591, 2003.

McDowell-Boyer, L. M., Hunt, J.R., and Sitar, N., *Water Resour. Res. 22,* 1901, 1986.

McKay Larry D. and Cherry John A., A field example of bacteriophage as tracers of fracture flow, *Environ. Sci. Technol, 27,* 1075-1079, 1993.

Mclinn Eugene L. and Rehm Bernd W., Biodegradation of petroleum hydrocarbons in fractured, unsaturated dolomite at a field site, *GWMR*, fall, 73-80, 1997.

Medema, G.J., Payment, P., Dufour, A., Robertson, W., Waite, M., Hunter, P., Kirby, R., Andersson, Y.. Safe drinking water: an ongoing challenge. In: Dufour *et al.* (Eds.), *Assessing Microbial Safety of Drinking Water: Improving Approaches and Methods,* World Health Organization, 2003. ISBN 92 4154630, 2003.

Pang, L., and J. Simunek, Evaluation of bacteria-facilitated cadmium transport in gravel columns using the HYDRUS colloid-facilitated solute transport model, *Water Resour. Res., 42, W12S10,* doi:10.1029/2006WR004896, 2006.

Ross Nathalie *et al.*, Clogging of a limestone fracture by stimulating groundwater microbes, *Wat. Res., Vol. 35, No. 8,* 2029-2037, 2001.

Ross Nathalie and Bickerton Greg, Application of biobarriers for groundwater contaminant at fractured bedrock sites, *Remediation,* Summer, 5-21, 2002.

Ross, Nathalie *et al.*, Ecotoxicological assessment and effects of physicochemical factors on biofilm development in groundwater conditions, *Environmental Science and Technology, Vol. 32, No. 8,* 1105-1111, 1998.

Saiers James E., Ryan Joseph N., Introduction to special section on colloid transport in subsurface environments, *Water Resources Research, Vol. 42, W12S01,* doi:10.1029/2006WR005620, 2006.

Sekerak Bethany, Development of an interfacial tracer test for DNAPL entrapped in discrete fractured rock, M.A.Sc thesis, Civil Engineering, McMaster University, 2004.

Shaw, J.C., Bramhill, B., Wardlaw, N.C., & Costerton, J.W., Bacterial fouling in a model core system, *Appl. Environ. Microbial, 49,* 693-701, 1985.

Smith, M. S., Thomas, G.W., White, R.E., and Retonga, D, *J. Environ. Qual., 14,* 87, 1985.

Stumm, W., Morgan, J.J.. *Aquatic Chemistry*, 3rd ed. Wiley, New York, 1996.

Torkzaban, S., S. M. Hassanizadeh, J. F. Schijven, and H. H. J. L. van den Berg, Role of air-water interfaces on retention of viruses under unsaturated conditions, *Water Resour. Res., 42, W12S14,* doi:10.1029/2006WR004904, 2006.

Trefy, M.G., & Jognston, C.D., Pumping test analysis for a tidally forced aquifer, *Ground Water, 36,* 4327-433, 1998.

Tsang, Y. W., Usage of 'equivalent apertures' for rock fractures as derived from hydraulic and tracer tests, *Water Resour. Res., 28(5),* 1454-1455, 1992.

Tufenkji, N., Application of a dual deposition mode model to evaluate transport of Escherichia coli D21 in porous media, *Water Resour. Res., 42, W12S11,* doi:10.1029/2005WR004851, 2006.

Vandevivere, P., & Baveye, P., Effect of bacterial extracellular polymers on the saturated hydraulic conductivity of sand columns, *Appl. Environ. Microbial, 58*, 1690-1698, 1992.

Yates, M. V. and Yates, S. R., *ASM News 56*, 324, 1990.

Zheng Qinghuai, Effect of aperture variability, specific discharge, and ionic strength on colloid transport in single fractrues, Ph.D. thesis, Civil Engineering, McMaster University,

Hamilton, Ontario, Canada, 2008.

Zheng Q., Dickson S. E., and Guo Y., On the appropriate "equivalent aperture" for the description of solute transport in single fractures: Laboratory-scale experiments, *Water Resources Research, Vol. 44, W04502,* doi:10.1029/2007WR005970, 2008.

Zvikelsky, O., and Weisbrod N., Impact of particle size on colloid transport in discrete fractures, *Water Resour. Res., 42, W12S08,* doi:10.1029/2006WR004873, 2006.

Appendix

A.

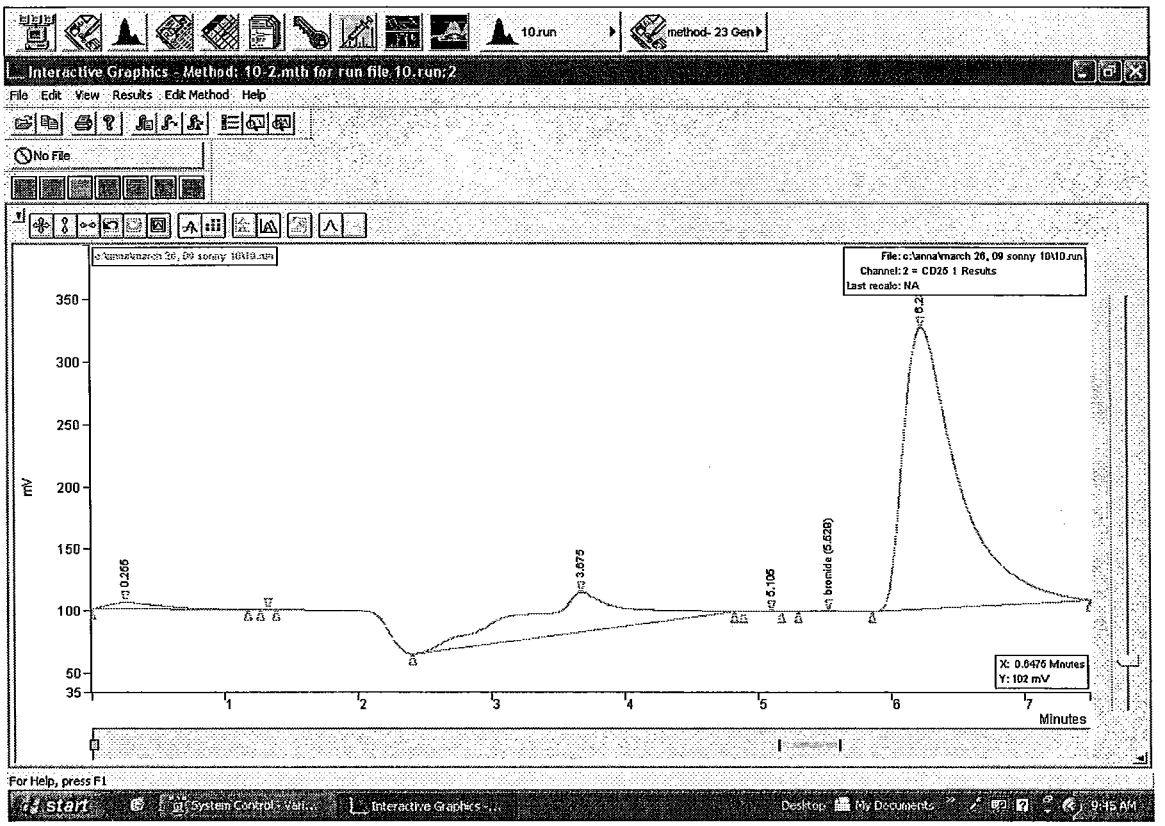

Figure A. Schematic chromatogram response curve.

B.

An example of calculation of error bars on Figure 4-3.

Part 1	**Time [hrs]**	**0.3**	**0.5**	**0.8**	**1.0**	**1.3**
	Q1 [cfu/mL]	860000	2157500	5150000	4850000	5350000
	min [cfu/mL]	830000	2140000	4900000	4800000	5200000
	median [cfu/mL]	900000	2255000	5400000	4900000	5500000
	max [cfu/mL]	1000000	4600000	6300000	6700000	7800000
	Q3 [cfu/mL]	947500	2525000	5850000	5800000	6650000
	Back-calculated median		15353333	35801667	9733333	11300000
Part 2	**1.5q**	131250	551250	1050000	1425000	1950000
	Q3+1.5q	1078750	3076250	6900000	7225000	8600000
	Q1-1.5q	728750	1606250	4100000	3425000	3400000
	top	1000000	3076250	6300000	6700000	7800000
	bot	830000	2140000	4900000	4800000	5200000
	No. Pore Volumes Flushed	0.12	0.24	0.36	0.48	0.60
Part 3	**log bac-cal median**		7.186203	7.553903	6.988262	7.053078
	log median	5.954243	6.353147	6.732394	6.690196	6.740363
	log top	6	6.488022	6.799341	6.826075	6.892095
	log bot	5.919078	6.330414	6.690196	6.681241	6.716003
	top2	0.045757	0.134875	0.066947	0.135879	0.151732
	bot2	0.035164	0.022733	0.042198	0.008955	0.024359

Above is a sample of CFU records of F1 from time 0.3-1.3 hour on 0.1 cm/min.
Part 1 is the quartile function from original CFU data. Part 2 is the conversion of quartile function. 1.5 q is 1.5 times (Q3-Q1), and makes Q3 plus 1.5q, Q1 minus 1.5q. Compare those numbers with maximum and minimum number from Part 1. Make the smaller number between Q3+1.5q and maximum the top of error bars, the larger number between Q1-1.5q and minimum the bottom of the error bars. Part 3 takes the log function of Part 2, and plots the final figure.

C.

a) F1 1 cm/min

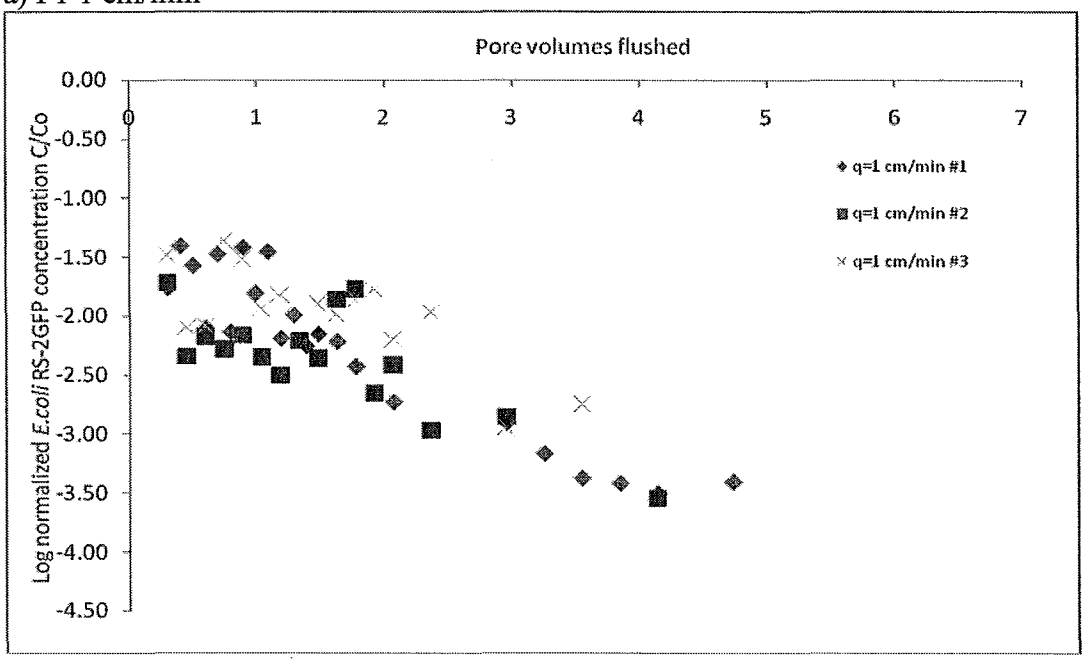

b) F1 0.1 cm/min

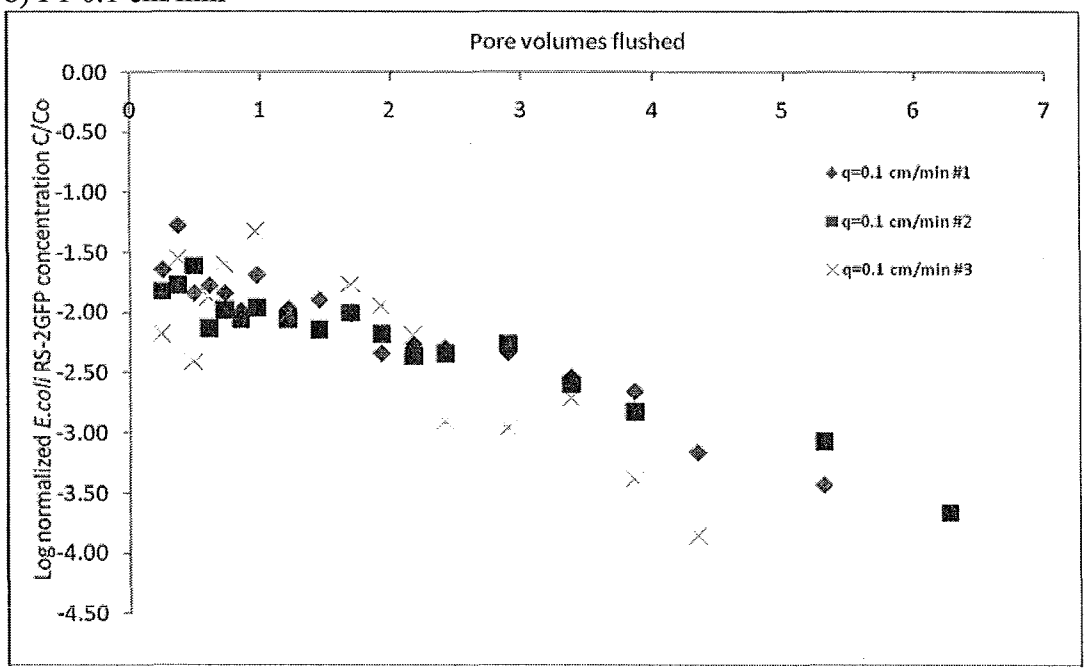

c) F2 1 cm/min

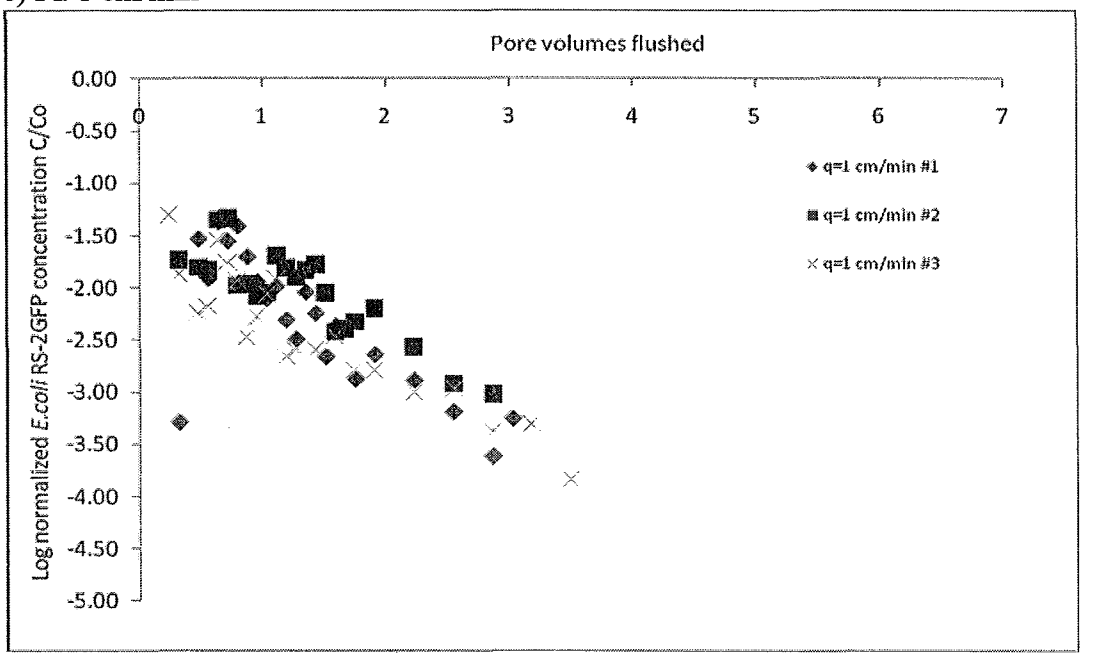

d) F2 0.1 cm/min

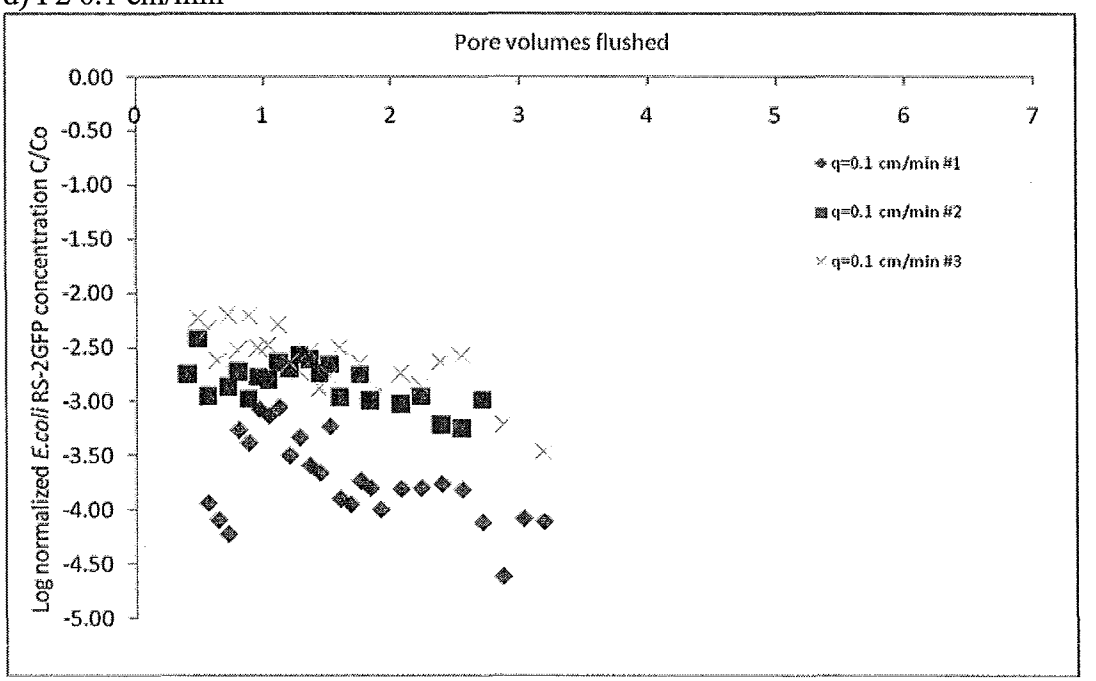

e) F3 0.1 cm/min

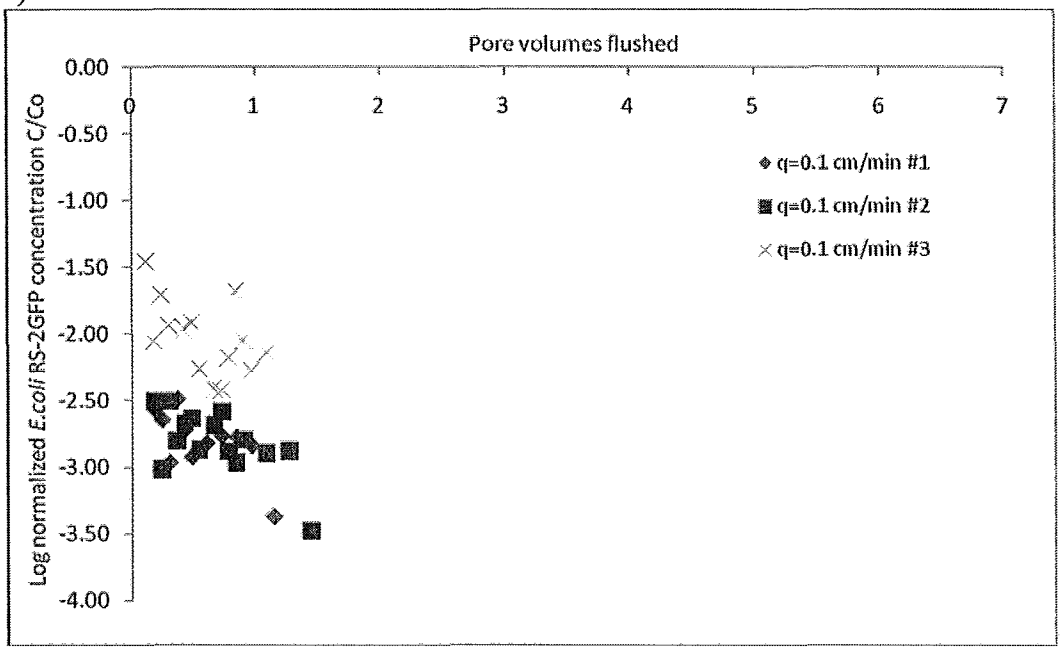

f) F3 1 cm/min

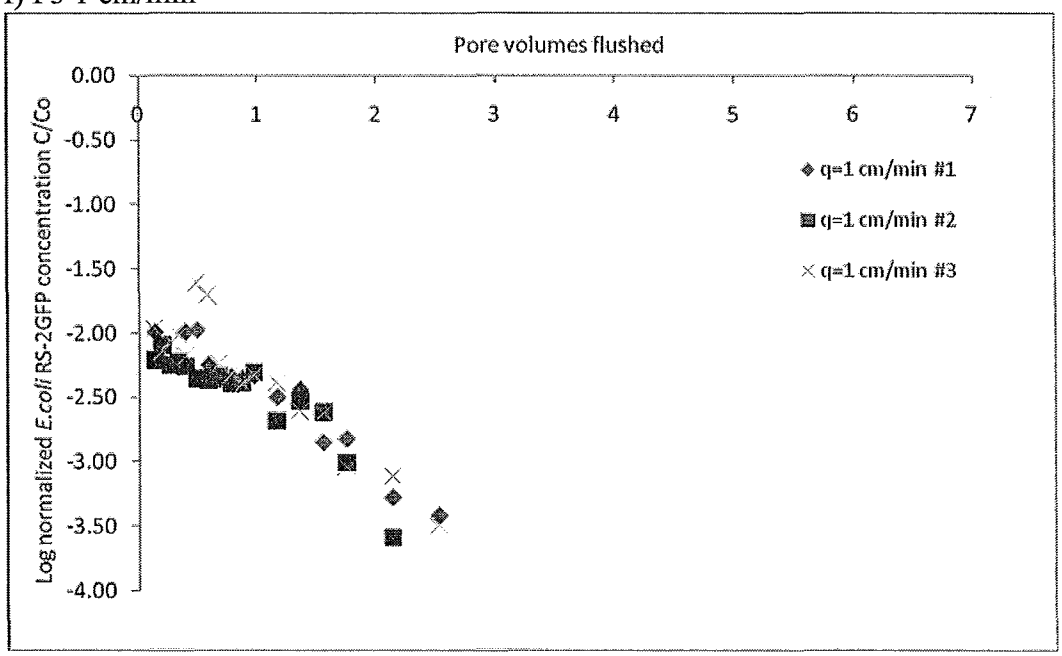

Figure C. Log normalized *E.coli* RS-2GFP concentrations in 1 and 0.1 cm/min, for a), b) F1, c), d) F2, and e), f) F3.